2014

RESPONSE OF FILLED CORRUGATED SANDWICH STRUCTURES TO SHOCK LOADING AT HIGH TEMPERATURES

Payam Fahr
University of Rhode Island, payam_fahr@my.uri.edu

RESPONSE OF FILLED CORRUGATED SANDWICH STRUCTURES TO SHOCK LOADING AT HIGH TEMPERATURES

BY

PAYAM FAHR

A THESIS SUBMITTED IN PARTIAL FULFILLMENT OF THE

REQUIREMENTS FOR THE DEGREE OF

MASTER OF SCIENCE

IN

MECHANICAL ENGINEERING AND APPLIED MECHANICS

UNIVERSITY OF RHODE ISLAND

2014

MASTER OF SCIENCE THESIS

OF

PAYAM FAHR

APPROVED:

Thesis Committee:

Major Professor Arun Shukla

D.M.L. Meyer

K. Wayne Lee

Nasser H. Zawia
DEAN OF THE GRADUATE SCHOOL

UNIVERSITY OF RHODE ISLAND
2014

ABSTRACT

The dynamic response of filled corrugated steel sandwich panels was investigated under combined extremes of blast loading and high temperature heating. The objective of this project was to study blast mitigation and the thermo-mechanical response of panels using a polymer based syntactic foam and mortar as a filler material. These materials were selected due to their thermal resistivity.

In this study, silicone resin (with an operating temperature range between -53°C to 232°C) and two types of glass bubbles were selected as materials to develop a heat resistive syntactic foam. The mechanical properties of the foam were investigated, in ambient temperatures, before and after high-temperature heat treatment (of 500°C), by quasi-static compression experiments. It was observed that plateau stress increases after introduction of glass bubbles in silicone, enhancing the energy absorption properties for both specimens with and without heat treatment.

To produce repeatable blast loading, a shock tube was utilized. Pressure history was recorded using pressure transducers located in the shock tube muzzle. High speed photo-optical methods utilizing Digital Image Correlation (DIC) coupled with optical band-pass filters and high-intensity light source, were utilized to obtain the real-time deformation at high temperature while a third camera captured side-view deformation images. The shock pressure profiles and DIC analysis were used to obtain the impulse imparted to the specimen, transient deflection, in plane strain and out-of-plane velocity of the back face sheet.

Shock tube experiments were performed to investigate the blast response of corrugated steel sandwich panels filled with a silicone based syntactic foam filler at

room and high temperature. It was observed that using the syntactic foam as a filler material, decreased the front face and back face deflections by 42% and 27%, respectively, compared to an empty panel. The highest impulse was imparted on the specimen at room temperature and subsequently lower impulses with increasing temperature. Due to increasing ductility in steel with high temperature, the specimens demonstrated an increase in back face deflection, in-plane strain and out-of-plane velocity with increasing temperatures with weld failure being the primary form of core damage.

High temperature blast experiments were also performed on mortar filled corrugated steel sandwich panels. Mortar is a common building material that can withstand extreme temperatures. It was observed cement based mortars are thermally resilient enough to be used as a filler material for high temperature applications. The highest impulse was imparted on the specimen at room temperature and subsequently lower impulses with increasing temperature. A temperature difference of at least 300ºC was observed across the thickness of the specimen for all heating conditions. Due to increasing ductility in steel with high temperature, the specimens demonstrated an increase in back face deflection, in-plane strain and out-of-plane velocity with increasing temperatures with weld failure being the primary form of core damage.

ACKNOWLEDGMENTS

First and foremost, I would like to express my gratitude to Dr. Arun Shukla for his guidance and support during my graduate career. His patience and approach to problem solving often left me asking questions I never knew existed, and thus truly expanding my knowledge. By allowing us to make our own mistakes, he encourages us to find creative solutions to extract the physics behind novel experiments while gently keeping us on track. He is an incredible professor and mentor, and a truly inspirational human being. His contribution to furthering knowledge in solid mechanics and engineering is profound, yet while humble, he is always thinking ahead to the next interesting puzzle that warrants investigation. I am truly honored to be one of his graduate students.

I would also like to extend my appreciation to Dr. D.M.L. Meyer who has been an unofficial role model during my undergraduate and graduate career. I consider myself lucky to have been able to take every course offered by Dr. Meyer during my time as a student at URI. Her 'knack' for explaining difficult material in simple elegance makes tackling challenging problems less daunting. Her enthusiasm for teaching and her command of course material made it easy to look forward to each class, even at 8 a.m. after a one hour bus commute. As well as being an outstanding professor, she has been a counselor for which I am deeply grateful.

I would like to thank all of my lab mates in the Dynamic Photomechanics Laboratory: Frank LiVolsi, Prathmesh Parrikar, Nicholas Heeder, Michael Pinto, Anil Rajesh Kumar C, Kim McCarthy, and Emad Makki. I'd also like to acknowledge past DPML members: Nathanial Gardner, Jefferson T. Wright and Christopher O'Connell

for their support and encouragement as well as all the undergraduate students who have helped with manufacturing and experimentation. There have been many sleepless nights and difficult experiments which required, at times, 17 continuous hours to complete. Without everyone's collaboration and willingness to help, the lab will not have excelled to where it is today. In addition, I would also like to Joe Gomez, Dave Ferreira, Jim Byrnes, Rob D'Ambrosca and the rest of the mechanical engineering department faculty and staff.

The financial support provided by the Department of Homeland Security under Grant Number: 2008-ST-061-T20002-04 is greatly acknowledged.

Last but not least, I would like to thank my parents for being most tolerant of my long and bumpy academic path. Their support, patience and understanding throughout my studies is rivaled by none.

PREFACE

The present study investigated the behavior of corrugated sandwich structures filled with different materials under combined extremes of high temperature blast loading. The sandwich panels were comprised of AISI 1018/A36 steel face sheets with alternating layers of corrugated steel forming a lattice core. A syntactic foam was developed, using silicone and glass microspheres, and its properties were investigated. Sandwich panels were filled with syntactic foam and blast performance was compared with an empty panel as well as at elevated temperatures. The use of mortar as a filler material was also investigated at extreme temperatures. Real-time deformation images were captured using high speed photography to provide further insight into the core response and full field rear face deformations. This thesis is prepared using the manuscript format.

Chapter 1 presents the method for developing a silicone based syntactic foam by introducing two different types of glass bubbles, provided by 3M Company, at different weight percentages (henceforth wt%). The materials were characterized using a screw-driven universal testing machine. Samples were tested both as prepared and after heat treating at elevated temperatures. This chapter followed the formatting guidelines for and was published by *Acta Physica Polonica A*.

Chapter 2 investigates the blast response of corrugated sandwich panels when filled with syntactic foam. Two studies were performed: (1) a comparison of the blast performance between empty and filled panels and (2) experiments investigating the response of filled panels under three different temperature environments up to 500°C. A shock tube was utilized to load the specimen while three high speed cameras

obtained images later used in analysis. This chapter followed the formatting guidelines specified by the Journal of *Sandwich Structures and Materials*.

Chapter 3 investigates the blast response of corrugated sandwich panels when filled with mortar, a common building material comprised of cement and sand aggregate. Four series of experiments were performed each at different temperature environments up to 900°C. A shock tube was utilized to load the specimen while three high speed cameras obtained images later used in analysis. This chapter followed the formatting guidelines specified by the Journal of *Sandwich Structures and Materials*.

Chapter 4 provides a summary of the major experimental findings obtained during the development of a syntactic foam, the dynamic response of syntactic foam filled corrugated structures under high temperature shock loading, and the dynamic response of mortar filled corrugated structures under high temperature shock loading. This chapter concludes with suggestions for future work to compliment or enhance the studies contained within this thesis.

TABLE OF CONTENTS

LIST OF TABLES

CHAPTER 1

TABLE PAGE

CHAPTER 2

TABLE PAGE

CHAPTER 3

TABLE PAGE

LIST OF FIGURES

CHAPTER 1

FIGURE PAGE

CHAPTER 2

FIGURE PAGE

CHAPTER 3

FIGURE PAGE

CHAPTER 1

DEVELOPMENT OF A POLYMER BASED SYNTACTIC FOAM FOR HIGH TEMPERATURE APPLICATIONS

by

Murat Yazici, Payam Fahr , Arun Shukla, Ş. Güneş and S.K. Akay

Published in Acta Physica Polonica A

Corresponding Author: Murat Yazici

Uludag University

Engineering Faculty Automotive Engineering Deptartment

Tr16059 Görükle Kampüsü, Nilüfer, Bursa, Turkey

Phone: +90 (224) 294-2630

Email Address: myazici@uludag.edu.tr

Abstract

Syntactic foams are one of the most widely used close cell structured foams. They are used for industrial applications on account of their good acoustical attenuation, excellent strength to weight ratio, vibration isolation, and dielectric properties. These foams are fabricated by incorporation of hollow particles in a matrix material. In this study, silicone resin (with an operating temperature range between -53°C to 232°C) and two types of glass bubbles were selected as materials to develop a heat resistive syntactic foam. Both types of glass bubbles were incorporated into the silicone resin at three different mass percentages (10%, 20%, and 30%) reducing the density of the silicone by as much as 50%. The mechanical properties of the foam were investigated, in ambient temperatures, before and after high-temperature heat treatment (of 500°C), by quasi-static compression experiments. It was observed that plateau stress increases after introduction of glass bubbles in silicone, enhancing the energy absorption properties for both specimens with and without heat treatment. It can be concluded that syntactic foams with a silicone base matrix can be used for applications with heat resistance, low weight and high compression strength requirements.

1. Introduction

Many applications demand the use of light weight materials, but often at the cost of reduced strength. Foams can provide significant weight saving structures but their applications are limited by their low strength and modulus. In recent years considerable efforts have been invested in developing methods of introducing porosity

in materials without causing detrimental effects on the mechanical properties of material [1]. Syntactic foams are a class of porous materials in which manufactured by filling a polymeric matrix with hollow spheres called microspheres or micro balloons. Syntactic foams are sometimes described as three-phase composites, considering interstitial voids within the matrix to be the third phase [2, 3]. Compared with standard foams (containing blown gas bubbles only), syntactic foams are often preferred in weight-sensitive applications, for which their enhanced mechanical properties and tailorability make them useful [4, 5]. Several compositions of nano-scale reinforced syntactic foams are now developed for further enhancement in mechanical and thermal properties [6, 7]. As a class of advanced lightweight composites, syntactic foams have been widely employed in more and more engineering applications, e.g., marine equipment for deep sea operations [8], aircraft components, spacecraft solid rocket booster nose cone filling, thermal insulation for deep sea pipelines [9–11], core materials of sandwiches [12,13] and structural components in the aerospace industry [14]. While a wide body of literature is now available on room-temperature mechanical properties of syntactic foams, relatively few efforts are found focused on thermal properties such as coefficient of thermal expansion [15], thermal conductivity [4, 16] and high temperature behavior [17]. In spite of the abundant literature regarding various thermoplastic and thermo set resin based syntactic foams; few studies consider silicone rubber based syntactic foams [18, 19]. According to the authors' investigations, there is no current literature about silicone based high temperature resistive syntactic foams.

In this study, novel high temperature resistive polymer based syntactic foams were developed. Compression properties of the foams are compared with respect to glass bubble percentage variation in specimens with and without heat treatment.

2. Experimental Procedure

High temperature closed cell syntactic foam was produced by using platinum silicone resin and two different type glass bubble contributions at 10, 20, 30 wt%. A liquid silicone rubber resin (MoldStar® 30) was used as a matrix material, obtained by mixing two supplied components (A and B) which are mixed 1A:1B by volume. This easy to use platinum silicone features relatively low viscosities (According to ASTM D2393/12500 cps) and vacuum degassing is not required for most applications. The pot life is 45 minutes and cure time is 6 hours at room temperature. MoldStar30® has 30A Shore hardness. Tensile strength (ASTM D412) is 2.90 [MPa] and Elasticity Modulus is 0.66 [MPa]. Cured Mold Star® rubber is heat resistant up to 232 ºC [20]. Closed-cells structure was obtained after reinforcement with glass bubbles. Glass bubbles (Figure 1a) were obtained from 3M Company with the product codes: A16/500 and A20/1000. The properties of these bubbles are given in Table 1. The glass bubbles are thermally stable up to the 600°C, depending on the duration of exposure.

Table 1 - Properties of the glass bubbles [21]

	Test Pressure [MPA](PSI)	Density [g/cc]	Particle Size [µm]	Thermal Conductivity [W/m.K] at 20°C
A16/500	3.44 (500)	0.16	115	0.06-0.16
A20/1000	6.90 (1000)	0.20	105	0.06-0.16

A syntactic foam was produced by mixing silicone rubber and glass bubbles by hand. After mixing for 20 minutes, the raw material was filled in a wax mold and compressed by hand. The specimen was designed to be cylindrical with a diameter of 25 mm and a height of 17mm. High temperature heating of specimens was performed by applying a constant temperature of 500±10 °C to one side of the specimen for a duration of one hour. During this time, the specimen's opposite surface was left exposed to ambient temperatures. Temperatures were recorded on both surfaces using thermocouples.

Figure 1 Images of glass bubbles and specimens
a) Glass bubbles b) Virgin syntactic foam (30% GB1000)
c) Heat treated syntactic foam (30% GB1000) and temperature measurement points.

The density of the foam was obtained by weighing a specimen on a weight scale, with a sensitivity of 0.0001g, and calculating the volume based on the specimen geometry. Compression experiments were performed by using Instron Universal 5585 universal testing machine with a 1 mm/min cross head speed. Experiments were performed at room temperature for specimens with and without heat treatment. The microstructures were investigated by using an SEM microscope.

3. Results and Discussions

Syntactic foam densities decreased with the addition of glass bubbles in higher percentages. In syntactic foams containing 30% glass bubbles by weight, the density decreased 63% using A20/1000 glass bubbles (henceforth GB1000) and 68% using A16/500 glass bubbles (henceforth GB500). Room temperature quasi static experiments were performed on the syntactic foams to ascertain the glass bubbles' weight percentage effect on compression strength and energy absorbing capabilities. The selected glass bubbles have a low failure compression strength, they collapsed during the syntactic foams' compression. Because of this, the foams' stress v. strain plots show more plateau regions, suggesting greater energy absorbing properties. The variations of the quasi-static compression behavior are given in Figure 2 for both GB500 and GB1000 syntactic foams. It is observed that the virgin silicone rubber behaves as a viscoelastic material and that the introduction of glass bubbles increases the plateau stress of the material. Figures 2a and 2b show the results of compression tests between the two syntactic foams, GB500 and GB1000, with the different wt% of glass bubbles with their respective crush strengths as : 3.44 [MPa] for A16/500 and 6.90 [MPa] for A20/1000.

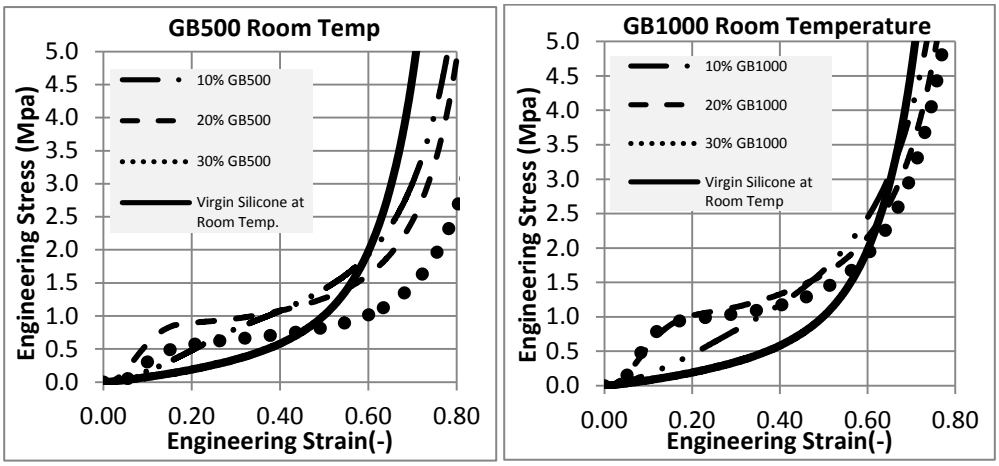

Figure 2 Plots of stress-strain variation from quasi-static compression of the developed syntactic foams a) GB500 syntactic foam b) GB1000 syntactic foam

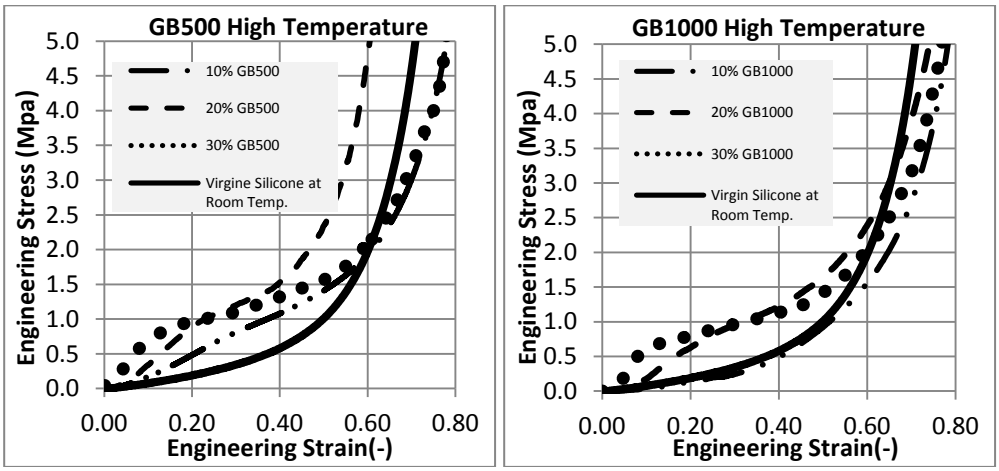

Figure 3 Plots of stress-strain variation from quasi-static compression of the developed syntactic foams after high-temperature heat treatment a) GB500 syntactic foam b) GB1000 syntactic foam

Table 2 - Density of the syntactic foams.

	wt% of Glass bubbles	**Density [kg/m^3]**
GB500	10%	739.78
	20%	472.25
	30%	360.38
GB1000	10%	747.95
	20%	539.57
	30%	409.61
Silicone Rubber Resin	-	1120

The specimens that were heat treated (at constant temperature of 500 ºC) were originally light blue in color. The color, originating from the heated surface, started to change white and after about 20 minutes, stabilized at less than 1/3 of the specimens section height (see Figure 1b). During heating, the face exposed to ambient temperature was measured, and a steady state surface temperature of 130 °C was obtained. When heated to 500 ºC, the glass bubbles remain intact within the syntactic foam (Figure 4a). Because of maximum temperature sensitivity of the glass bubble is around 600 ºC, any heating beyond this temperature, the glass bubbles would rupture (Figure 4b). For the purpose of this study, heating was limited to 500 °C. The white section is more brittle and heat resistive than the virgin syntactic foam. After heating, the foam developed into a two layered foam structure. The front layer (heat treated surface) is brittle and heat resistive (Figure 1c), while the back layer exhibits more elastic and plastic properties similar to the unheated syntactic foams (Figure 1b). In

Figure 3, the results from quasi-static compression of high-temperature heat treated specimens are given. It was observed that plateau stress and plateau region sizes depend on the wt% of glass bubbles.

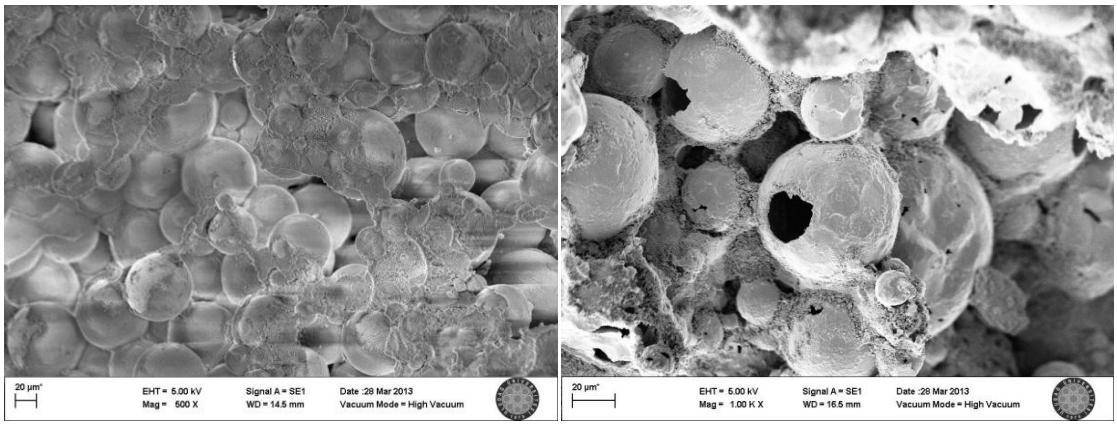

Figure 4 SEM microscopy of syntactic foam
a) 500 °C Heat treated 30% GB1000 syntactic foam 500X SEM picture
b) 750 °C Heat treated 30% GB 1000 syntactic foam 1000X SEM picture

Figures 2 and 3 show that heating the specimens, from one face, does not affect the compression properties considerably of the developed syntactic foam.

4. Conclusions

In this study, high temperature resistive silicone based syntactic foams were developed. The effect of post high temperature heating on material properties were investigated using quasi-static compression tests. Results obtained can be summarized as follows:

1) A High temperature resistive layer forms when the silicone syntactic foam is subjected to heating on one surface, 2) Foam is transformed to a two layer structure during high temperature heating (brittle and soft layers), 3) The foam shows very good

heat resistivity with the brittle layer working as a heat barrier, 4) Compression strength properties were not affected after heating processes, 5) The insulative properties of silicone rubber improved with higher weight percentages of glass bubbles, 6) The introduction of glass bubbles lowers the density of silicone rubber, 7) During compression tests, the Plateau (crush) regions increased by introducing higher amounts of glass bubbles improving energy absorption properties.

Acknowledgement

The authors acknowledge the financial support provided by 3M Ind. & Transp. Business En. & Adv. Mat. Div. Murat YAZICI acknowledges the financial support of the TUBITAK 2219 Int. Post Doc. Research Fellowship Program.

References

[1] N. Gupta, V.C. Shunmugasamy, *Mater Sci and Eng A.* **528**, 7596 (2011). DOI: 10.1016/j.msea.2011.06.073

[2] V. Shabde, K. Hoo, G. Gladysz, *J Mater Sci.* **41**, 4061 (2006). DOI: 10.1007/s10853-006-7637-x

[3] G. Gladysz, B. Perry, G. McEachen, J. Lula, *J Mater Sci.* **41**, 4085 (2006). DOI: 10.1007/s10853-006-7646-9

[4] N. Gupta, E. Woldesenbet, P. Mensah, *A. Compos Appl Sci Manuf.* **35**,103 (2004). DOI:10.1016/j.compositesa.2003.08.001

[5] N. Gupta, K. Kishore, E. Woldesenbet, S. Sankaran, *J Mater Sci.* **36**, 4485 (2001). DOI:10.1023/a:1017986820603

[6] R. Poveda, S. Achar, N. Gupta, *JOM J Miner Met Mater Soc.* **64**, 1148 (2012). DOI:10.1007/s11837-012-0402-5

[7] M. Dimchev, R. Caeti, N. Gupta, *Mater Des.* **31**, 1332 (2010). DOI:10.1016/j.matdes.2009.09.007

[8] V.T. Phan, D. Choqueuse, J. Y. Cognard, L. Sohier, *Prog Org Coat.* **76**, 341(2013). DOI: 10.1016/j.porgcoat.2012.09.028

[9] C.I. Stuckey, T. R. Reinarts, D. Davis, *AIP Conf. Proc.* **552**, 2 98 (2001). DOI: 10.1063/1.1357938

[10] F. Grosjean, N. Bouchonneau, D. Choqueuse,V. Sauvant-Moynot, *J Mater Sci.* **44**, 1462 (2009). DOI:10.1007/s10853-008-3166-0

[11] N. Bouchonneau, V.Sauvant-Moynot, D.Choqueuse, F.Grosjean, E.Poncet, D. Perreux, *J Petrol Sci Eng.* **73**,1 (2010). DOI:10.1016/ j.petrol.2010.03.023

[12] A. Corigliano, E. Rizzi, E. Papa, *Compos Sci Technol.* **60**, 2169 (2000). DOI: 10.1016/S0266-3538(00)00118-4

[13] L. Bardella, F. Genna, *Int J Solids Struct* **38**, 307 (2001). DOI: 10.1016/S0020-7683(00)00025-1

[14] E. S. Weiser, T. F. Johnson, T. L. S. Clair, Y. Echigo, H. Kaneshiro, *High Perform Polym.* **12**,1 (2000). DOI: 10.1088/0954-0083/12/1/301

[15]. V. Shunmugasamy, D. Pinisetty, N. Gupta, *J Mater Sci.* **47**, 5596 (2012). DOI:10.1007/s10853-012-6452-9

[16] M. Porfiri, N. Nguyen, N. Gupta, *J Mater Sci.* **44**, 1540 (2009). DOI:10.1007/s10853-008-3040-0

[17] T. Lin, N. Gupta, A. Talalayev, *J Mater Sci.* **44**, 1520 (2009). DOI:10.1007/s10853-008-3074-3

[18] T. Muthukumar, A. Aravinthan, K. Lakshmi, R. Enkatesan, L. Vedaprakash, M. Doble, *Int. Biodeterior Biodegrad.* **65** ,2 76 (2011). DOI: 10.1016/j.ibiod.2010.11.012

[19] M. Kessler and A. Schnettler. *IEEE Trans. Dielectr Electr Insul.***17**, 898 (2010). DOI:10.1109/TDEI.2010.5492264

[20] http://www.smooth-on.com/Silicone-Rubber-an/c2/index.html

[21] www.3M.com/oilandgas

CHAPTER 2

DYNAMIC RESPONSE OF FILLED CORRUGATED STRUCTURES UNDER COMBINED EXTREME ENVIRONMENTS

by

Payam Fahr, Murat Yazici, Arun Shukla

Prepared for submission to Journal of Sandwich Structures and Materials

Corresponding Author: Arun Shukla

Dynamic Photomechanics Laboratory

Department of Mechanical, Industrial and Systems Engineering

University of Rhode Island

206 Wales Hall, 92 Upper College Rd

Kingston, RI, 02881, USA

Phone: +1-401-874-2283

Email Address: shuklaa@egr.uri.edu

Abstract

Shock tube experiments were performed to investigate the blast response of corrugated steel sandwich panels filled with a silicone based syntactic foam filler at room and high temperature. The syntactic foam filler was prepared by mixing a two-part silicone with glass microspheres and its microstructure and mechanical properties were characterized. A shock tube apparatus, capable of testing materials at temperatures up to 900°C, was used to generate the shock loading. High speed photo-optical methods utilizing Digital Image Correlation (DIC) coupled with optical band-pass filters, and a high-intensity light source, were utilized to obtain the real-time deformation at high temperature while a third camera captured side-view deformation images. The shock pressure profiles and DIC analysis were used to obtain the impulse imparted to the specimen, transient deflection, in plane strain and out-of-plane velocity of the back face sheet. It was observed that using the syntactic foam as a filler material, decreased the front face and back face deflections by 42% and 27%, respectively, compared to an empty panel. At high temperatures the silicone based syntactic foam decomposes into silica, a stable and non-hazardous byproduct. The highest impulse was imparted on the specimen at room temperature and subsequently lower impulses with increasing temperature. Due to increasing ductility in steel with high temperature, the specimens demonstrated an increase in back face deflection, in-plane strain and out-of-plane velocity with increasing temperatures with weld failure being the primary form of core damage.

1. Introduction

In this study, the response of corrugated steel sandwich structures were evaluated during high temperature shock loading using measurements taken by high speed optical methods. Blast loading is simulated using a shock tube apparatus outfitted with heating nozzles to provide uniform specimen heating during experimentation. A syntactic foam was developed to fill the corrugated structures using silicone and 3M Glass Bubbles. The demands for tailorable multifunctional structures are ever increasing in industries ranging from defense, automotive, aerospace and naval. Sandwich panels offer many benefits over their monolithic counterparts for mitigating blast energy and have the potential to act as thermal insulators. Extensive studies have been conducted on various core configurations from closed cell, lattice corrugation, pyramidal truss, honeycomb and composite functional graded structures[1-12]. Xue and Hutchinson established the benefits of sandwich panels over monolithic plates due to compressibility of the core allowing longitudinal shear and axial stiffness. Core response was divided into three parts: fluid structure interaction, core compression, and beam bending [13]. Core response can be characterized as stiff or soft depending on the mid-span velocity versus time curve of the front and rear of the panel [3]. The back face of a stiff core will respond almost immediately after shock impingement of the front face, whereas a soft core response will exhibit a delay during fluid structure and core compression stages of panel response. Filled core configurations have been investigated using a variety of filler materials including PVC, styrene and metallic foams [5, 14, 15]. Langdon et al explored the different failure mechanisms associated with varied core densities, showing that a

stiffer core resists damage better than soft cores at higher impulse. Wang et al found that functionally grading a core from soft to stiff reduced dynamic pressures felt on the back face, limiting the damage imparted on the panels. Novel materials, such as syntactic foams, show improved energy absorption and may even be used in some high temperature applications [16-19]. Syntactic foams are comprised of particles, used to enhance or modify material properties, that are suspended in a matrix material ranging from rubber or elastomer, ceramics and even metal. A recent study, by Abotula et al, investigated the response of monolithic metallic plates subjected to shock loads at high temperatures, but no studies have been performed on filled sandwich panels with this combined extreme environment [20]. The syntactic foam filled panels exhibit a stiff core response and superior blast mitigation compared to unfilled panels. The use of syntactic foam also creates a good thermal barrier for temperatures up to 500°C.

2. Materials and Specimen

Syntactic foam filler

High temperature closed cell syntactic foam was produced in house using platinum silicone resin and A20/1000 Glass Bubbles supplied by 3M Company. A liquid silicone rubber resin (MoldStar® 30), used as a matrix material, was obtained by mixing two supplied components (A and B) which are mixed 1A:1B by volume. This easy to use platinum silicone features relatively low viscosities (According to ASTM D2393/12500 cps), and vacuum degassing is not required for most applications. The pot life of this particular silicone is 45 minutes and cure time is about 6 hours at room temperature. By introducing the glass bubbles to ensure proper

curing, the specimens were given a minimum of 6 days before experiments were performed. MoldStar30® has 30A Shore hardness. Tensile strength (ASTM D412) is 2.90 MPa and modulus is 0.66 MPa. Cured Mold Star® rubber is heat resistant up to 232 ºC. When glass microspheres are added to a silicone matrix, the material's density is lowered and due to sacrificial collapse, quasi-static compression tests show energy absorbent foam-like material behavior. Closed cells were obtained after adding glass bubbles, at 30% by weight, obtained from 3M Company with the product code: A20/1000. To investigate the effects of extreme temperatures on the microstructure of syntactic foam, SEM microscopy was used. At high temperature, the silicone begins to decompose into silica, however, Figure 1(a) shows the glass bubbles remain intact after being heated to a temperature of 500°C. Figure 1(b) depicts syntactic foam that was heated to 750°C at which point, the glass bubbles rupture. This verifies the manufacturers specifications stating material properties may change at temperatures above 600°C.

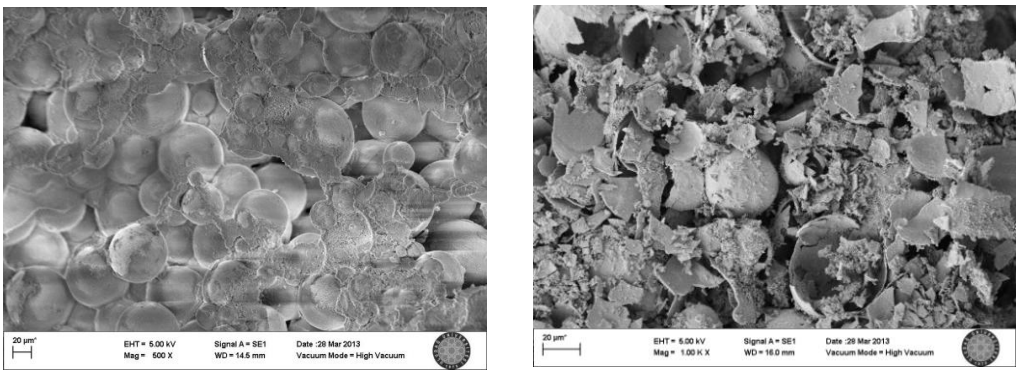

(a) **(b)**

Figure 1 - SEM images of syntactic foam

Compression tests of silicone containing 30 wt% of Glass Bubbles were performed using an Instron 5585 material testing system. Samples were tested before and after heat treatment to 500°C. The results of compression tests, seen in Figure 2, show that the syntactic foam experiences plastic yielding around 1MPa. A crush plateau is observed between a strain of 0.1 and 0.5, after which the specimen steadily enters the densification regime reaching a final densification strain of 0.7. The post-heated specimen observes a lower yield stress but behaves similarly to the room temperature sample.

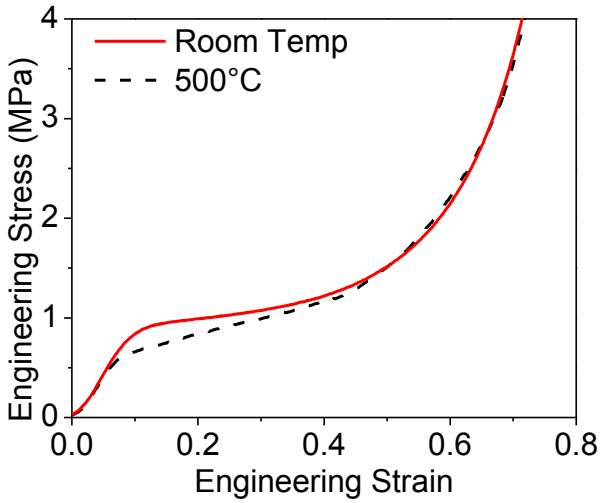

Figure 2- Stress-strain curves of syntactic foam before and after heating to 500°C

1018 Steel

Steel was used to construct the sandwich panels as it is a common building material that can be recycled with desirable material properties in both strength and temperature resistance. The decrease in yield stress due to thermal effects can be represented by the Johnson-Cook constitutive model, Equation 1[21]. The Johnson-Cook

parameters of 1018 steel, seen in Table 1, were used to calculate the stress strain behavior of steel at room and elevated temperature [22]. Temperature, T, was varied between experimental temperatures of 25 ºC, 330 ºC and 500 ºC. A plot of the calculated stress-strain behavior for 1018 Steel at various experimental temperatures can be seen in Figure 3. Due to the effects of thermal softening, the yield stress decreases as temperatures increase, thus it was predicted that plastic deformation of the face sheets will increase at elevated temperature given the same applied load.

$$\sigma = (\sigma_o + B\varepsilon^n)(1 + C \ln \frac{\dot{\varepsilon}}{\dot{\varepsilon}_o})(1 - T_*^p) \tag{1}$$

where,

$$T_* = \frac{T - T_r}{T_m - T_r} \tag{2}$$

Table 1. Johnson-Cook parameters of Cold Rolled 1018 Steel

σ_o (MPa)	B (MPa)	n	C	$\dot{\varepsilon}$ (s^{-1})	$\dot{\varepsilon_0}$ (s^{-1})	p	T_m (K)
560	300	0.32	7.6×10^{-3}	10	5×10^{-6}	0.55	1773

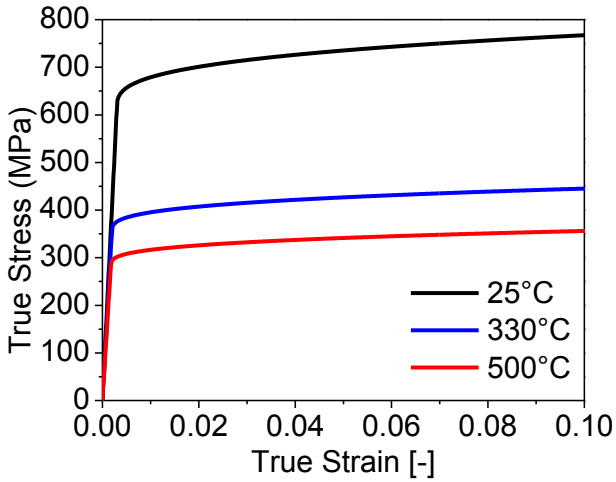

Figure 3 - Calculated stress-strain behavior of 1018 steel at different temperatures

Sandwich panel

Each specimen is composed of two 1018 steel face sheets with the dimensions: 203.2 mm length, 50.8 mm width, and 1.6 mm thickness. The core is constructed by using four layers of corrugated G90 galvanized steel strips, with a 29 gauge thickness, stacked back to back. A form was created from aluminum matching the pitch and length of the sinusoidal-shaped features of the corrugated sheets. The sheets were then clamped between the mold which was fastened to an X-Y table of a Bridgeport milling machine. An abrasive wheel was used to reduce sheet deformation by providing constant contact during the cutting process. The corrugated material was cut to a width of 50.8 mm, the same as the face sheets. The sandwich panel was assembled by welding the outer nodes of alternating corrugated layers, forming the core, and then by spot welding the monolithic face sheets. Table 2 lists the specifications of an empty sandwich panel, seen in Figure 4. The filler material was extruded through the

sandwich panel and then a speckle pattern was applied for DIC, seen in Figure 5. The mass of a filled corrugated sandwich panel is 480 grams.

Table 2. Specifications of empty corrugated sandwich panel

Parameter	Length (mm)	Width (mm)	Height (mm)	Mass (g)	Areal Density ($kg \cdot m^{-2}$)
Value	203.2	50.8	27.4	377.7	36.6

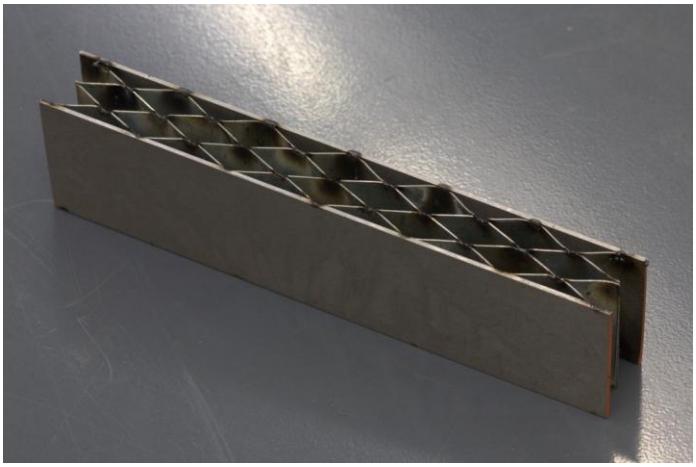

Figure 4 - Corrugated Sandwich Panel

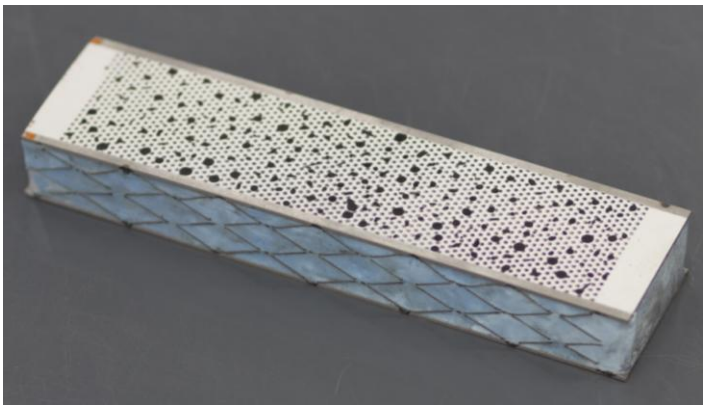

Figure 5 - Filled Corrugated Sandwich Panel prepared for DIC

3. Experimental Procedures

Shock tube

A shock tube apparatus, as seen in Figure 6(a), was utilized to simulate a blast in a controlled environment. With a length of 8 m, the shock tube consists of a driver and driven section. The high-pressure driver section and the low pressure driven section are separated by a Mylar diaphragm. The driver section is then pressurized using helium and pressure difference across the diaphragm is created. Once this pressure difference reaches a critical value, the diaphragm ruptures resulting in a rapid release of gas creating a shock wave, which travels down the tube to a convergence section, impart dynamic loading on the specimen in the form of a planar wave front. The muzzle diameter at the specimen end is 38.1 mm. Two pressure transducers (PCB102A) are mounted at the end of the muzzle section, to measure the incident and reflected pressure profiles during the experiment which are recorded using an oscilloscope. A schematic of the muzzle dimensions and sensor locations can be seen in Figure 6(b). The specimen was placed in the supports and positioned 3 mm away from the end of the muzzle. The support fixtures ensured simply supported boundary conditions with a span of 152.4 mm. To reduce the effects of friction during deformation, the sandwich panels are positioned over a block, where contact is only on the edge of the back face. The sandwich panel is then secured to the simple support using Nickel-Chrome wire, with a diameter of 0.05 mm, which easily breaks during shock loading and deformation.

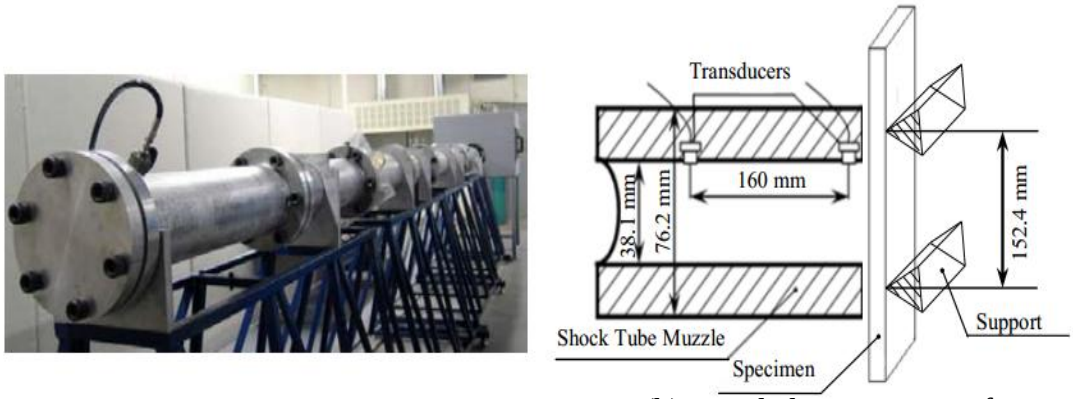

(a) Shock Tube (b) Detailed Dimensions of

Figure 6 - Shock Tube and Muzzle Detail

In the first part of this study, both empty and filled sandwich panels are compared at room temperature. A single diaphragm of Mylar with a thickness of 0.127 mm was selected to generate a shock wave loading that impinged on the specimen with an average incident peak pressure of approximately 0.35 MPa, a reflected peak pressure of approximately 1.32 MPa, an incident shock wave speed of 741 ms^{-1} and a reflected shock wave speed of 203 ms^{-1}. The shock wave generated had a short rise time (~70 μs) and showed an exponential decay period of approximately 6ms. The final part of this study investigated the response of filled sandwich panels under three different temperature conditions: ambient temperature, 330°C and 500°C. A single diaphragm of Mylar with a thickness of 0.254mm (10 mil) was chosen to generate shock wave loading with an incident peak pressure of approximately 0.44 MPa, a reflected peak pressure of approximately 1.77 MPa, an incident shock wave speed of 820 ms^{-1} and a reflected shock wave speed of 265 ms^{-1}. The rise time and decay period were approximately the same as with the 5mil diaphragm, approximately 6 ms. Figure 7 shows a typical pressure profile obtained from the sensor closest to the specimen at room temperature.

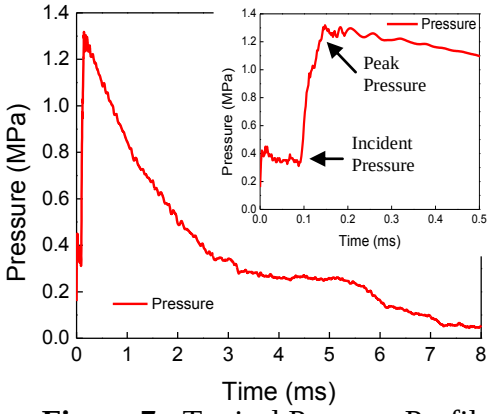

Figure 7 - Typical Pressure Profile

High temperature shock tube setup

The shock tube was modified to heat the back face of the specimen before shock impingement. Four propane nozzles were directed at the rear of the specimen and calibrated to give an even temperature distribution across the surface. A 1018 steel monolithic plate was used representing the rear face sheet of the sandwich panel, therefore having dimensions of 203.2 mm length, 50.8 mm width, and 1.6 mm thickness. Three thermocouples were positioned on the specimen along the vertical axis at the center and ~38mm above and below the center and were affixed to the monolithic plate using resistive spot welding. Figure 8 shows the heating setup with the nozzles directed at the specimen. After adjusting the nozzle orientations and flow rate, the temperature was recorded during calibration. A typical plot of the temperature distribution obtained on the back face on the points of the vertical axis is shown in Figure 9. After obtaining even heating on the back face, a filled specimen was used to then record the temperature on the front face (loaded area) to study the transient thermal response of the panels.

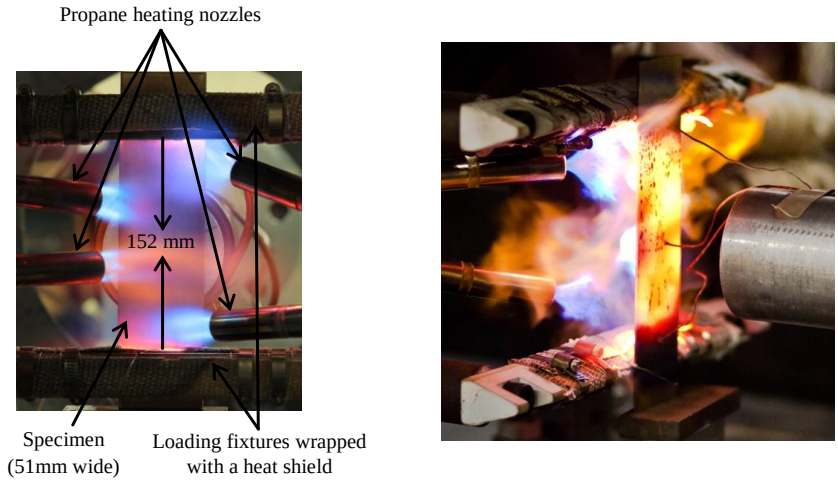

Figure 8 - Heated Shock Tube Setup and Heating Calibration

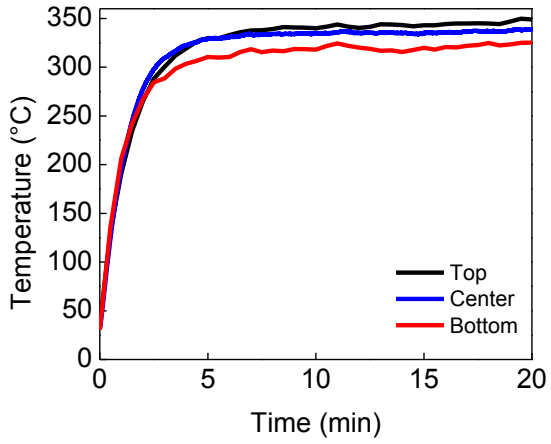

Figure 9 - Typical Recording of Temperature Calibration

High speed photography system

A high speed digital photography system was utilized to capture deformation images at high frame rates during shock loading. The experimental setup, shown in Figure 10, consisted of a back-view 3D Digital Image Correlation (DIC) system with two synchronized Photron SA1 cameras facing the back side of the specimen to capture full field deflection and strain information. The DIC cameras used in these

studies operated at 50,000 frames per second at a resolution of 192x400 pixels for a one second time duration. Subset size of 8.4 mm was selected for performing DIC analysis and the displacement resolution ± 0.02 mm. Another Photron SA1 Camera, positioned perpendicular to the shock tube and specimen, was utilized to capture deflection information and core response during shock loading. Though all cameras were triggered simultaneously, the side view camera was independently controlled, and was operated at 18,000 frames per second with a resolution of 384x752. Results obtained from MATLAB analysis of side view images are subject to an accuracy of ± 0.27 mm.

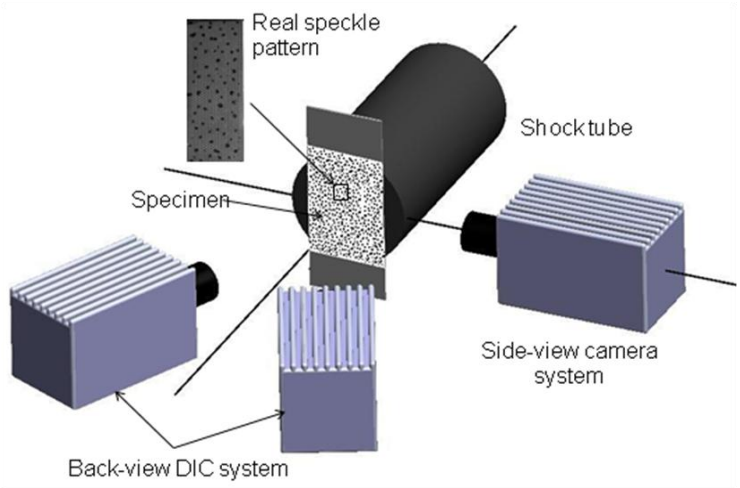

Figure 10 - DIC setup with side view camera

High temperature DIC system under shock loading

Heating a specimen to high temperatures poses difficult challenges when it comes to using optical methods to capture specimen deformation. To eliminate the influence of thermal radiation on image quality during heating, a DIC setup developed by Abotula et al was used. A band-pass filter was used permitting the transmission of

light in the blue wavelengths between 410-490nm. To ensure sufficient contrast for high speed imaging, the need for a high intensity light source was realized. A Cordin, Model 659, high energy flash lamp was used which has a maximum capacity of 1100 Joules regardless of single flash duration. The lamp was set to illuminate the specimen for a duration of 8 ms, which gives a power of 137.5 kW. Figure 11(a) shows an image of a specimen exhibiting the effects of black body radiation as the surface is heated between the simple support fixture. Comparing this image to Figure 11(b), it is observed that the use of an optical band-pass filter helps eliminate contributions of lower frequency wavelengths, increasing contrast of the speckle pattern which is required for DIC optical analysis.

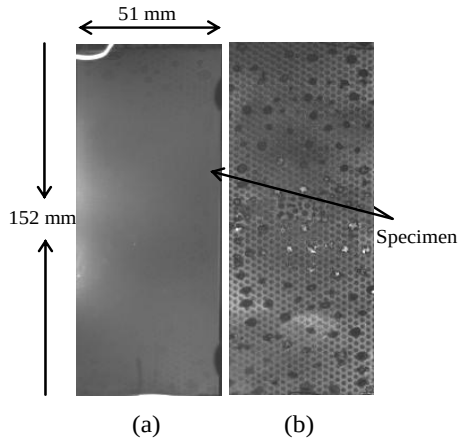

Figure 11 - Images of specimen without (a) and with (b) use of filter at high temperature

4.Results and Discussion

A comparison was made between empty and filled sandwich structures, conducted at room temperature, using a pressure of 1.25 MPa to evaluate the benefit of using syntactic foam as a filler material. Three experiments were performed for both the filled and unfilled cases. The full-field deformation history of the back face

was obtained by DIC and is displayed in Figure 12. Images for the empty and filled panels were analyzed using Vic-3d and are displayed under the same temporal resolution and fixed contour scale for comparative purposes. The back face of the empty specimen, displayed in Figure 12(a), shows the panel steadily deforming until reaching maximum around *t*=4 ms before rebounding. The filled panel exhibits a stiff response as it deflects less, and reaches its maximum nearly 1 ms sooner when compared to the empty sample.

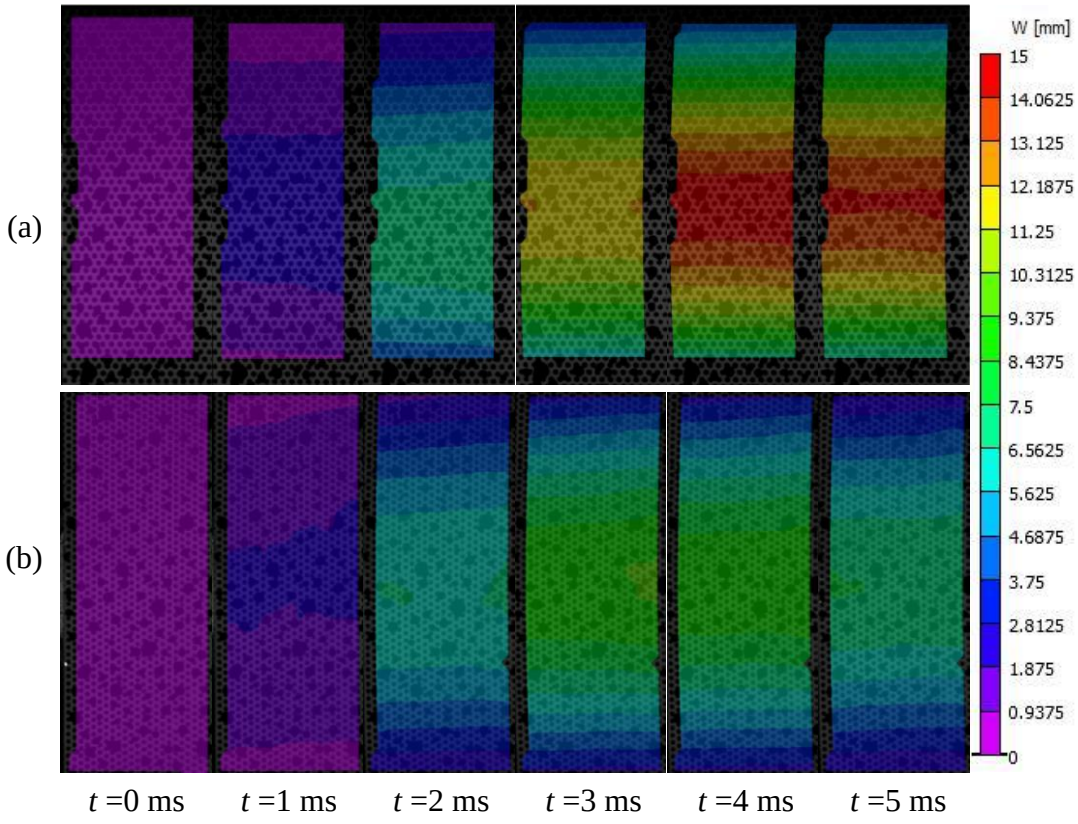

Figure 12 - Full-field deformation history of
(a) Empty sandwich panel
(b) Syntactic foam filled sandwich panel

To better understand core behavior, images from the side view camera were also analyzed. In the following images, the impinging shock propagated from the left side of each frame to the right side; both cases are compared within the same temporal

duration, starting from an undeformed state at time $t = 0$. The transient behavior of the empty corrugated sandwich panel can be seen in Figure 13(a). Fluid structure interaction and core compression phase of core response begins immediately from time of shock impingement. Elastic deformation of the corrugated layers can be seen throughout the core until about t=0.4 ms when the back face begins to deform. This shows an initial decoupled response of the core. The front face sheet deflects more than the back face and plastic deformation and buckling of the core can be observed near the load area. Core compression continued along the horizontal axis through the specimen width until it reaches its maximum, after about t=2.5 ms, at which point several welds failed due to shearing about the neutral axis. The corrugated core adjacent to the front face experiences compression while the opposing region stretches under tension as the back face continues to deflect. The filled panel, shown in Figure 13(b), shows minimal core compression due to the presence of the foam filler. A stiff core response is observed as it enters global bending by t=1ms and begin to shear along the neutral central axis at t=1.6 ms. By t=3 ms, maximum deflection is observed as well as separation of the filler from the corrugation is observed as well as nodal weld shearing between the core and front face sheet.

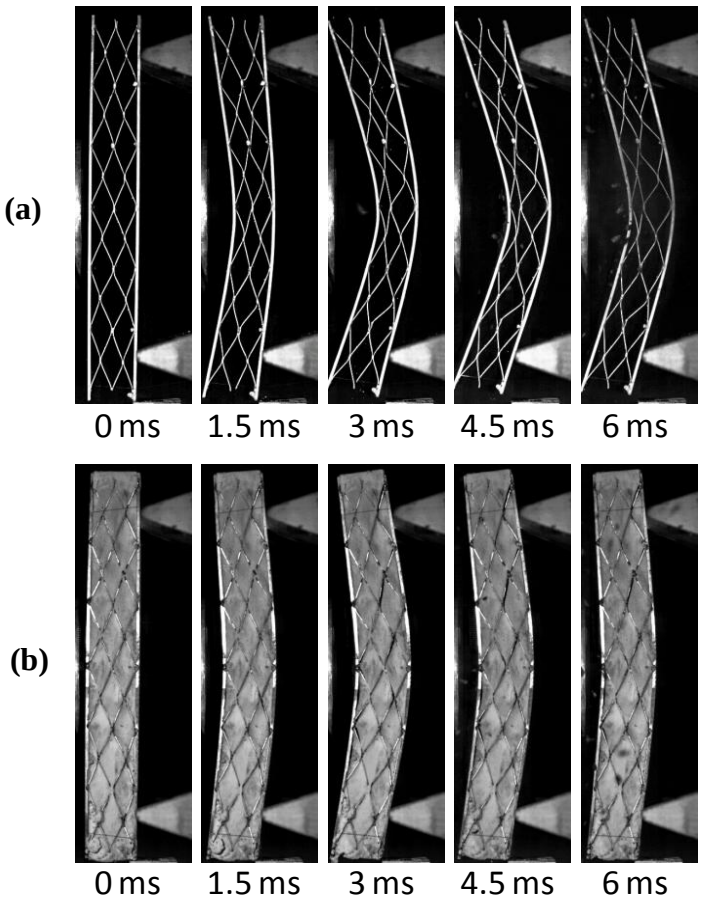

Figure 13 - Real-time deformation of empty and filled sandwich panels

The deflections of both front and back face sheets are plotted in Figure 14(a) and displays a decoupled panel response as the back face dwells briefly after the front face begins deforming . The empty sample exhibited maximum front face deflection of 16 mm by *t*= 4ms while the back only deflected 12.8 mm due to the compression of the core. The filled panel, seen in Figure 14 (b) experienced a coupled core response as the delay between face sheets was very small, around 0.25 ms. The filled sample obtained maximum deflections of 9.4mm around *t*=3.4 ms. Using the syntactic foam as a filler material, decreased the front face and back face deflections by about 42% and 27%, respectively.

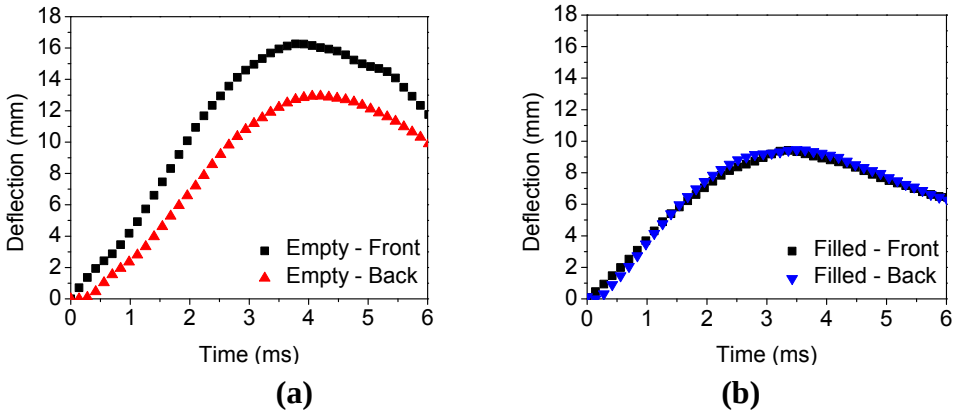

Figure 14 - Front and back face deflection for empty and filled sandwich panels

Core compression can be calculated taking the difference of front and back face deflections. Figure 15 shows the amount of core compression versus time for both the empty and filled specimens. It can be seen that the core of the empty specimen compresses about 5.5mm by t=2.5ms at which point the panel experiences bends globally then rebounds. Recalling the accuracy of side-view analysis, the core compression experienced by the filled panel is considered negligible.

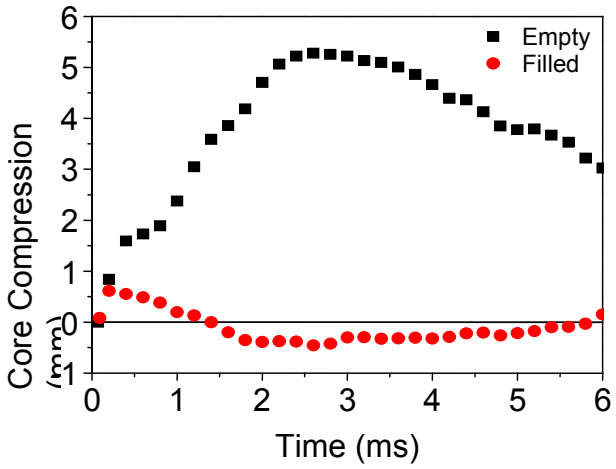

Figure 15- Core compression for empty and filled sandwich panels

One of the primary goals for creating an energy absorbent sandwich panel is to decrease panel deflections that may be impacted by a dynamic load while trying to keep a low areal density. The back face deflections of the filled panel, W_{filled}, can be scaled for comparative purposes using the mass of the empty panel as reference. The scaled values for back face deflection, W^*_{filled}, can be calculated using the expression shown in Equation 3. The scaled deflection has been plotted in Figure 16.

$$W^*_{filled} = \left(\frac{m_{filled}}{m_{empty}}\right) * W_{filled} \tag{3}$$

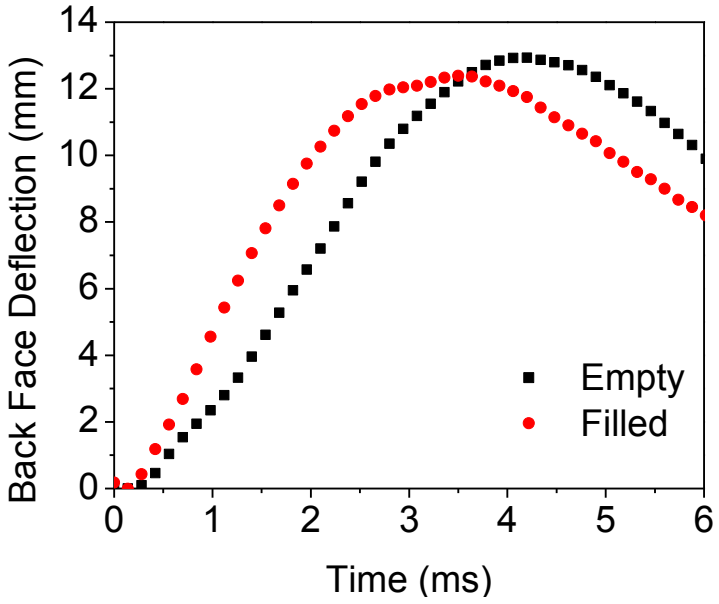

Figure 16 - Panel deflections after scaling with respect to mass

It can be seen that although the filler material adds more mass to the panel, there is still a 5% reduction in back face deflection even after scaling with respect to the mass of the empty panel. Due to its increased stiffness, the filled specimen reaches its peak back face deflection sooner than the empty corrugation with observable core damage being nodal weld shearing throughout the core and face sheet, followed by global bending. The empty specimen, however, experienced buckling and bending of independent core ligaments as well as shearing of nodal points within the core.

Permanent deformation of the corrugated steel sandwich panels was visually inspected and documented using a digital camera. In post-mortem, the empty specimen, shown in Figure 17(a), exhibits plastic deformation of 16.1mm for the front face sheet and 11.9 mm for the rear face sheet. The core permanently compressed by 8% of its original width in the center of the specimen. From high speed video playback, it was seen that welds at the interface between the core and rear face sheet failed under tension while the specimen rebounded. Permanent core deformation is visible, displaying compression near front face and extension near the back face.

Since the foam filler does not bond to metals, it is assumed that delamination contributes little to energy lost in the core compared to other composite materials or adhered structures. Due to the stiff response of the core, no localized buckling is observed and most of the damage is attributed to weld shearing both within the core as well as the nodes joining the corrugation to face sheets. Plastic deformation of the face sheets is present with negligible core compression. Permanent back face deflection of the filled panel, shown in Figure 17 (b), is 5.5mm.

(a)

(b)

Figure 17 - Post mortem images of empty and filled comparison

The use of a syntactic foam has proven to enhance blast response of sandwich panels, therefore, experiments were then conducted using a higher pressure of 1.77 MPa to investigate the effects high temperature has on the response of filled sandwich panels. Experiments were conducted using temperatures of 25˚C, 330˚C and 500˚C. Specimens, whose back face was heated to 330˚C and 500˚C, were held at temperature for 20 minutes before the application of shock loading to ensure a steady state temperature through the thickness of the specimen. A 3mm standoff between the specimen and the muzzle was used for each experiment to protect pressure transducers from excessive heating. The transient thermal response of the filled sandwich panels up to the point of shock impingement can be seen in Figure 18(a) and Figure 18(b) for experiments conducted with back face temperatures of 330˚C and 500˚C respectively.

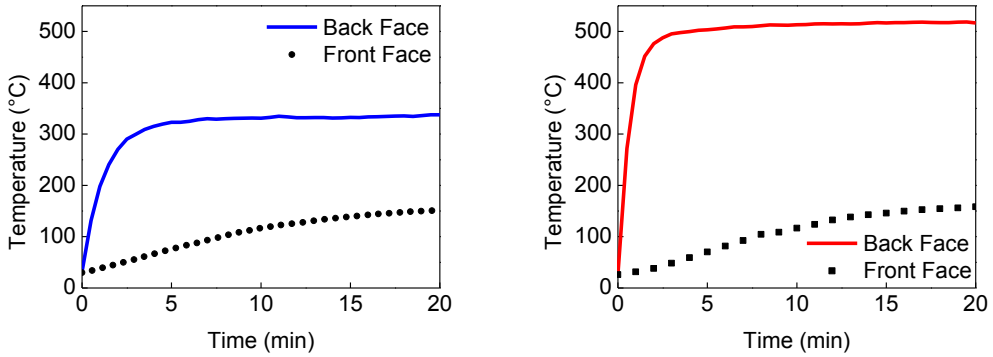

Figure 16 - Temperature response of syntactic foam filled sandwich panels

For the 330˚C case, steady state back face temperature is achieved after 7 minutes while the front face stabilizes to 150˚C after 20 minutes. For the 500˚C case, it only takes 4 minutes for the back face to reach steady state while the front face also reaches 150˚C after 20 minutes. The real-time observations of the transient behavior for syntactic foam filled sandwich structures at varying temperatures was taken using the side view camera. For all cases, the panels exhibited a coupled response with the back face sheet deforming soon after the front. Figure 19 shows the real-time observations from room temperature experiments. The panel showed signs of weld shearing by t= 0.6ms along the vertical central axis. At t=1.5ms, separation of the filler from the corrugation is observed as well as welds shearing on both the front and back face sheet. Maximum back face deflection occurs around t=3.64ms. No notable buckling was observed.

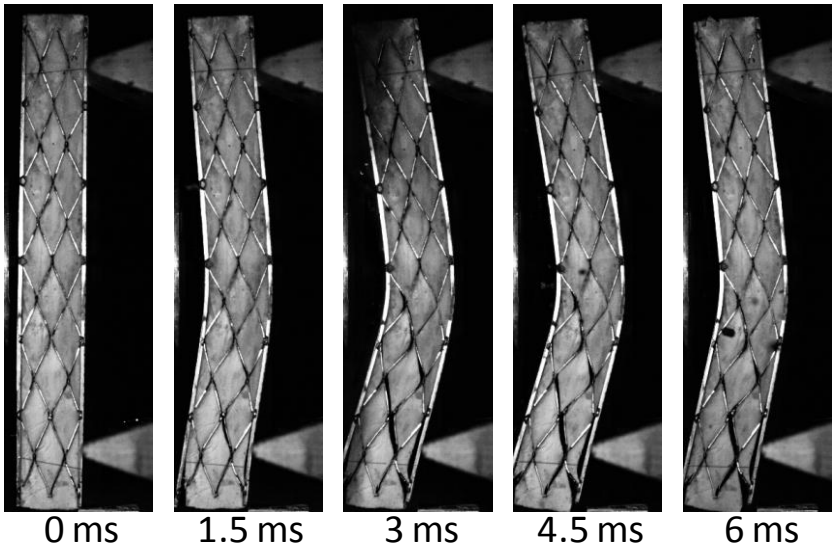

Figure 19 - Real - time deformation of samples at 25˚C

At 330˚C, the sandwich panel, shown in Figure 20, shows signs of bulging from the side of the specimen as the filler material is heated. First signs of weld shearing occurred at t=0.7ms along the vertical central axis. However, unlike the room temperature series, more weld failures are present throughout the core, resulting in more substantial filler material separation. Despite the additional failures within the core, the face sheets/core interface remained intact. Maximum back face deflection occurred around t=3.7ms then the specimen begins to rebound.

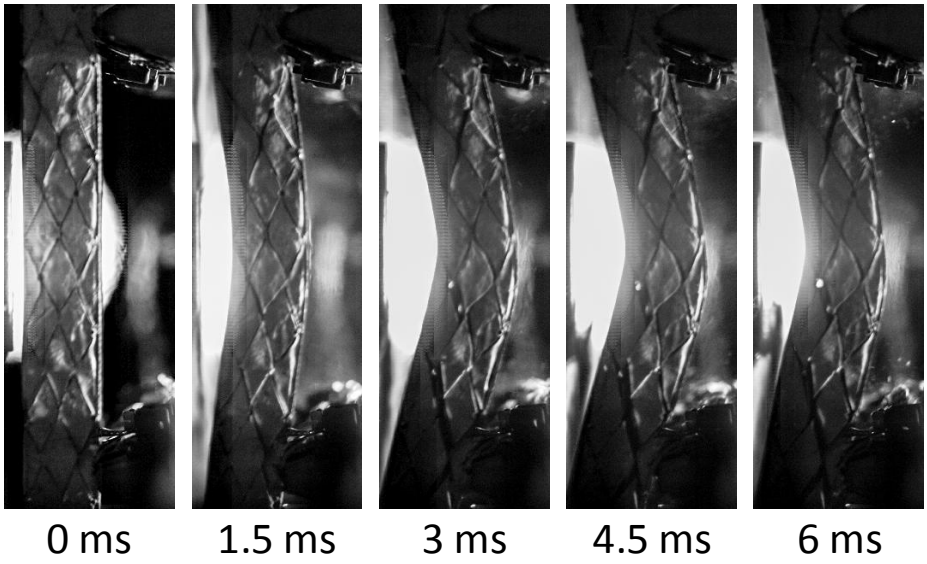

Figure 20- Real - time deformation of samples at 330˚C

The specimen heated to 500˚C, seen in Figure 21, also displays material swelling while being heated. Condensed water vapor is dispersed by the impinging shock, causing a brief obstruction in side view images due to its illumination by the flash, seen at t=1.5 ms. More material adjacent to the heated surface has decomposed at this temperature causing brittle fragments to be ejected as the specimen deforms. Maximum back face deflection occurs around 7ms and due to increased ductility, the specimen plastically deforms without rebound.

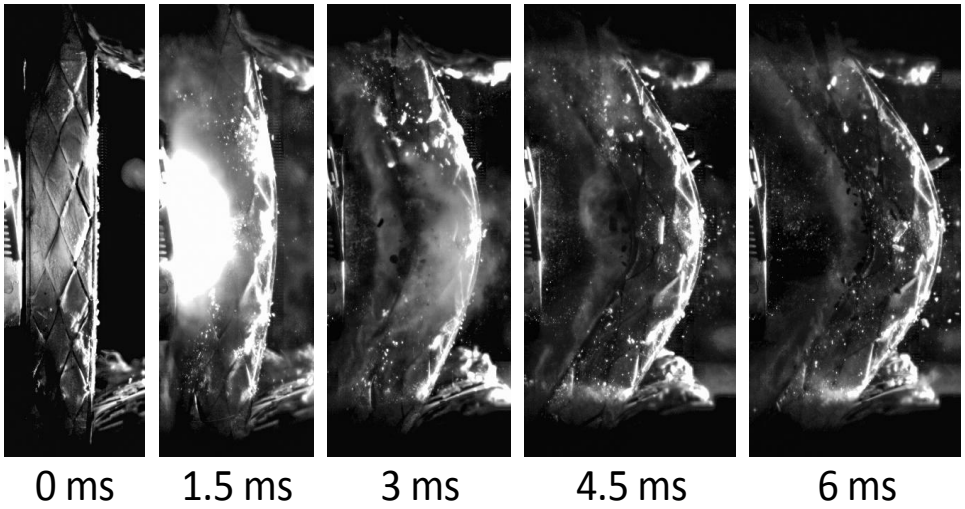

Figure 21 - Real - time deformation of samples at 500˚C

The pressure history for each experiment is given in Figure 22(a). Since pressures are measured from within the muzzle the profiles recorded are dependent on the specimen deflection. Pressures decay more rapidly with elevated temperatures due to an increase in ductility allowing specimens to deflect for longer durations of time with higher maximum deflections. Impulse imparted to the specimen, plotted in Figure 22(b), can be calculated by integrating the force-time data of the reflected pressure profile. It can be seen that all panels experience the same impulse until about t=1ms. The room temperature specimen obtained a maximum impulse of 3.4 Ns. When the temperature increased from room temperature to 500°C, the maximum impulse imparted decreased by approximately 15% (from 3.4 Ns to 2.9 Ns).

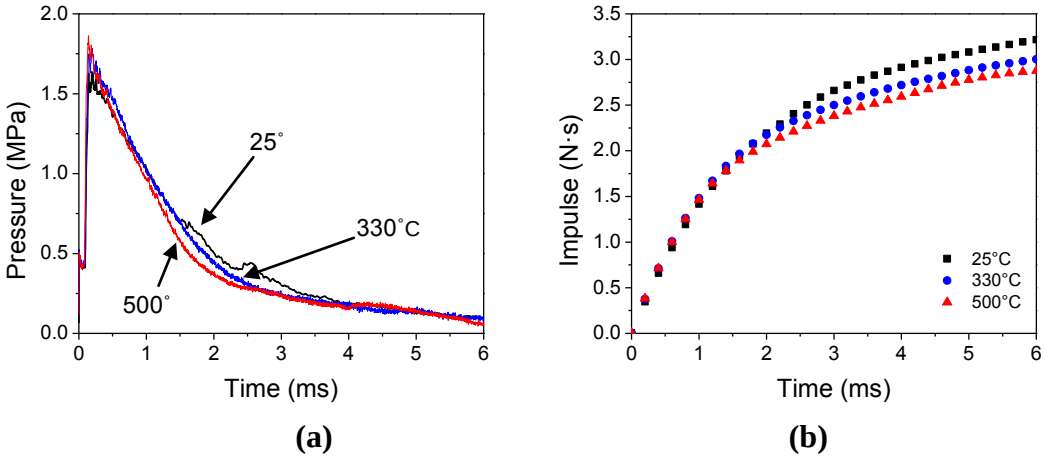

(a) **(b)**

Figure 22 - Pressure profile and impulse plots for temperature experiments

The mean mid-point deflection of the back face were obtained by DIC and plotted in Figure 23(a). For all experiments, the back face starts to deflect around 0.2ms after the shock impinges the front face of the panel. The maximum deflection for the room temperature experiments was 14.7mm, occurring at t=3.8ms. The experiments conducted at 330˚C, behave similarly to room temperature. Panel stiffness was not affected at this temperature as the material property of steel remained unaffected with such a small temperature gradient through the specimen thickness. Specimens heated to 330˚C and 500˚C showed maximum deflections of 15.4 mm and 37mm at 3.7ms and 8ms, respectively.

The average in-plane strain-rate observed in these experiments was 10 s^{-1}. Using the Johnson-Cook parameters listed in Table 2, the stress–strain curves of 1018 Steel were constructed for 25 °C, 330 °C, 500 °C temperatures at a strain-rate of 10 s^{-1}. From these stress–strain curves, it was determined that the flow stress at 330 °C had decreased by 42 % when compared to room temperature and as a result, the mid-

point back-face deflection had increased by 5 %. In comparison to room temperature, the value of flow stress at 500 °C decreased by 54%. Due to a significant decrease in flow stress values at these temperatures, the back-face deflections at 500 °C showed an increase of 152%. Calculating the stiffness as a function of temperature is more complex with sandwich structures compared to monolithic plates. While heating occurs on one face, there is a gradation of the elastic modulus of both the steel coupled with property changes in syntactic foam through the thickness of the specimen which changes the stiffness of the structure. As temperatures increase, the stiffness of the panel decreases towards the heated surface. At higher temperatures, however, the overall structural stiffness and strength of the welds are decreased, causing failure on both front and back face sheets, resulting in an increase in deflections. It is noted that though the 500˚C specimens exhibited extreme deflections, the samples never ejected from the simple supports.

The out-of-plane velocities are plotted in Figure 23(b) showing substantial increase for the 500˚C when compared to the room and 330˚C experiments. As steel becomes more ductile, the resistance to bending decreases, allowing the panel to deform at a higher rate. For the experiments conducted at 25˚C and 330˚C the max out of plane velocity occurred at 1 ms and were within 2% of each other at 7.32 m/s and 7.46 m/s, respectively. The specimens then reach a point of maximum deflection, and begin to rebound at t=4 ms. For the 500˚C case, the out-of-plane velocity reached 10.62 m/s, occurring around t=1.3 ms, 46% higher compared to room temperature, and then decreases until the end of the event.

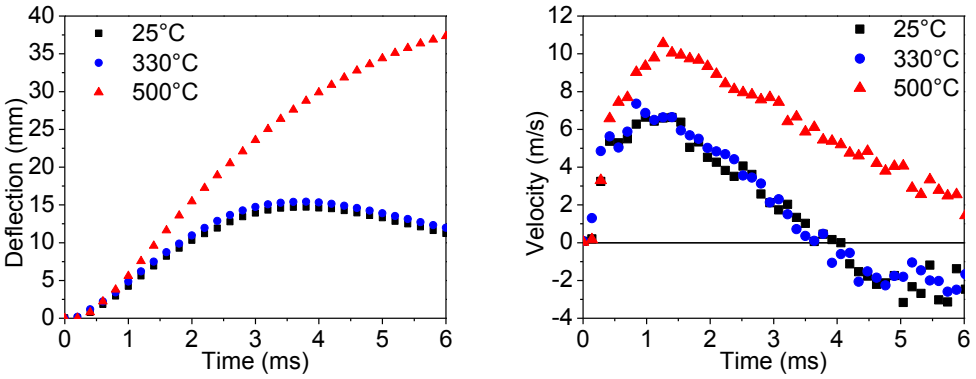

(a) **(b)**

Figure 23 - Out-of-plane deflection and velocity plots for temperature experiments

The in-plane-strain (ε_{yy}) information, displayed in Figure 24, exhibited an increasing trend as temperatures increased. After 0.2ms, the back face for all specimens showed significant bending, resulting in higher in-plane strains (ε_{yy}). At room temperature, the maximum in-plane strain of the specimens was around 0.39% at t=2.9 ms. For the 330˚C case, a maximum in-plane strain of 0.51% was observed at t=4.1 ms. For the 500˚C case, the in-plane strain reached 0.6% and continued to increase until the end of the event. In comparison to the room temperature experiments, the specimens at 330˚C and 500˚C showed an increase in ε_{yy} of 31% and 54%, respectively.

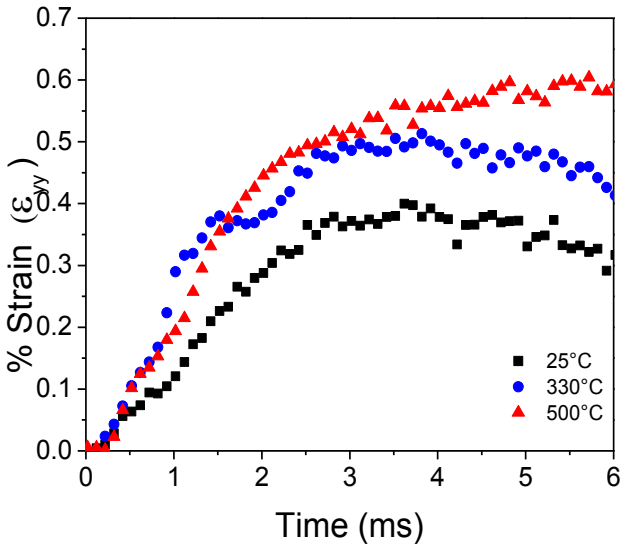

Figure 24 - In-plane strain (ε_{yy}) for temperature experiments

Permanent deformation of the corrugated steel sandwich panels was visually inspected and documented using a digital camera. In post-mortem, the samples from room temperature experiments, pictured in Figure 25, shows front face separation along with separation of filler material. Weld shearing is present, primarily along the central axis with filler material separating from the corrugated core. Permanent plastic deformation of the back face sheet is 8.5 mm.

Figure 25 - Post-mortem image of 25˚C specimen

Samples from 330˚C, seen in Figure 26, shows higher plastic deformation when compared to room temperature. Core failure due to weld breakage is more prominent. It was noted that the filler material showed a white discoloration 3 mm into the panel originating from the heated face. This white region is a result of the decomposition of silicone leaving silica, carbon dioxide and carbon monoxide as a byproduct of combustion. Permanent plastic deformation of the back face sheets is 12 mm.

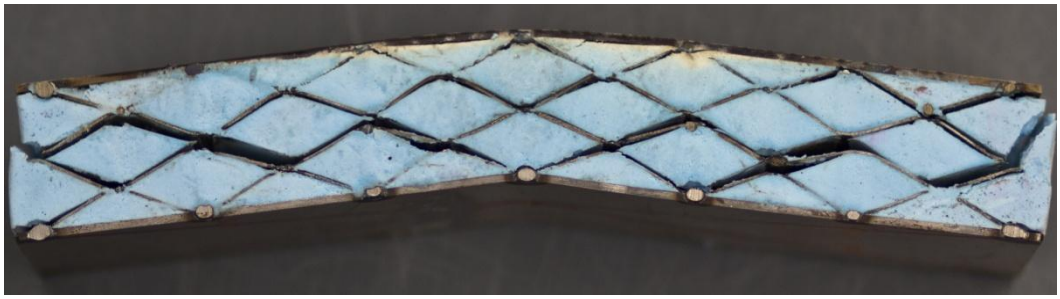

Figure 26- Post-mortem image of 330˚C specimen

The specimen heated to 500˚C, shown in Figure 27, also shows a decomposed layer of the filler material measuring at a depth of roughly 15mm into the panel originating from the heated face. The post mortem specimen shows significant core failure, major deflection and separation of both face sheets. The corrugated core appears to retain a majority of its filler material. Due to decreased stiffness as a result of weld breakage along the face sheets, inner core separation is present. Minor core buckling can be seen in the core near the load area due to the extreme panel deformation and front face sheet separation. Plastic deformation of the back face sheet is measured to be 41 mm.

Figure 27- Post-mortem image of 500˚C specimen

5. Conclusions

A series of experiments were conducted to investigate the shock resistance of corrugated sandwich panels with and without a syntactic foam filler as well as the response of syntactic foam filled panels to shock loading at room and high temperatures. The following is the summary of the results:

1. The syntactic foam filled corrugated panels show superior blast mitigation compared to unfilled panels. The presence of syntactic foam decreased back face deflections by 27% given the same applied pressure. The filled panels exhibit a stiffer core response in comparison to unfilled panels that demonstrate core compression and softer response

2. Syntactic foam maintains its structural integrity up to 500˚C as glass bubbles do not rupture. Though the yield stress is slightly lower at higher temperature, the material properties are not significantly affected.
3. When heated, the panels maintained a minimum temperature difference of 180˚C between the front and back face (25.4 mm). This gradient grew larger with increasing temperature. A temperature gradient of nearly 350˚C was observed for 500˚C experiments.
4. The maximum back face deflection of specimens at 500˚C was approximately 152% higher than those at room temperature.
5. The maximum in-plane-strain (ε_{yy}) showed an increase of 54% as temperatures increased from room temperature to 500˚C.
6. Due to decreased ductility of steel with increasing temperature, the integrity of the welds was weakened at 500˚C. Coupled with a gradation of elastic modulus through the panel thickness, the stiffness decreased toward the heated surface resulting in larger deformation.

Acknowledgements

The authors gratefully acknowledge the financial support provided by the Department of Homeland Security under Grant Number: 2008-ST-061-T20002-04. The authors also wish to express gratitude to 3M Company for the generous contribution of materials used in this study.

References

1. Ajdari A, Jahromi BH, Papadopoulos J, Nayeb-Hashemi H and Vaziri A. Hierarchical honeycombs with tailorable properties. *International Journal of Solids and Structures*. 2012; 49: 1413-9.
2. Dharmasena KP, Wadley HNG, Xue Z and Hutchinson JW. Mechanical response of metallic honeycomb sandwich panel structures to high-intensity dynamic loading. *International Journal of Impact Engineering*. 2008; 35: 1063-74.
3. Liang C-C, Yang M-F and Wu P-W. Optimum design of metallic corrugated core sandwich panels subjected to blast loads. *Ocean Engineering*. 2001; 28: 825-61.
4. Wadley HNG, Dharmasena KP, O'Masta MR and Wetzel JJ. Impact response of aluminum corrugated core sandwich panels. *International Journal of Impact Engineering*. 2013; 62: 114-28.
5. Wang E, Gardner N and Shukla A. The blast resistance of sandwich composites with stepwise graded cores. *International Journal of Solids and Structures*. 2009; 46: 3492-502.
6. Wright J, Hebert R and Shukla A. The Response of Graded Corrugated Steel Armor to Blast Loading. To Be Published.
7. Xiong J, Vaziri A, Ma L, Papadopoulos J and Wu L. Compression and impact testing of two-layer composite pyramidal-core sandwich panels. *Composite Structures*. 2011; 94: 793-801.
8. Yang Y, Fallah AS, Saunders M and Louca LA. On the dynamic response of sandwich panels with different core set-ups subject to global and local blast loads. *Engineering Structures*. 2011; 33: 2781-93.

9. Hassan MZ, Guan ZW, Cantwell WJ, Langdon GS and Nurick GN. The influence of core density on the blast resistance of foam-based sandwich structures. *International Journal of Impact Engineering*. 2012; 50: 9-16.
10. Rubino V, Deshpande VS and Fleck NA. The dynamic response of end-clamped sandwich beams with a Y-frame or corrugated core. *International Journal of Impact Engineering*. 2008; 35: 829-44.
11. Tekalur SA, Shukla A and Shivakumar K. Blast resistance of polyurea based layered composite materials. *Composite Structures*. 2008; 84: 271-81.
12. Ebrahimi H and Vaziri A. Metallic sandwich panels subjected to multiple intense shocks. *International Journal of Solids and Structures*. 50: 1164-76.
13. Xue Z and Hutchinson JW. A comparative study of impulse-resistant metal sandwich plates. *International Journal of Impact Engineering*. 2004; 30: 1283-305.
14 .Langdon GS, von Klemperer CJ, Rowland BK and Nurick GN. The response of sandwich structures with composite face sheets and polymer foam cores to air-blast loading: Preliminary experiments. *Engineering Structures*. 2012; 36: 104-12.
15. Liu H, Cao ZK, Yao GC, Luo HJ and Zu GY. Performance of aluminum foam-steel panel sandwich composites subjected to blast loading. *Materials & Design*. 2013; 47: 483-8.
16. Li G and Jones N. Development of rubberized syntactic foam. *Composites Part A: Applied Science and Manufacturing*. 2007; 38: 1483-92.

17. Yazici M, Fahr P, Shukla A, Günes S and Akay SK. Development of a Polymer Based Syntactic Foam for High Temperature Applications. *Acta Physica Polonica A***.** 2014; 125(2), 526-528

18. Song B, Chen W and Frew DJ. Dynamic Compressive Response and Failure Behavior of an Epoxy Syntactic Foam. *Journal of Composite Materials*. 2004; 38: 915-36.

19. Jhaver R and Tippur H. Characterization and modeling of compression behavior of syntactic foam-filled honeycombs. *Journal of Reinforced Plastics and Composites*.

20. Abotula S, Heeder N, Chona R and Shukla A. Dynamic Thermo-mechanical Response of Hastelloy X to Shock Wave Loading. *Experimental Mechanics*, 2013, 10.1007/s11340-013-9796-4.

21. Johnson G.R. and Cook W.H.. *Proc. 7th Int. Symp. on Ballistics*, The Hague, The Netherlands, 1983, 541–47.

22. Vural M, Ravichandran G and Rittel D. Large strain mechanical behavior of 1018 cold-rolled steel over a wide range of strain rates. *Metallurgical and Materials Transactions A*. 2003; 34: 2873-85.

CHAPTER 3

DYNAMIC RESPONSE OF MORTAR FILLED CORRUGATED STRUCTURES TO HIGH TEMPERATURE BLAST LOADING

by

Payam Fahr, Arun Shukla

Prepared for submission to Journal of Sandwich Structures and Materials

Corresponding Author: Arun Shukla

Dynamic Photomechanics Laboratory

Department of Mechanical, Industrial and Systems Engineering

University of Rhode Island

206 Wales Hall, 92 Upper College Rd

Kingston, RI, 02881, USA

Phone: +1-401-874-2283

Email Address: shuklaa@egr.uri.edu

Abstract

The dynamic behavior of mortar filled corrugated sandwich structures heated to temperatures up to 900°C was studied using a shock tube apparatus. High speed photo-optical methods utilizing Digital Image Correlation (DIC) coupled with optical band-pass filters, and high-intensity light source, were utilized to obtain the real-time deformation at high temperature while a third camera captured side-view deformation images. The shock pressure profiles and DIC analysis were used to obtain the impulse imparted to the specimen, transient deflection, in plane strain and out-of-plane velocity of the back face sheet. It was observed that cement based mortars are thermally resilient enough to be used as a filler material for high temperature applications. The highest impulse was imparted on the specimen at room temperature and subsequently lower impulses with increasing temperature. A temperature difference of at least 300ºC was observed across the thickness of the specimen for all heating conditions. Due to increasing ductility in steel with high temperature, the specimens demonstrated an increase in back face deflection, in-plane strain and out-of-plane velocity with increasing temperatures with weld failure being the primary form of core damage.

1. Introduction

The dynamic response of corrugated steel sandwich structures filled with mortar was investigated using shock tube apparatus and high speed optical methods. The shock tube apparatus outfitted with heating nozzles to provide uniform specimen heating during experimentation. Mortar is commonly found in building material comprised of cement and sand aggregate. It is able to withstand high temperatures and is cost effective compared to more exotic materials. Sandwich panels offer many benefits over their monolithic counterparts for mitigating blast energy and have the potential to act as moderate heat barriers. Extensive studies have been conducted on various core configurations from closed cell, lattice corrugation, pyramidal truss, honeycomb and composite functional graded structures [1–11]. Xue and Hutchinson established the benefits of sandwich panels over monolithic plates due to compressibility of the core allowing longitudinal shear and axial stiffness. Core response was divided into three parts: fluid structure interaction, core compression, and beam bending[12]. Core response can be characterized as stiff or soft depending on the mid-span velocity versus time curve of the front and rear of the panel[3]. The back face of a stiff core will respond almost immediately after shock impingement of the front face, whereas a soft core response will exhibit a delay during fluid structure and core compression stages of panel response. Filled core configurations have been investigated using a variety of filler materials including PVC, styrene and metallic foams, syntactic foams and cements [13–15]. Langdon et al explored the different failure mechanisms associated with varied core densities, showing that a stiffer core resists damage better than soft cores at higher impulse. A recent study, by Abotula et al,

investigated the response of monolithic metallic plates subjected to shock loads at high temperatures, and Sohel et al conducted static experiments using Steel-Concrete-Steel sandwich structures for marine and off-shore structures [13,16]. There have been very few studies investigating the blast response of heated sandwich panels to such extreme temperatures. The material response of concrete and mortars are of great interest in civil applications. There have been several studies investigating the effects of extreme temperature on the strength of concretes and mortars with different mixture formulations[18–25]. Results from these investigations show a decrease in compressive strength as temperatures increase with variations depending on material composition. Despite a decrease in strength, cements and mortars are resilient enough to withstand extreme temperatures, providing a cost effective option for a filler material while maintaining superior blast resistance in temperatures up to 900°C.

2. Materials and Specimen

1018 Steel

Steel was used to construct the sandwich panels as it is a common building material that can be recycled with desirable material properties in both strength and temperature resistance. The decrease in yield stress due to thermal effects can be represented by the Johnson-Cook constitutive model, Equation 1[26]. The Johnson-Cook parameters of 1018 steel, seen in Table 1, were used to calculate the stress strain behavior of steel at room and elevated temperature[27]. Temperature, T, was varied between experimental temperatures of 23ºC, 500ºC, 700ºC and 900ºC. A plot of the calculated stress-strain behavior for 1018 Steel at various temperatures can be seen in Figure 1. Due to the effects of thermal softening, the yield stress decreases as

temperatures increase, thus it was predicted that plastic deformation of the face sheets will increase at elevated temperature for a given load.

$$(\sigma_o + B\varepsilon^n)(1 + C\ln\frac{\dot{\varepsilon}}{\dot{\varepsilon}_o})(1 - T_*^p)\,\sigma \tag{1}$$

where,

$$T_* = \frac{T - T_r}{T_m - T_r} \tag{2}$$

Table 1. Johnson-Cook parameters of Cold Rolled 1018 Steel

σ_o (MPa)	B (MPa)	n	C	$\dot{\varepsilon}$ (s^{-1})	$\dot{\varepsilon_0}$ (s^{-1})	p	T_m (K)
560	300	0.32	$7.6x10^{-3}$	10	$5x10^{-6}$	0.55	1773

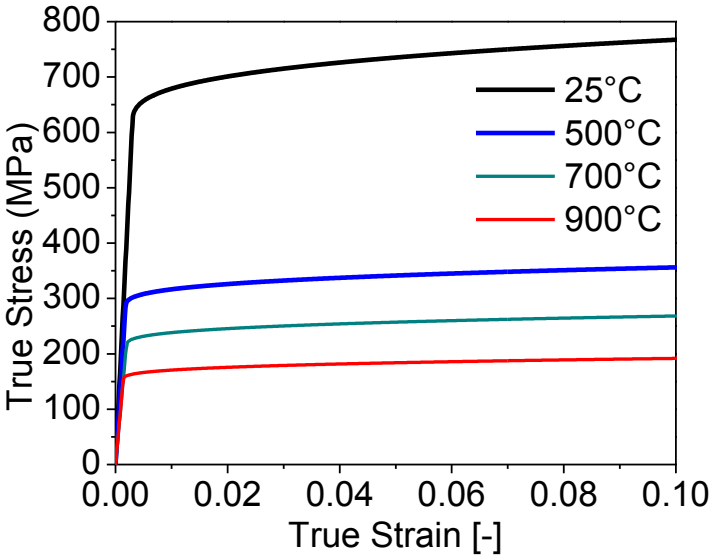

Figure 1 - Stress-strain behavior of 1018 steel at various experimental temperatures

Sandwich panel

Each specimen is composed of two 1018 steel face sheets with the dimensions: 203.2 mm length, 50.8 mm width, and 1.6 mm thickness. The core is constructed by using four layers of G90 corrugated galvanized steel strips, with a 29 gauge thickness, stacked back to back. A form was created from aluminum matching the pitch and length of the sinusoidal-shaped features of the corrugated sheets. The sheets were then clamped between the mold which was fastened to an X-Y table of a Bridgeport milling machine. An abrasive wheel was used to reduce sheet deformation by providing constant contact during the cutting process. The corrugated material was cut to a width of 50.8 mm, the same as the face sheets. The sandwich panel was assembled by welding the outer nodes of alternating corrugated layers, forming the core, and then by spot welding the monolithic face sheets. Table 2 lists the specifications of an empty sandwich panel, seen in Figure 2.

Table 2. Specifications of empty corrugated sandwich panel

Parameter	**Length (mm)**	**Width (mm)**	**Height (mm)**	**Mass (g)**	**Areal Density ($kg \cdot m^{-2}$)**
Value	203.2	50.8	27.4	377.7	36.6

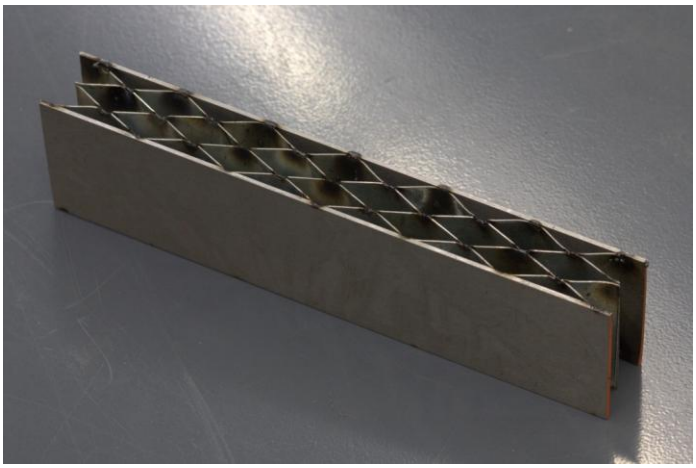

Figure 2 - Corrugated Sandwich Panel

Mortar

Mortar is a very common building material used to bind construction blocks such as: brick, stone and cinderblocks. It is a paste comprised of cement and sand aggregate which cures and can be used to fill cracks and gaps in structures. Quickrete® Mortar Mix (No. 1102) was used to fill the sandwich structures in this study and complies with ASTM C 270 property requirements as a Type N mortar. Yazici et al found that the relative compressive strength of ordinary portland cement based mortars decreased to 62%, 48%, and 35% after being exposed to temperatures of 450°C, 600°C, and 750°C respectively[23]. Considering the *minimum* compressive strength for this product is listed by the manufacturer as 5.2 MPa, then even at 750°C, the compressive strength will drop to 1.82 MPa which is above the peak target pressure of 1.7 MPa used in experiments. Combined with the stiffness of the sandwich panel, it is assumed that the compression of the mortar itself will be minimal, therefore, no further material characterization was performed. The mortar was prepared by thoroughly mixing 250 grams of Quikrete Mortar Mix with 50 grams of water. The mix was then poured into the core of the sandwich panel leaving an empty

region, two cells in depth, adjacent to the front face sheet. This was done to promote core compression while maintaining an barrier of air to help facilitate insulation. While the mixture was solid within a day, it was allowed to set for a week before experimentation. The mass of a filled corrugated sandwich panel is 617 grams. An image of the filled corrugated structure can be seen in Figure 3.

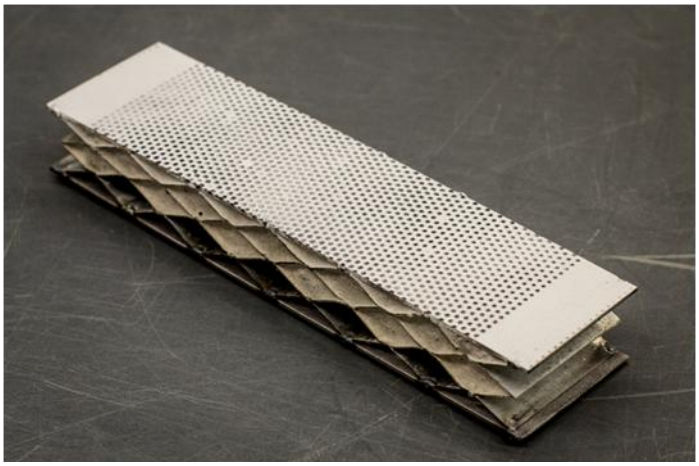

Figure 3 - Image of mortar filled sandwich panel

3. Experimental Procedures

Shock tube

A shock tube apparatus, as seen in Figure 4(a), was utilized to simulate a blast in a controlled environment. With a length of 8 m, the shock tube consists of a driver and driven section. The high-pressure driver section and the low pressure driven section are separated by a Mylar diaphragm. The driver section is then pressurized using helium and pressure difference across the diaphragm is created. Once this pressure difference reaches a critical value, the diaphragm ruptures resulting in a rapid

release of gas creating a shock wave, which travels down the tube to a convergence section, impart dynamic loading on the specimen in the form of a planar wave front. The muzzle diameter at the specimen end is 38.1 mm. Two pressure transducers (PCB102A) are mounted at the end of the muzzle section, to measure the incident and reflected pressure profiles during the experiment which are recorded using an oscilloscope. A schematic of the muzzle dimensions and sensor locations can be seen in Figure 4(b). The specimen was placed in the supports and positioned 3 mm away from the end of the muzzle. The support fixtures ensured simply supported boundary conditions with a span of 152.4 mm. To reduce the effects of friction during deformation, the sandwich panels are positioned over a block, where contact is only on the edge of the back face. The sandwich panel is then secured to the simple support using Nickel-Chrome wire, with a diameter of 0.05 mm, which easily breaks during shock loading and deformation.

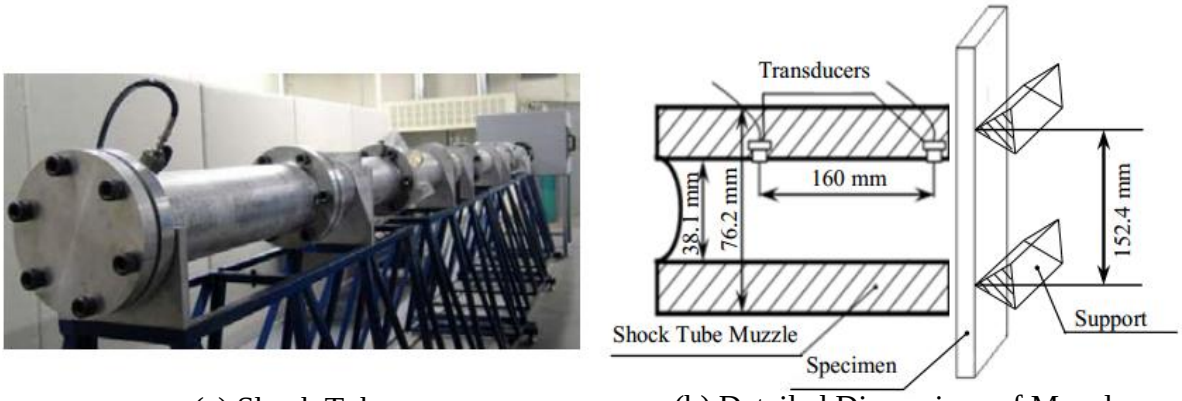

(a) Shock Tube (b) Detailed Dimensions of Muzzle

Figure 4 - Shock Tube and Muzzle Detail

A single diaphragm of Mylar with a thickness of 0.254 mm was selected to generate a shock wave loading that impinged on the specimen with an average incident peak pressure of approximately 0.5 MPa, a reflected peak pressure of

approximately 1.77 MPa, an incident shock wave speed of 821 ms^{-1} and a reflected shock wave speed of 200 ms^{-1}. The shock wave generated had a short rise time (~70 μs) and showed an exponential decay period of approximately 6ms. The response of filled sandwich panels were investigated at room temperature and under three different high temperature conditions: 500°C, 700°C and 900°C. Figure 5 shows a typical pressure profile obtained from the sensor closest to the specimen at room temperature.

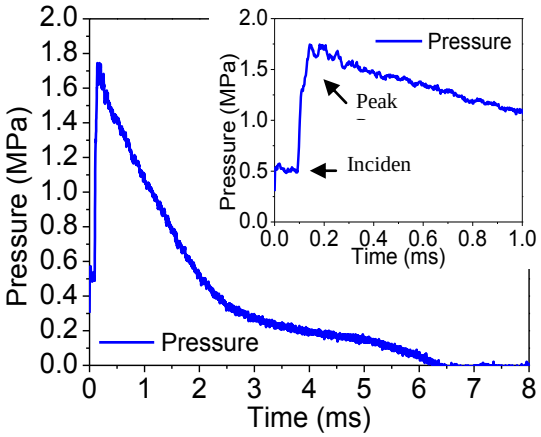

Figure 5 - Typical Pressure Profile

High temperature shock tube setup

The shock tube was modified to heat the back face of the specimen before shock impingement. Four propane nozzles were directed at the rear of the specimen and calibrated to give an even temperature distribution across the surface. Figure 6(a) shows an image of the heating setup with the nozzles directed at the specimen. A 1018 steel monolithic plate was used representing the rear face sheet of the sandwich panel, therefore having dimensions of 203.2 mm length, 50.8 mm width, and 1.6 mm thickness. Three thermocouples were positioned on the specimen along the vertical axis at the center and ~38mm above and below the center and were affixed to the monolithic plate using resistive spot welding. After adjusting the nozzle orientations

and flow rate, the temperature was recorded to calibrate the temperature across the specimen, seen in Figure 6(b).

A typical plot of the temperature distribution obtained on the back face on the points of the vertical axis are shown in Figure 7. After obtaining even heating on the back face, a filled specimen was used to then record the temperature on the front face (loaded area to study the transient thermal response of the panels.

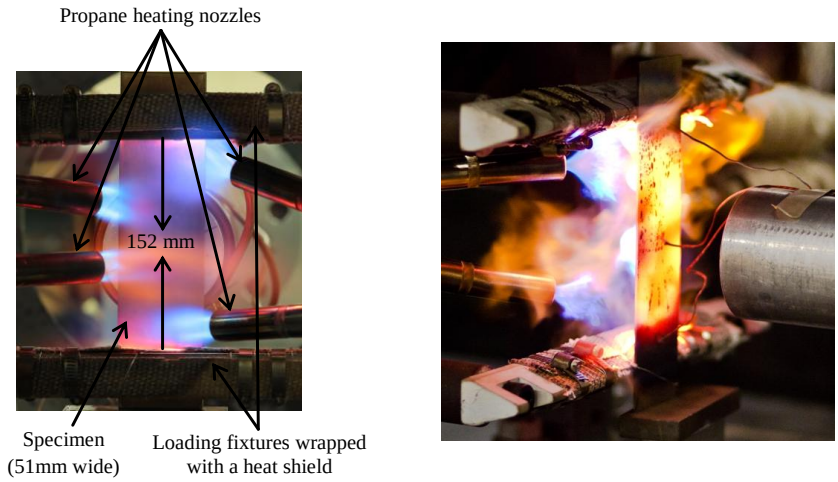

Figure 6 - Heated Shock Tube Setup and Heating Calibration

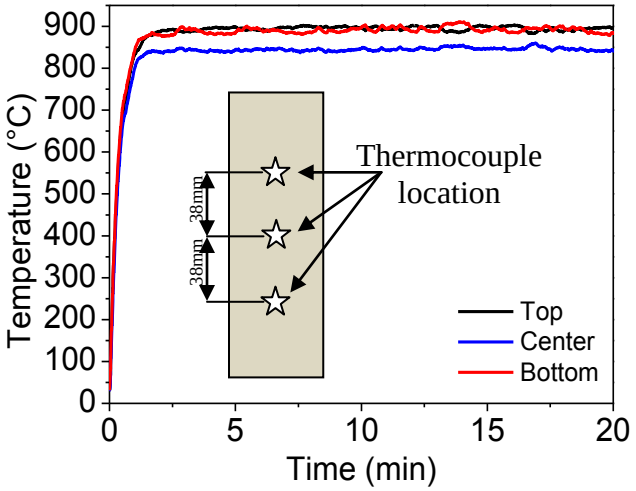

Figure 7 - Typical recording during temperature calibration

High speed photography system

A high speed digital photography system was utilized to capture deformation images at high frame rate during shock loading. The experimental setup, shown in Figure 8, consisted of a back-view 3D Digital Image Correlation (DIC) system with two synchronized Photron SA1 cameras facing the back side of the specimen to capture full field deflection and strain information. The DIC cameras used in these studies operated at 50,000 frames per second at a resolution of 192x400 pixels for a one second time duration. Subset sizes between 8-12 mm were used for performing DIC analysis to reduce decorrelation for some high temperature experiments. The displacement resolution of this technique is $\pm$ 0.02 mm. Another Photron SA1 Camera, positioned perpendicular to the shock tube and specimen, was utilized to capture deflection information and core response during shock loading. Though all cameras were triggered simultaneously, the side view camera was independently controlled, and was operated at 18,000 frames per second with a resolution of 384x752. Results obtained from MATLAB analysis of side view images are subject to an accuracy of ± 0.27 mm.

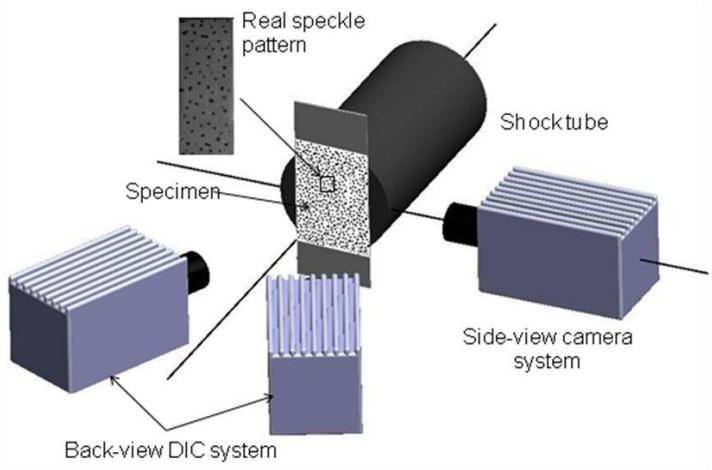

Figure 8 - DIC setup with side view camera

High temperature DIC system under shock loading.

Heating a specimen to high temperatures poses difficult challenges when it comes to using optical methods to capture specimen deformation. To eliminate the influence of thermal radiations on image quality during heating, a DIC setup developed by Abotula et al was used. A band-pass filter was used permitting the transmission of light in the blue wavelengths between 410-490nm. To ensure sufficient contrast for high speed imaging, the need for a high intensity light source was realized. A Cordin, Model 659, high energy flash lamp was used which has a maximum capacity of 1100 Joules regardless of single flash duration. The lamp was set to illuminate the specimen for a duration of 8 ms, which gives a power of 137.5 kW. Figure 9(a) shows an image of a specimen exhibiting the effects of black body radiation as the surface is heated between the simple support fixture. Comparing this image to Figure 9(b), it is observed that the use of an optical band-pass filter helps eliminate contributions of lower frequency wavelengths, increasing contrast of the speckle pattern which is required for DIC optical analysis.

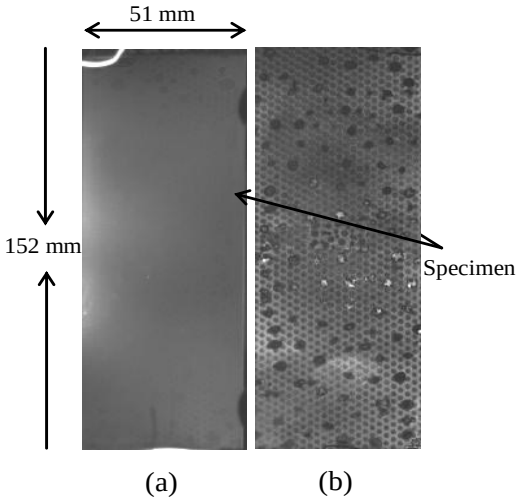

Figure 9 - Images of specimen without (a) and with (b) use of filter at high temperature

4. Results and Discussion

Before blast loading, the transient thermal response of the panels was recorded with three thermocouples placed in the same location as in the temperature calibration. Small variations were noted across the length of the specimen, the warmest temperatures usually recorded by the center thermocouple. Figure 10 shows a typical temperature history plot comparing the average front face and back face temperatures for an experiment over a duration of 20 minutes. The final temperatures and times required for the front face (FF) and back face (BF) to reach steady state have been recorded in Table 3.

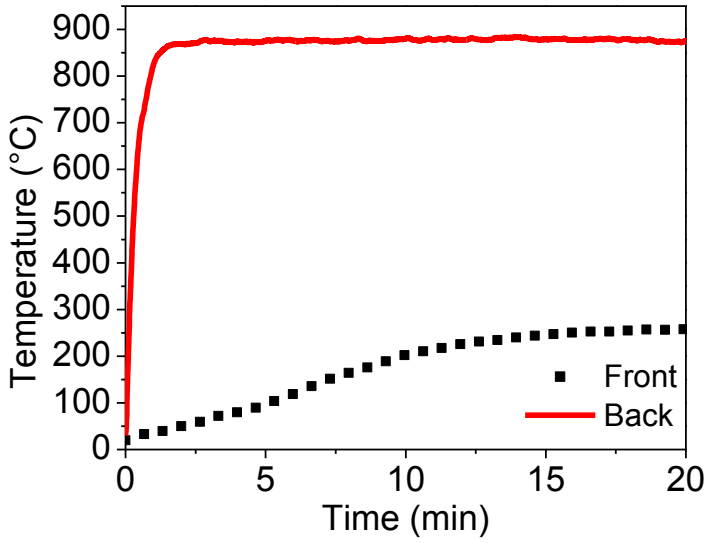

Figure 10 - Typical temperature history plot for front and back face during heating

Table 3. Results of temperature measurement and times to reach steady state

	BF Temp (˚C)	BF $Time_{ss}$ (min)	FF Temp (˚C)	FF $Time_{ss}$ (min)
500˚C Experiments	512 ± 15	8	204 ± 8	20
700˚C Experiments	716 ± 15	5	226 ± 15	16
900˚C Experiments	874 ± 28	2.5	260 ± 16	16

Mortars are not usually considered insulative with a thermal conductivity of 1.27 W/m-K, but compared to steel with a thermal conductivity of 52 W/m-K, the main form of heat transfer is likely to be via conductive thermal bridging of the steel corrugated core. Using the temperature history for each series, the difference in face sheet temperature is plotted in Figure 11, using the expression $\Delta T = T_b - T_f$, where T_b and T_f are back face and front face temperatures, respectively. ΔT peaks after instantaneous heating of the back face and gradually tapers as heat is transferred through the core to the front face until it plateaus reaching steady state. It can be seen that as back face temperatures increase, the steady state difference in temperature also improves. The panels maintain a gradient of at least 300°C through the thickness and an even larger gradient with increasing temperatures.

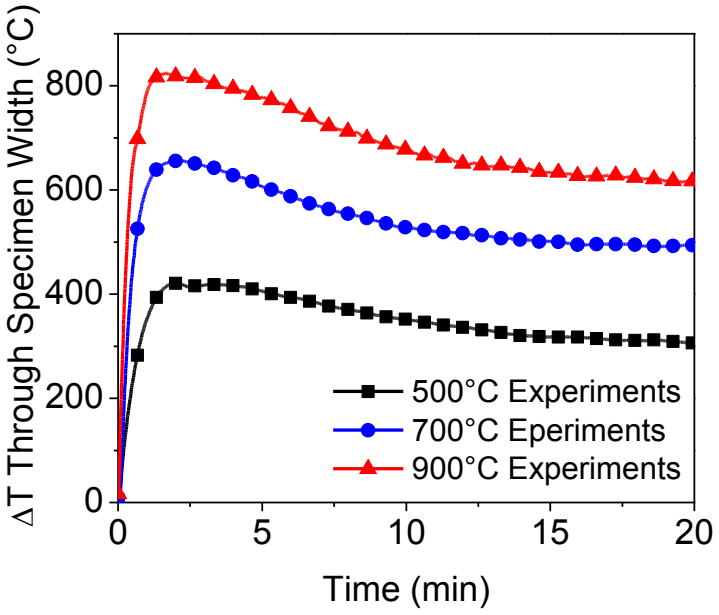

Figure 17- Temperature difference through thickness of specimens

The pressure history for each experiment is given in Figure 12. Since pressures are measured from within the muzzle the profiles recorded are dependent on the specimen deflection. Pressures decay more rapidly with elevated temperatures due to an increase in ductility allowing specimens to deflect for longer durations of time with higher maximum deflections. Impulse imparted to the specimen, plotted in Figure 13, can be calculated by integrating the force-time data of the reflected pressure profile. Since the overall time period of reflected pressure profile was longest at room temperature, the room temperature specimen obtained a maximum impulse of 5.6 Ns. When the temperature increased from room temperature to 900°C, the maximum impulse imparted decreased by approximately 56% (from 5.6 Ns to 3.1 Ns).

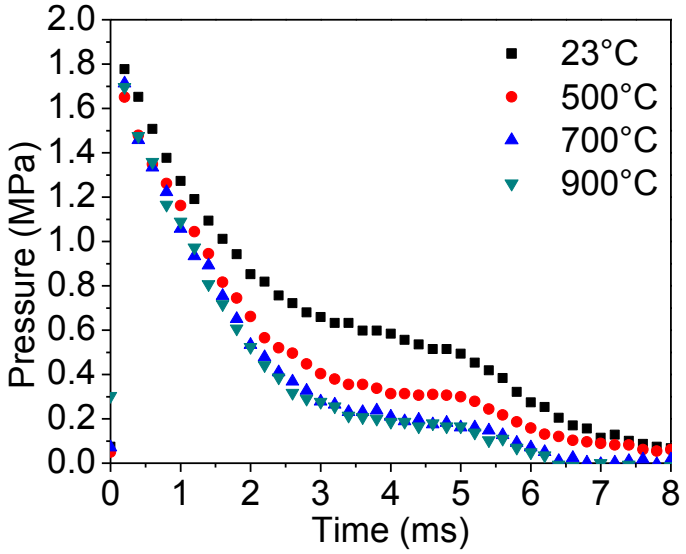

Figure 12 - Pressure profiles of mortar filled sandwich panels

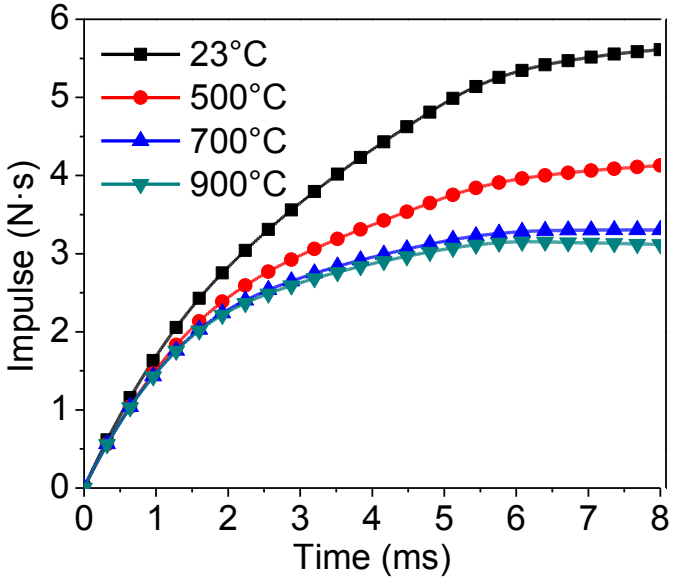

Figure 13 - Impulse of mortar filled sandwich panels

The mean mid-point deflection of the back face for different temperatures were obtained by DIC and plotted in Figure 14. All specimens behave similarly until about

t = 1 ms. The maximum deflection for the room temperature specimen was 5.2mm , occurring at t = 2.8 ms began to reverberate. For the same incident pressure loading, the specimens at higher temperatures continued to deform for a longer duration of time due to thermal softening and lower values of flow stress. At 900°C, the specimen deformed for twice the duration as the room temperature sandwich panel. Specimens heated to 500°C , 700°C , and 900°C showed a maximum deflections of 10.6 mm, 18.2 mm, and 20.7 mm at 3.6 ms, 5.6 ms and 5.6ms, respectively.

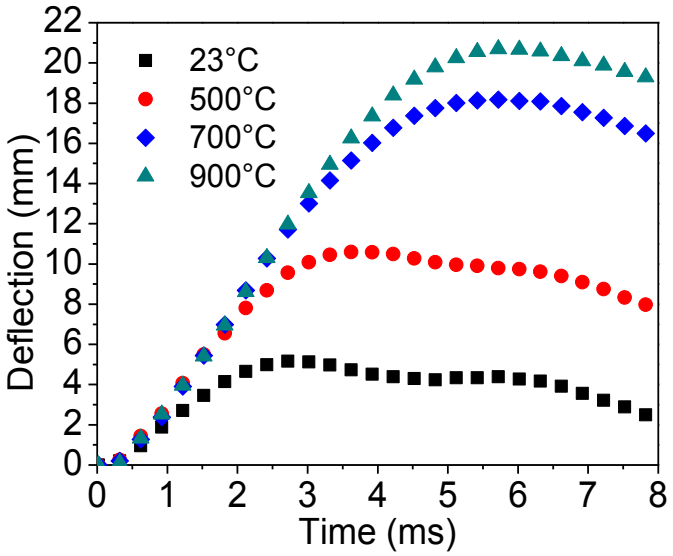

Figure 14 - Mid-point back face deflection of mortar filled sandwich panels

The average in-plane strain-rate observed in these experiments was 10 s^{-1}. Using the Johnson-Cook parameters listed in Table 1, the stress–strain curves of 1018 Steel were constructed for 23 °C, 500 °C, 700 °C and 900°C with a strain-rate of 10 s^{-1}. From these stress–strain curves, it was determined that the flow stress at 500 °C had decreased by 54 % when compared to room temperature and as a result, the mid-point back-face deflection had increased by 104%. In comparison to room

temperature, the value of flow stress at 700 °C decreased by 66% increasing deflections by 250%. Flow stress for 900°C decreases by 76% resulting in an increased back face deflection of nearly 300%. Calculating the stiffness as a function of temperature is more complex with sandwich structures compared to monolithic plates. While heating occurs on one face, there is a gradation of the elastic modulus of steel coupled with property changes of mortar through the thickness of the specimen which changes the stiffness of the structure. It is noted that though the 900˚C specimens exhibited extreme deflections, the samples never ejected from the simple supports.

The out-of-plane velocities are plotted in Figure 15 showing an increasing trend with increasing temperature. As steel becomes more ductile, the resistance to bending decreases, allowing the panel to deform at a higher rate. The room temperature experiments reached a maximum velocity of 3m/s at t = 0.7 ms before slowing and rebounding shortly after t = 3 ms. The specimens heated to 700˚C and 900˚C both exhibited a 100% increase in velocity reaching 6 m/s after t = 2 ms and rebounds after t = 6ms.

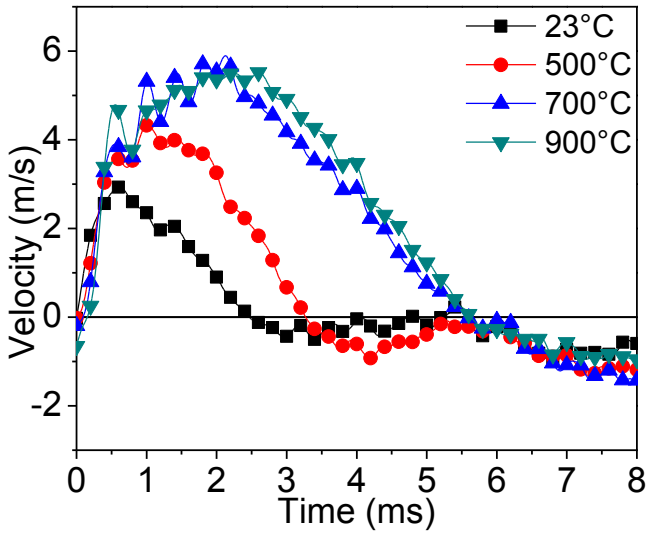

Figure 15 - Mid-point out-of-plane velocity of mortar filled sandwich panels

The in-plane-strain (ε_{yy}) information, displayed in Figure 16, exhibited an increasing trend as temperatures increased. After 0.2ms, the back face for all specimens showed significant bending, resulting in higher in-plane strains (ε_{yy}). At room temperature, the maximum in-plane strain of the specimens were around 0.14% at t = 2.3 ms. For the 500˚C case, a maximum in-plane strain of 0.31% was observed at t = 3.0 ms. For sandwich panels heated to 700˚C, in-plane strain reached a maximum of 0.53% by t = 6.0 ms. For 900°C experiments, the maximum in-plane strain was shown to be nearly 1% and continued to increase until the end of the event. In comparison to the room temperature experiments, the specimens at 500˚C, 700°C and 900˚C showed an increase in ε_{yy} of 121%, 278%, and 614%, respectively. It is important to disclose that the strain resolution of the DIC technique is 200 micro-strain which translates to ± 0.02% strain.

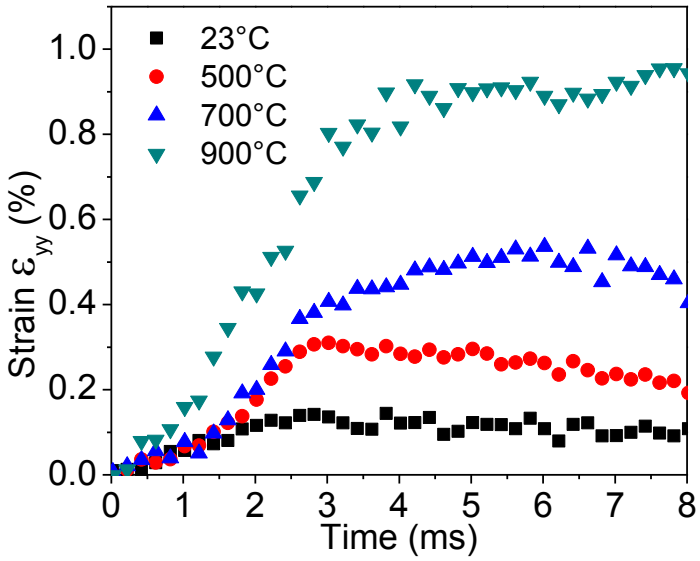

Figure 16 - Mid-point in-plane strain of mortar filled sandwich panels

The real-time observations of the transient behavior for mortar filled sandwich structures under shock loading for different temperatures are shown in Figure 17. The shock wave is propagating from left side of the image to the left side, causing deformation in the specimens. Time t = 0 ms corresponds to the beginning of the event where the shock wave impinged on the specimen. The time scale is kept the same to provide a comparison of panel response up to the point of maximum deflections obtained by the 900˚C experiments. The images were later used to calculate the mid-point deflections in the specimens front face. At room temperature, 500˚C and 700˚C, the specimens experience little core compression, however, the 900˚C experiments showed more significant weld failure about the neutral axis, reducing stiffness and allowing further deformation of core ligaments.

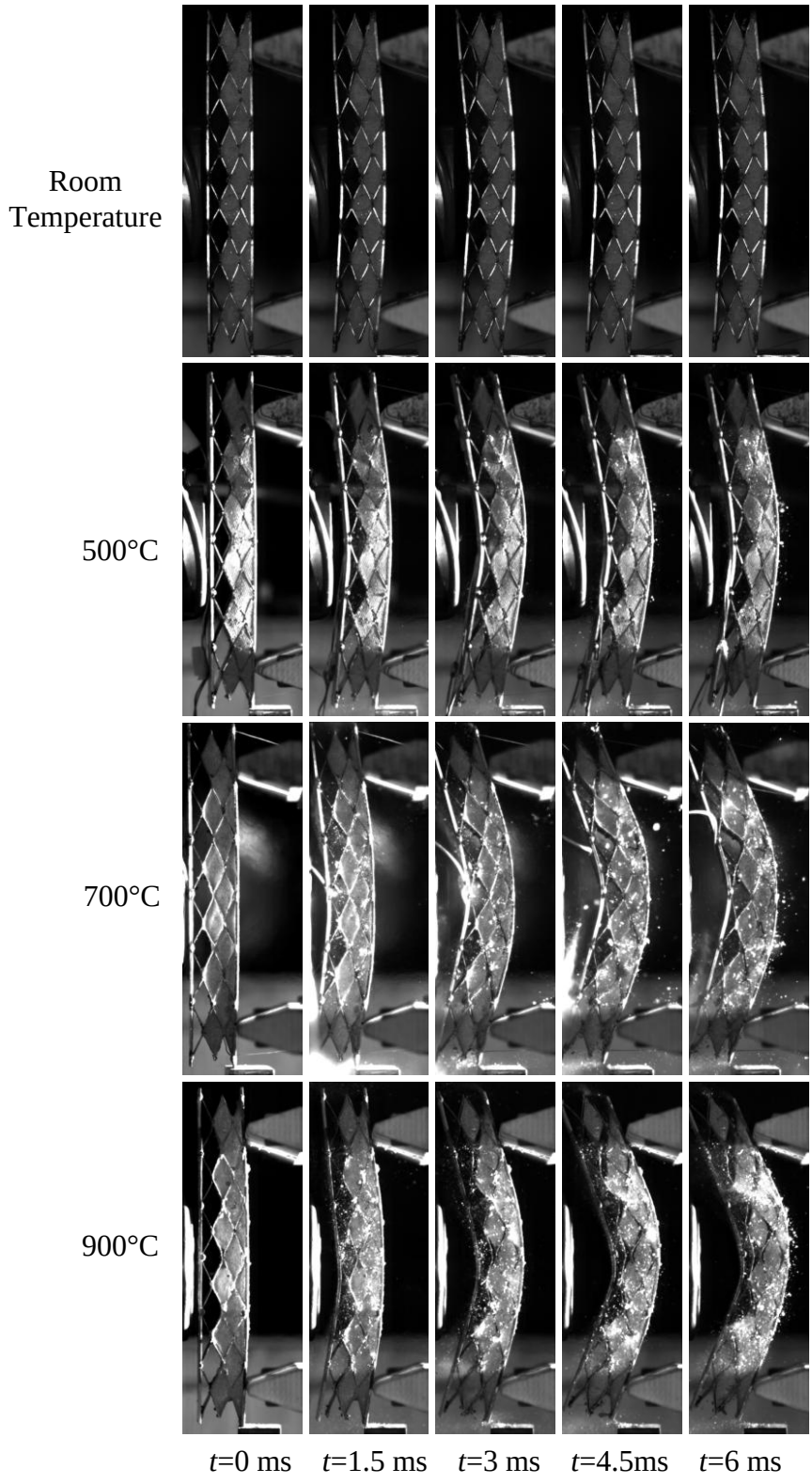

Figure 17 - Real-time side-view deformation images of mortar filled sandwich panels at different temperatures

From the side view analysis, there was evidence to suggest extremely minor core compression increasing at higher temperatures, up to 1.5 mm. Recalling the displacement resolution, the deviation was large enough for the difference in core compression between samples to be considered negligible.

To understand the amount of work done on specimens by shock loading, it is necessary to evaluate the deflection-time data from high speed side view images and the force-time data collected by pressure transducers [28]. This can be used to the evaluate the amount of energy used for panel deformation at different temperatures. It is assumed that the pressure pulse delivered by shock loading is planar, the work done on specimen can be approximated by integrating the pressure-deflection profile for every point inside the shock loading area using Equation 3, plotted in Figure 18. This energy imparted into the specimen is equal to the summation of energies used in panel response outlined in found in Equation 4.

$$E_{specimen} = \oint_{S_{shock\ tube}} \left(\int P_{reflected}(t) * dl_{deformation} \right) dS \tag{3}$$

where

$$E_{specimen} = E_{deformation} + E_{kinetic} + E_{dissipated} \tag{4}$$

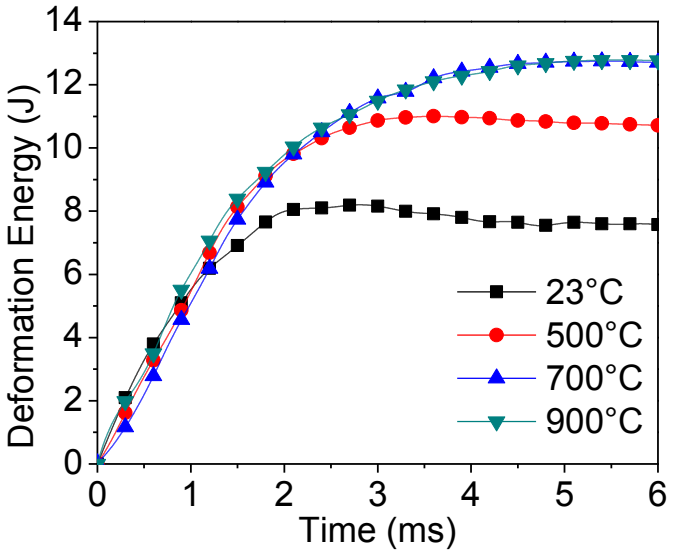

Figure 18 - Deformation energy of mortar filled sandwich panels at various temperatures

The work done on samples for experiments conducted at room temperature and 500˚C showed maximum of 8.2 J and 11.0 J, respectively. A maximum of 12.7 J was observed for both the 700˚ and 900˚C experiments. The work done for the two highest temperatures was approximately 55% higher than at room temperature. This indicates that the specimens at higher temperature absorbed significantly more energy during the shock loading process. Even though the impulse was lower at higher temperatures, the specimen absorbed more energy, resulting in higher deflections. Due to increased ductility within the structure as temperatures increase, bending stiffness decreases. This allows for greater deflections for a given shock load, resulting in higher work done on the specimen during fluid structure interaction. With a 35% difference in flow stress of steel between 700˚C when and 900˚C, and with the presence of increased core damage in form of weld failure, the rear out-of-plane deflection was 12% higher

given the same amount of energy used for specimen deformation at 900˚C. This can also be observed from post-mortem images.

Permanent deformation of the corrugated steel sandwich panels was visually inspected and documented using a digital camera and is shown in Figure 18. In post-mortem, the samples from the room temperature experiments show no core damage as all welds are intact and there is no noticeable core buckling. Some of the mortar filler appears to have shifted slightly as the front and back face are permanently deformed by 3 mm. For the 500˚C experiments, a very few broken welds are present and are mostly located between the neutral axis and rear face sheet. Permanent plastic deformation of the rear sheet was 7 mm. The 700˚C and 900˚C experiments show the most core damage and plastic deformation. As temperatures increase, the flow stress decreases so drastically that the rear face sheet and corrugated layers become more ductile, effectively reducing the relative stiffness and compromising weld strength. For these temperatures, the brittle filler experienced cracking and portions were ejected as welds breakage and localized bending of the core ligaments allowed core separation. The permanent back face deflections for the 700˚C and 900 ˚C are 17 mm and 20 mm, respectively.

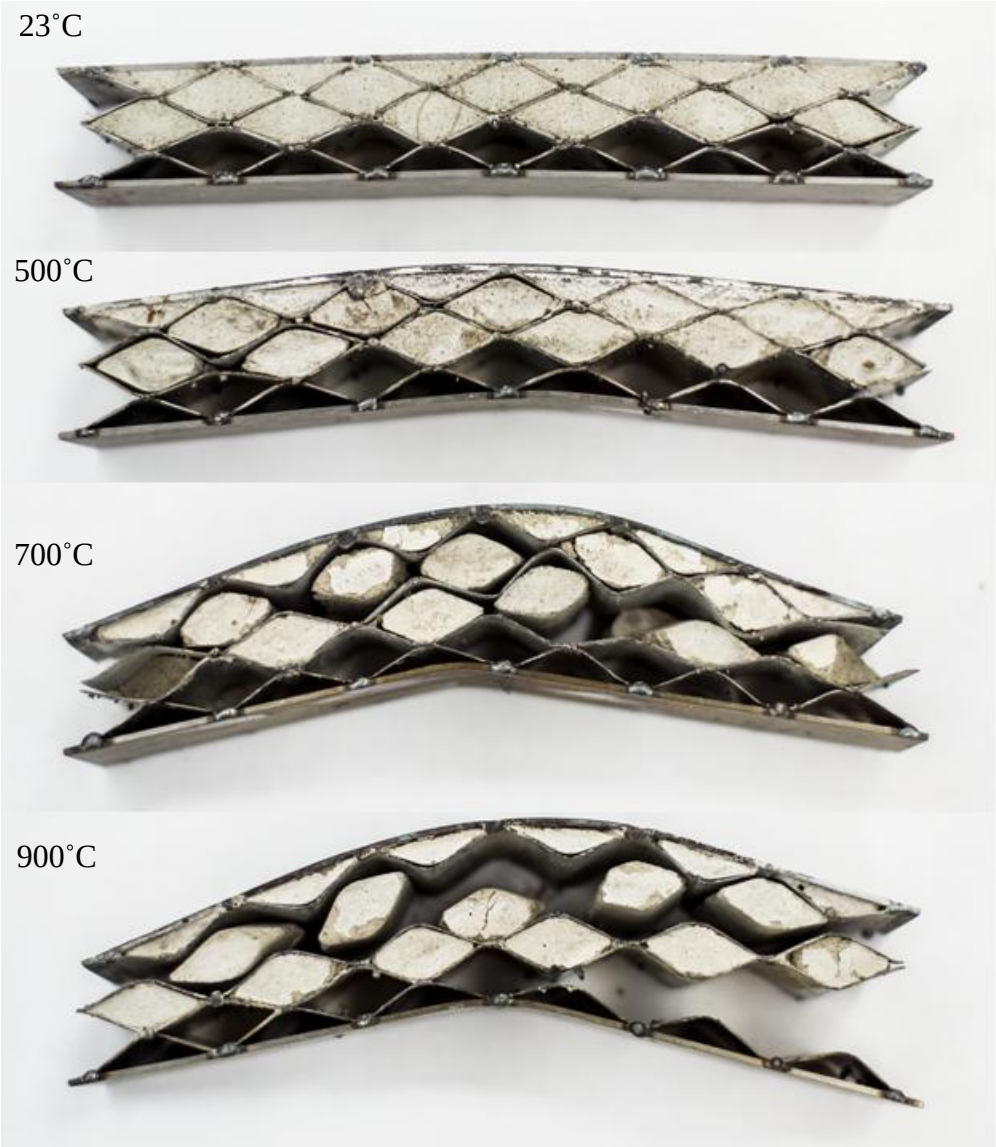

Figure 19 -Post-mortem images of mortar filled sandwich panels

5. Conclusions

A series of experiments was conducted to investigate the shock resistance of corrugated sandwich panels filled with mortar shock loading at room and high temperatures. The following is the summary of the results:

1. Mortar is thermally resilient and can be used as a filler material for sandwich panels to improve blast mitigation.

2. When heated, the panels maintained a minimum temperature difference of 300˚C between the front and back face (25.4mm).This gradient grew larger with increasing temperature. A temperature gradient of nearly 620˚C was observed when the back face was heated to 900˚C exhibiting good thermal qualities while maintaining a similar blast performance as 700˚C experiments.

3. The maximum back face deflection of specimens at 900˚C was approximately 300% higher than those at room temperature.
4. The impulse imparted into the specimen decreased as temperatures increased from room temperature to 900˚C.
5. The maximum in-plane-strain (ε_{yy}) showed an increase of 614% as temperatures increased from room temperature to 900˚C.
6. The amount of deformation energy aborbed by specimens increased by 55% as temperatures increased from room temperature to 900˚C.

Acknowledgements

The authors gratefully acknowledge the financial support provided by the Department of Homeland Security under Grant Number: 2008-ST-061-T20002-04.

References

1. Ajdari A, Jahromi BH, Papadopoulos J, Nayeb-Hashemi H, Vaziri A. Hierarchical honeycombs with tailorable properties. *Int J Solids Struct.* 2012 Jun 1;49(11–12):1413–1419.

2. Dharmasena KP, Wadley HNG, Xue Z, Hutchinson JW. Mechanical response of metallic honeycomb sandwich panel structures to high-intensity dynamic loading. *Int J Impact Eng.* 2008 Sep;35(9):1063–1074.

3. Liang C-C, Yang M-F, Wu P-W. Optimum design of metallic corrugated core sandwich panels subjected to blast loads. *Ocean Eng.* 2001 Jul;28(7):825–861.

4. Wadley HNG, Dharmasena KP, O'Masta MR, Wetzel JJ. Impact response of aluminum corrugated core sandwich panels. *Int J Impact Eng.* 2013 Dec;62:114–128.

5. Wang E, Gardner N, Shukla A. The blast resistance of sandwich composites with stepwise graded cores. *Int J Solids Struct.* 2009 Sep;46(18–19):3492–3502.

6. Zhang L, Hebert R, Wright JT, Shukla A, Kim J-H. Dynamic response of corrugated sandwich steel plates with graded cores. *Int J Impact Eng.* 2014 Mar;65:185–194.

7. Xiong J, Vaziri A, Ma L, Papadopoulos J, Wu L. Compression and impact testing of two-layer composite pyramidal-core sandwich panels. *Compos Struct.* 2012 Jan;94(2):793–801.

8. Hassan MZ, Guan ZW, Cantwell WJ, Langdon GS, Nurick GN. The influence of core density on the blast resistance of foam-based sandwich structures. *Int J Impact Eng.* 2012 Dec;50:9–16.

9. Rubino V, Deshpande VS, Fleck NA. The dynamic response of clamped rectangular Y-frame and corrugated core sandwich plates. *Eur J Mech - ASolids.* 2009 Jan;28(1):14–24.

10. Tekalur SA, Shukla A, Shivakumar K. Blast resistance of polyurea based layered composite materials. *Compos Struct.* 2008 Jul;84(3):271–281.

11. Ebrahimi H, Vaziri A. Metallic sandwich panels subjected to multiple intense shocks. *Int J Solids Struct.* 2013 Apr;50(7–8):1164–1176.

12. Xue Z, Hutchinson JW. A comparative study of impulse-resistant metal sandwich plates. *Int J Impact Eng.* 2004 Nov;30(10):1283–1305.

13. Langdon GS, von Klemperer CJ, Rowland BK, Nurick GN. The response of sandwich structures with composite face sheets and polymer foam cores to air-blast loading: Preliminary experiments. *Eng Struct.* 2012 Mar;36:104–112.

14. Bardella L, Genna F. Elastic design of syntactic foamed sandwiches obtained by filling of three-dimensional sandwich-fabric panels. *Int J Solids Struct.* 2001 Jan 11;38(2):307–333.

15. Liu H, Cao ZK, Yao GC, Luo HJ, Zu GY. Performance of aluminum foam–steel panel sandwich composites subjected to blast loading. *Mater Des.* 2013 May;47:483–488.

16. Abotula S, Heeder N, Chona R, Shukla A. Dynamic Thermo-mechanical Response of Hastelloy X to Shock Wave Loading. *Exp Mech.* 2014 Feb 1;54(2):279–291.

17. Sohel KMA, Richard Liew JY, Yan JB, Zhang MH, Chia KS. Behavior of Steel–Concrete–Steel sandwich structures with lightweight cement composite and novel shear connectors. *Compos Struct.* 2012 Dec;94(12):3500–3509.

18. Arioz O. Effects of elevated temperatures on properties of concrete. *Fire Saf J.* 2007 Nov;42(8):516–522.

19. Ergün A, Kürklü G, M. Serhat B, Mansour MY. The effect of cement dosage on mechanical properties of concrete exposed to high temperatures. *Fire Saf J.* 2013 Jan;55:160–167.

20. Husem M. The effects of high temperature on compressive and flexural strengths of ordinary and high-performance concrete. *Fire Saf J.* 2006 Mar;41(2):155–163.

21. Li M, Qian C, Sun W. Mechanical properties of high-strength concrete after fire. *Cem Concr Res.* 2004 Jun;34(6):1001–1005.

22. Poon C-S, Azhar S, Anson M, Wong Y-L. Comparison of the strength and durability performance of normal- and high-strength pozzolanic concretes at elevated temperatures. *Cem Concr Res.* 2001 Sep;31(9):1291–1300.

23. Yazıcı Ş, Sezer Gİ, Şengül H. The effect of high temperature on the compressive strength of mortars. *Constr Build Mater.* 2012 Oct;35:97–100.

24. Youssef MA, Moftah M. General stress–strain relationship for concrete at elevated temperatures. *Eng Struct.* 2007 Oct;29(10):2618–2634.

25. Yüzer N, Aköz F, Öztürk LD. Compressive strength–color change relation in mortars at high temperature. *Cem Concr Res.* 2004 Oct;34(10):1803–1807.

26. Johnson G.R. and Cook W.H.. *Proc. 7th Int. Symp. on Ballistics*, The Hague, The Netherlands, 1983, 541–47.

27. Vural M, Ravichandran G and Rittel D. Large strain mechanical behavior of 1018 cold-rolled steel over a wide range of strain rates. *Metallurgical and Materials Transactions A*. 2003; 34: 2873-85.

28. Wang E and Shukla A. Analytical and experimental evaluation of energies during shock wave loading. International Journal of Impact Engineering. 2010; 37: 1188-96.

CHAPTER 4

CONCLUSION AND RECOMMENDATIONS

Conclusions

This research experimentally investigated the properties of a polymer based syntactic foam as well as mortar for use as a filler material in corrugated steel sandwich structures. The objective of this project was to develop an understanding of the effects that extreme temperatures have on the blast response of filled corrugated sandwich panel. This in turn will provide a basis to further the development of tailorable multifunctional structures which could be used in many applications where it is necessary to mitigate blast energy and insulate persons or objects from extreme temperatures. The relevant findings from the present study are presented below.

1. A syntactic foam was developed using silicone and glass bubbles. The insulative properties of silicone rubber improved with higher weight percentages of glass bubbles do to the additional voids the hollow microspheres create and thus also lowering the density of the material. It was found that a layer forms when the silicone syntactic foam is subjected to heating on one surface, resistant to high temperatures. This layer transforms the material into a two layer structure during high temperature heating by creating a brittle and soft layer.
2. The foam shows very good heat resistivity with the brittle layer working as a heat barrier, as this segment of decomposed silicone leaves behind silica as well as carbon dioxide and carbon monoxide after combustion. Syntactic foam

maintains its structural integrity up to 500˚C with glass bubbles remaining intact.

3. The effect of post high temperature heating on material properties were investigated using quasi-static compression tests. The compression strength properties were not affected after heating processes, aside from a slight drop in yield stress. During compression tests, stress-strain plots show an increase in the crush plateau by introducing higher amounts of glass bubbles improving energy absorption properties compared to virgin silicone.
4. When investigating the shock resistance of corrugated sandwich panels with and without a syntactic foam filler, it was found that syntactic foam filled sandwich panels exhibited superior mitigation compared to unfilled panels. The filled panels exhibit a stiffer core response in comparison to unfilled panels that demonstrate core compression and softer response
5. During heating, the front face temperatures of syntactic foam filled panels never exceeded ~150˚C and a temperature difference of at least 180˚C and greater was observed for both heated experiments, highlighting the thermal barrier characteristics of syntactic foams. The syntactic foam stiffened the core despite gradation of elastic modulus through the specimen width, reducing deflection at 330˚C. Integrity of the welds were weakened at 500˚C, decreasing the panels overall stiffness causing larger deformation
6. Mortar proved to be thermally resilient and remains intact at extreme temperatures. It is prepared easily and can be used as a filler material for sandwich panels to improve blast mitigation.

7. When heated, the mortar filled panels maintained a minimum temperature difference of 300˚C between the front and back face (25.4mm).This gradient grew larger with increasing temperature. A temperature gradient of nearly 620˚C was observed when the back face was heated to 900˚C exhibiting good thermal qualities while maintaining a similar blast performance as 700˚C experiments.

8. Due to increasing ductility in steel at elevated temperatures, both the syntactic foam and mortar filled specimens demonstrated an increase in back face deflection, in-plane strain and out-of-plane velocity with increasing temperatures.

Recommendations

The current investigation has provided a basis for experimentally investigating the dynamic response of filled sandwich structures to high temperature blast loading. There, however, remains a significant body of work to be completed in this area to better understand the use of fillers and their insulative properties on the performance of sandwich structures. This work includes further experimental studies as well as computational studies. The proposed potential future projects are summarized as follows:

1. Develop a method to quantify the energy absorbed by the core due to failure and dissipation. MATLAB code exists to calculate the energy imparted by gasses, deformation energy and kinetic energy for a monolithic plate. These

calculations are contingent on the knowledge of the muzzle inner diameter. The stress field acting on the back face, the wave speed and inertia effects through this complicated core structure are unknown. This may require the generation of a finite element model which would then require validation and knowledge of simulation of welds.

2. Conduct well designed experiments exploring the thermal properties of syntactic foam with different percentages of glass bubbles and cenospheres. The addition of cenospheres may further increase the heat resistivity while introducing more local stress concentrations to promote sacraficial collapse of micrspheres. This will create a more energy absorbant insulative syntactic foam with expanded tailorability.
3. Perform quasi-static experiments on empty corrugated sandwich panels and find a way to model weld strength using finite element methods. Once the stiffness of the panel is assertained, a model can be created and simulations can be conducted using the pressure profiles gathered in experimentation. If the model is validated, with the experimental results, a variety of simulations can be conducted with different fillers, reducing the time required to carry out preliminary experiments. All material properties for fillers will need to be identified to apply to the simulation to ensure proper transient thermal response to the structure.
4. Explore funtional grading the filler material used in sandwich stuctures by greatly varrying the percentage of suspended particles. In past studies, Gardner et al. determined the most energy absorbant core configurations is graded soft

to firm from the direction of shock front. Using a rigid cement/morter on the back surface that can withstand extreme temperatures while grading the intermediate cells of the core with softer material may further reduce back face deflections.

5. Conduct experiments heating the front, shock impinging, surface and compare to the results of current research or simulation. This will investigate sandwich panel response with the temperature dependant gradation of elastic modulus in a different configuration; grading the structure opposite to what was tested in the current study. To fully understand the temperature distribution within the panel, imbedding thermocouples within the core might provide valuable information. With this information, boundary conditions can be established and the heat transfer through the specimen can be modeled with programs like COMSOL.
6. Numerically investigating the relation between the decrease in flow stress due to elevated temperature and the stiffness of the core with a gradation of elastic modulus throughout the panel thickness will help predict panel deflection as a function of temperature. M.H. Sadd has investigated plane non-homogeneous elasticity problems with various boundary conditions basing solution schemes using the Airy stress function, however, since dynamic loads applied by the shock tube usually induce bending moments that exceed the yield stress of the material, a deep understanding of plasticity will be required to formulate displacement approximation for complex, non-monlithic, beam bending problems.

7. Utilizing different sandwich structure construction. The use of perforated face sheets and corrugated layers may help diffuse blast energy by modifying the total area in which the shock impinges the speimen. If using a visco-elastic material to partially fill the panel, during core compression, energy may be dissipated by forcing the filler to 'flow' into empty cells which might further reduce deflections. Functionally grading the structure based on perforation or fill pattern can be useful in tailoing structures. Improving upon the bonding method for constructing sandwich panels will also prove beneficial. If brazing or similar bonding process were utilized, creating a permanant, high temperature resistant, adhesion across the specimen width, it is predicted that the stiffness of the panel will improve.

APPENDICES

APPENDIX A: PROCEDURE FOR MANUFACTURING PANELS

Preparing Corrugation

The test samples are sandwich panels consisting of a core and two face sheets. The core is comprised of four corrugated sheets, stacked in alternating front/back-face orientation. The galvanized steel corrugated sheets, as a raw material, is a commonly found building material and was delivered by Mechanical Metals, Inc. in Newton, Pennsylvania. For a visual reference, please refer to Figure 1. The sheets used in fabrication of this series of specimens were pre-trimmed to a rough dimension of approximately 60.96 centimeters (24 inches) by 91.44 centimeters (36 inches). The specifications of the corrugation are as follows: 29 gauge, 31.75mm x 6.35mm ($1\frac{1}{4}$ in x $\frac{1}{4}$ in), galvanized.

Figure 1. - Corrugated sheet as delivered from Mechanical Metals, Inc.

Four sheets, layered one on top of the other, were trimmed along the direction of the peaks/valley of the corrugation such that six raised features of the corrugation, and subsequently seven lower features. This resulted in three stacks of four corrugation layers with a width of 19.05 centimeters (7.5 inches) and the remaining length of 91.44 centimeters (36 inches).

In the past works, some corrugated sandwich structures were created by cutting the corrugations with a band saw. This causes major deformation and inconsistency since the corrugated sheets are to be stacked in four layers, it is imperative that the curvature of the corrugated sheets be preserved while cutting them into 50.8 millimeter (2 inch) strips. If any deformation were to occur, the total stack height would not be consistent, and would result in an non-symmetric core profile. A profile was created in SolidWorks and form was created out of aluminum using a CNC machine (see Schematic A and B). The form consisted of two parts, one component to be used as a base, and the other to be used to be used as a contoured clamp for both the raw material and the strip to be cut. Two counter bores were made in the base to allow for fastening on the X-Y Table of a Bridgeport Milling Machine. Holes were drilled and threaded into the base and the top was fastened using hex-cap bolts.

A 3 inch abrasive disc was used to cut the corrugated sheets, the first cut made to create a clean edge along the back face of the form. Figure 2 shows the aluminum form with the 90˚ Bridgeport attachment for the abrasive wheel.

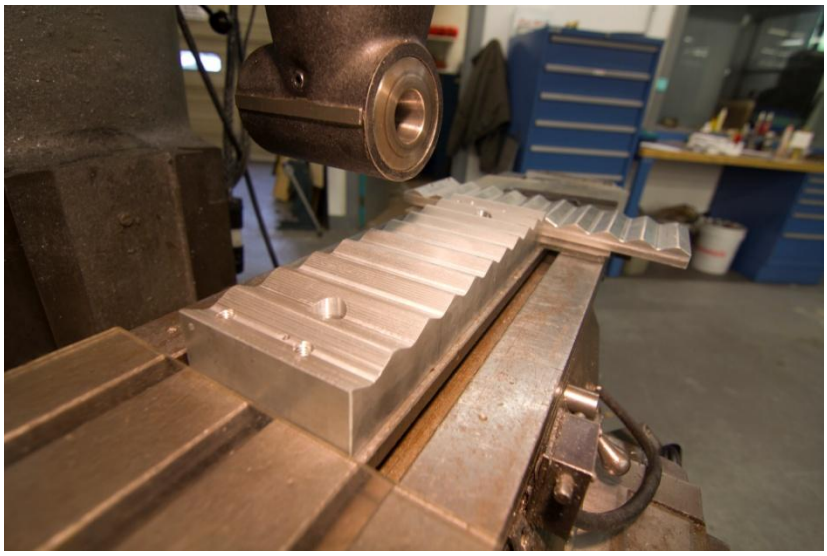

Figure 2. - Aluminum form to hold the corrugated sheets.

After the first cut was made, the table is indexed 50.8mm (2 inches) in the y-direction and a pass is made to trim the raw sheet to the desired dimensions for core construction. The corrugated layers were clamped together in various places to ensure that they would be indexed together after every cut without shifting. After each pass, the corrugated layers were indexed forward and aligned to the edge of the mold base. Because the table is already indexed 54mm ($2\ \frac{1}{8}$ inches) from the edge of the mold base each subsequent cut is made by mechanically translating the table in the X-direction. Figure 3 shows the final configuration for cutting corrugations. The bulk material as well as the piece to be trimmed are both clamped to reduce vibration and maintain curvature. Images of the corrugated layers after being cut, seen in Figure 4, show preserved curvature as well as smooth edges without requiring additional machine processes.

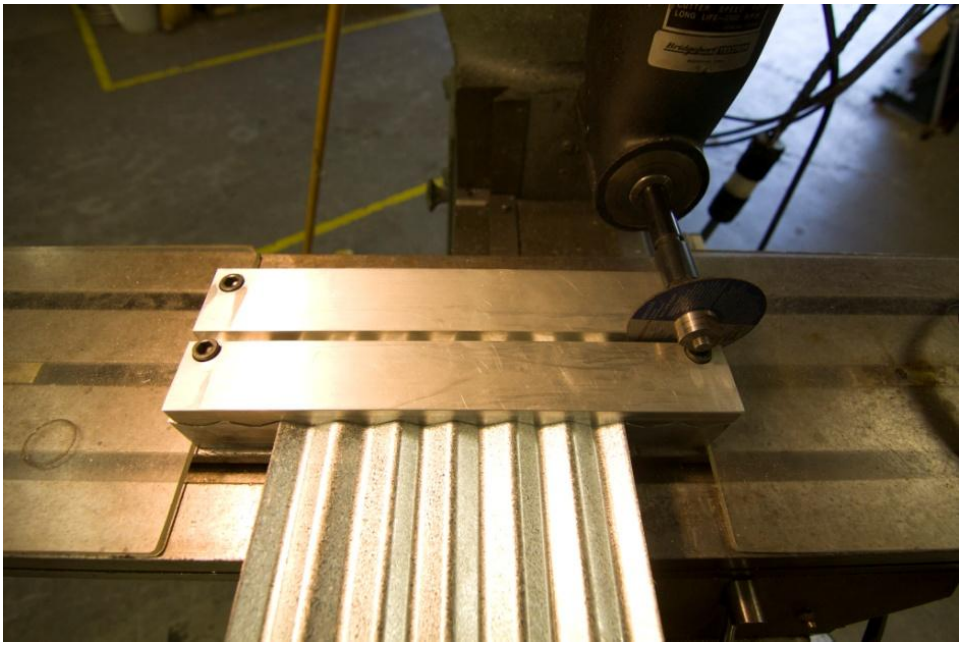

Figure 3. - Image of fixture and abrasive wheel in preparation to cut corrugations

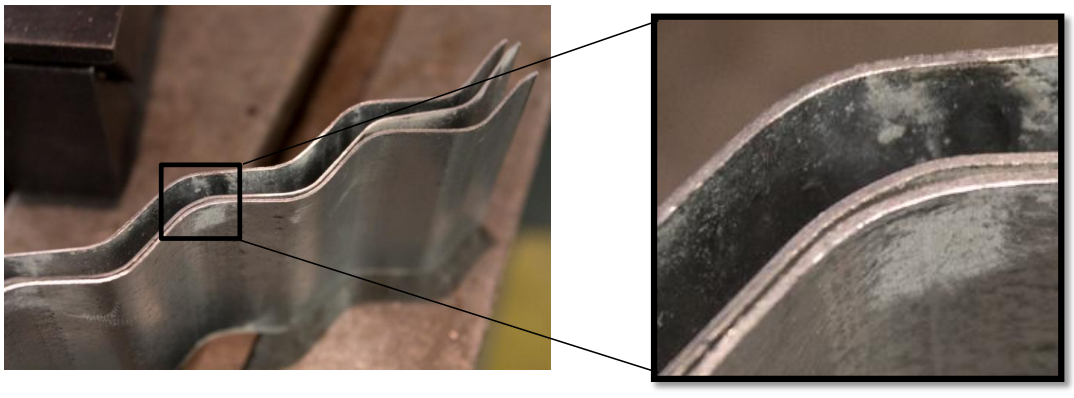

Figure 4. - Image corrugations after cutting process

Preparing Face Sheets

Flat bar stock was ordered with the following specifications: Mild Steel, 50.8mm (2 inches) width, 609.6mm (24 inches) length, 1.6mm ($\frac{1}{16}$ inches) thickness, Figure 5.

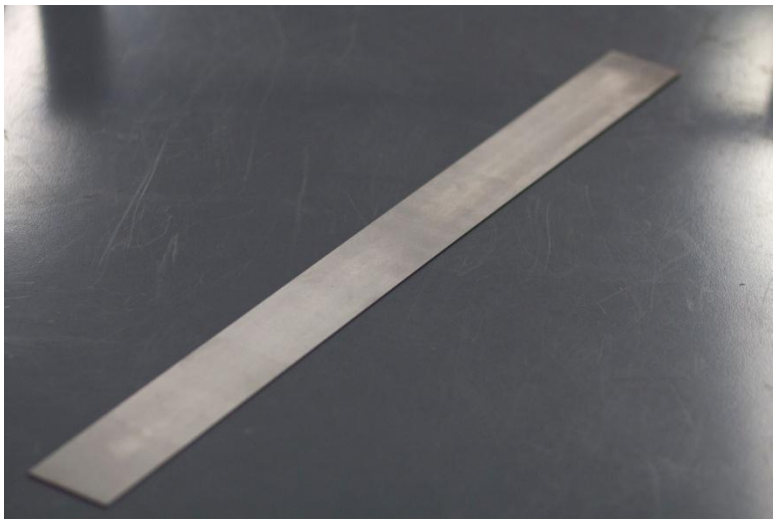

Figure 5. - Image of flat bar stock as ordered

The actual measured length was longer than 609.6mm (24 inches) therefore, the bar stock was partitioned into three portions with measurements of roughly 206.4mm ($8\frac{1}{8}$ inches), Figures 6 and 7 This overage in length proved to be beneficial as the edges were rough cut and would be made perpendicular using a Bridgeport. After marking the remaining flat bar stock, they were cut using a band saw, Figure 8.

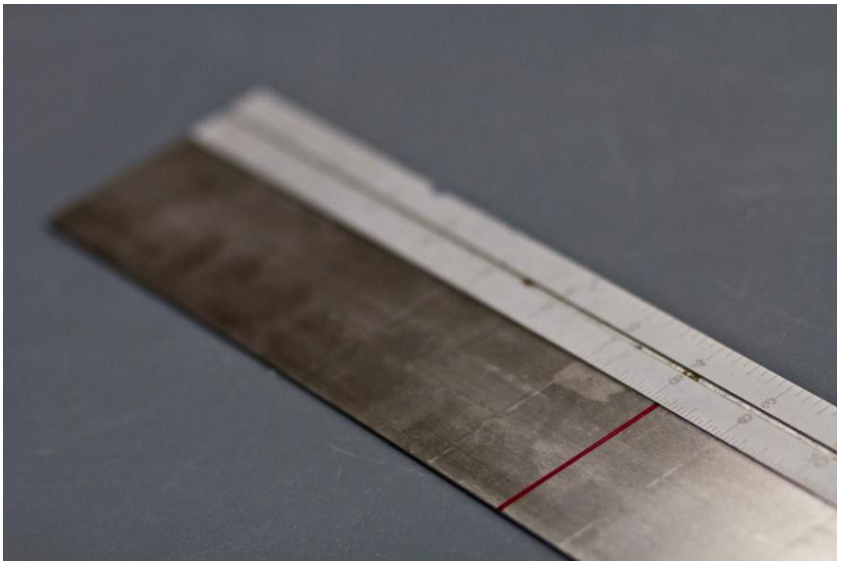

Figure 6. - Image of marks are made at a length of 206.375mm ($8\frac{1}{8}$ inches)

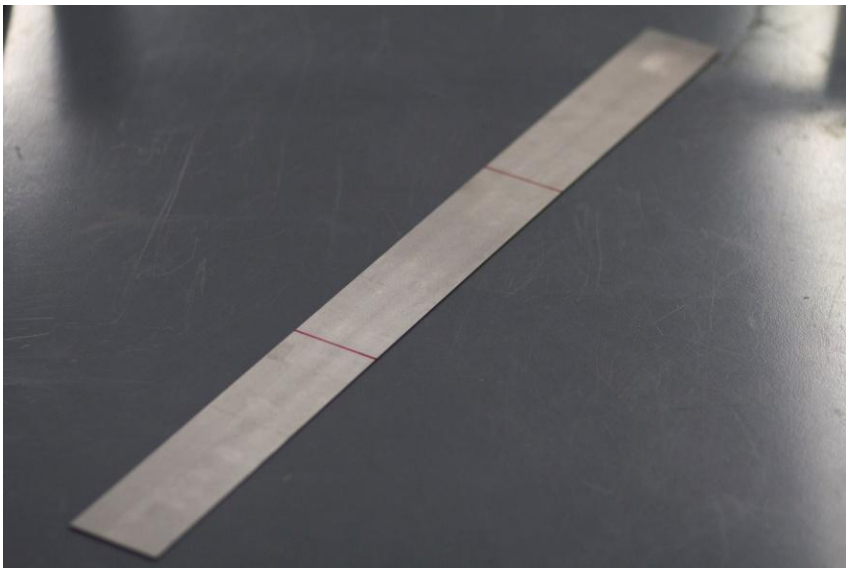

Figure 7. - Image of bar stock marked and ready to be cut

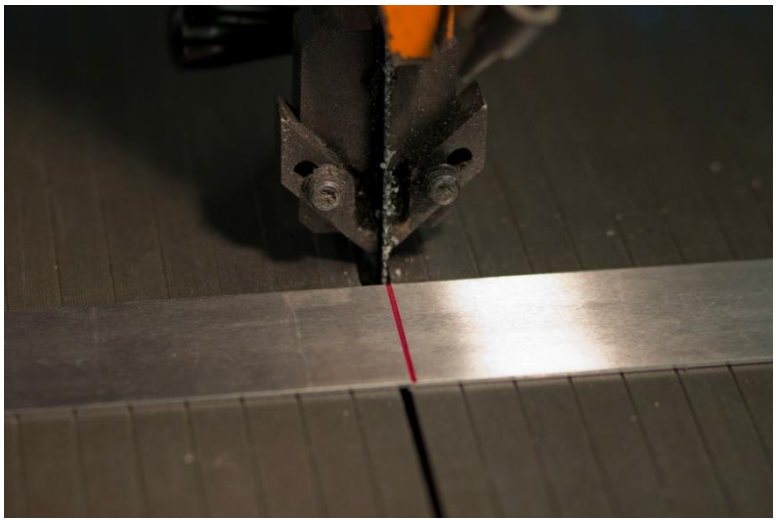

Figure 8. - Image of bar stock is cut using a band saw

With the face sheets cut, red marker was used to color both ends, Figure 10. This will serve as a visual indicator of whether or not material was removed during the milling process on the Bridgeport. The milling process is utilized to ensure that the ends are perpendicular to the length, and since it is a precision process, the final length of each face sheet will be consistent with one another.

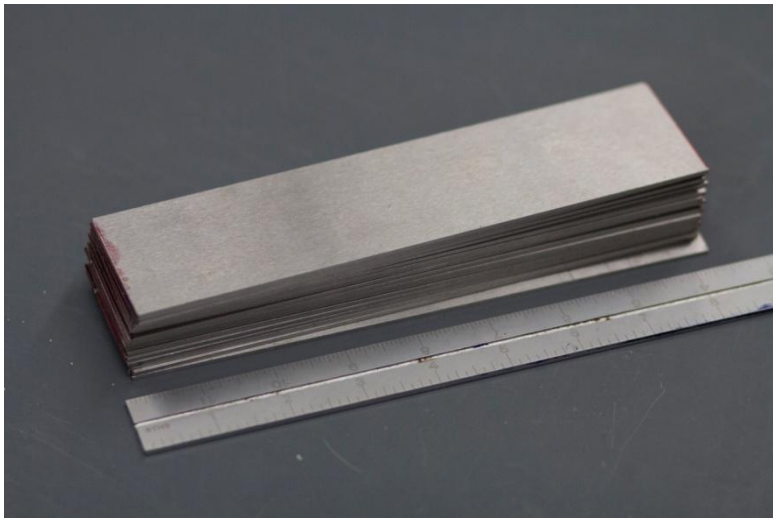

Figure 9. - Image of face sheets after being cut on the band saw

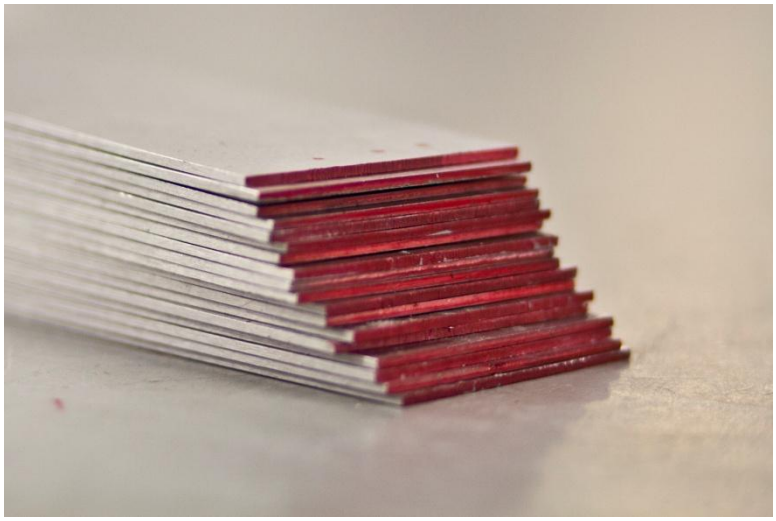

Figure 10. - Image of edges of face sheets marked with red marker

The face sheet with the smallest length is identified and placed in the vice of the Bridgeport milling machine. A mill stop is positioned at the end of the face sheet, depicted in Figure 11 .

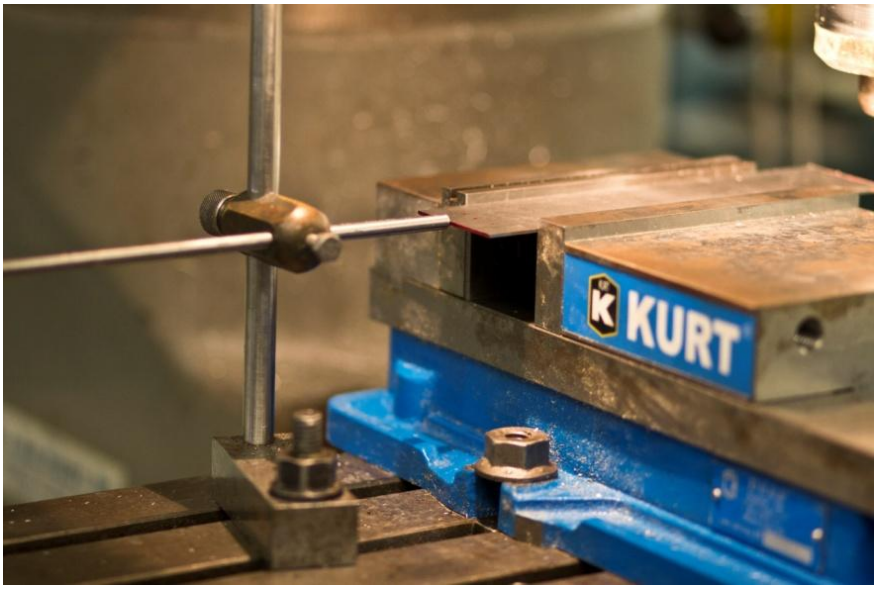

Figure 11. - Image of mill stop positioned at the center of the face sheet

With the shortest face sheet positioned in the vice, one pass is made removing a very small amount of material. The process is repeated with each face sheet until all are faced on one end, and now trimmed to similar lengths. The sheets are then reversed, such that the freshly machined end is now in contact with the mill stop, and the X-Y table is adjusted such that the edge of the end mill is located 8 inches from the mill stop, thus removing the remaining material required to achieve the desired length for the face sheets. The process is repeated until all face sheets have been machined on both ends to the same specification and no red markings remain, shown in Figure 12.

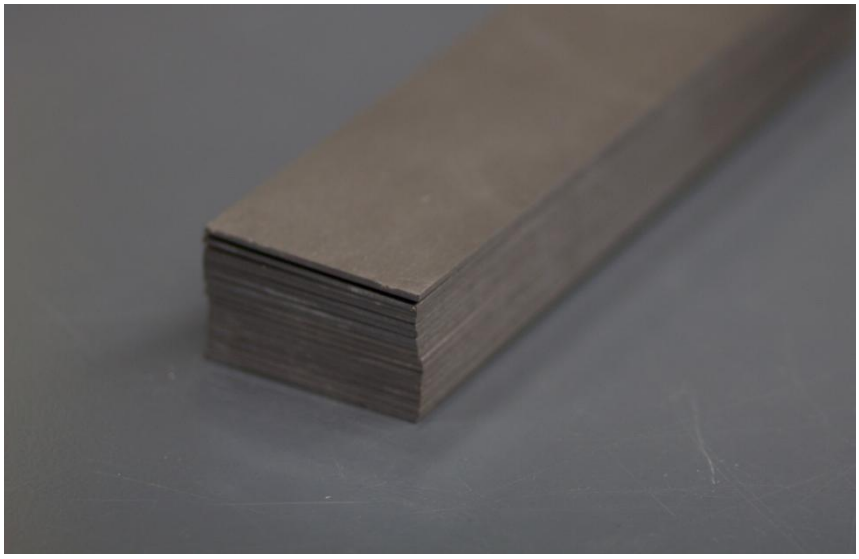

Figure 12. - Image of face sheets after milling edges to desired length

Preparing Sandwich Panel

A fixture comprised of two aluminum plates, one with a through clearance hole and the other with threaded holes. The prepared corrugated layers are stacked back to back in an alternating sinusoidal pattern and placed into the fixture while bolts are hand tightened just enough to apply small compressive force. This allows the layers from slipping drastically when trying to align the layers. The layers are then shifted individually to ensure the layers meet at local maximum and minimums of the sinusoidal shape. A Millermatic 250 metal inert gas welder (M.I.G.) is used to spot weld the nodes where each corrugated layer meet, shown in Figure 13. The process is repeated for the opposing side, thus completing the core element.

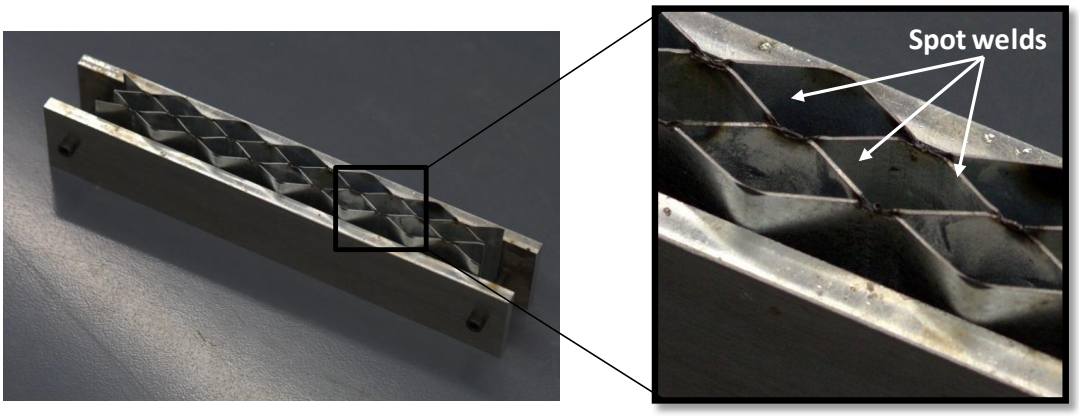

Figure 13. - Image of core being prepared in fixture

The bolts in the fixture are loosened slightly, allowing the face sheets to be moved into position. The center of the face sheet is marked on its edge and is then aligned to the center of the core element. The face sheets are then welded in a similar fashion, completing the sandwich structure, which can be seen in Figure 14.

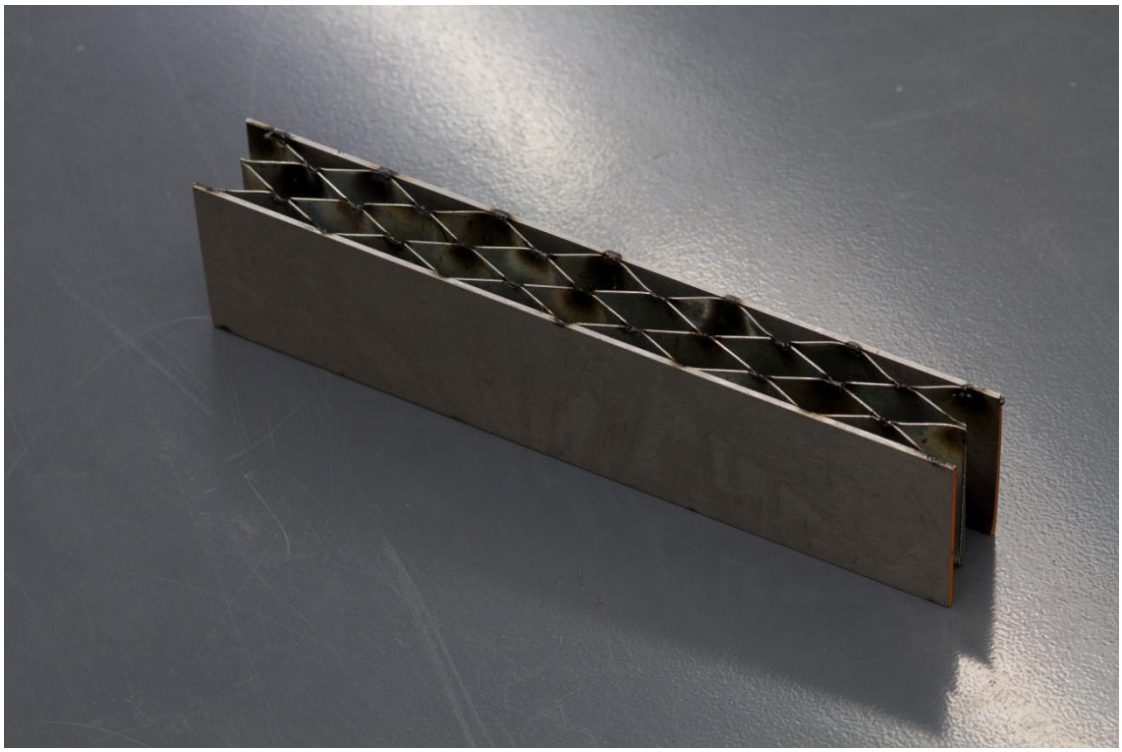

Figure 14. - Image of completed sandwich panel

Schematic A

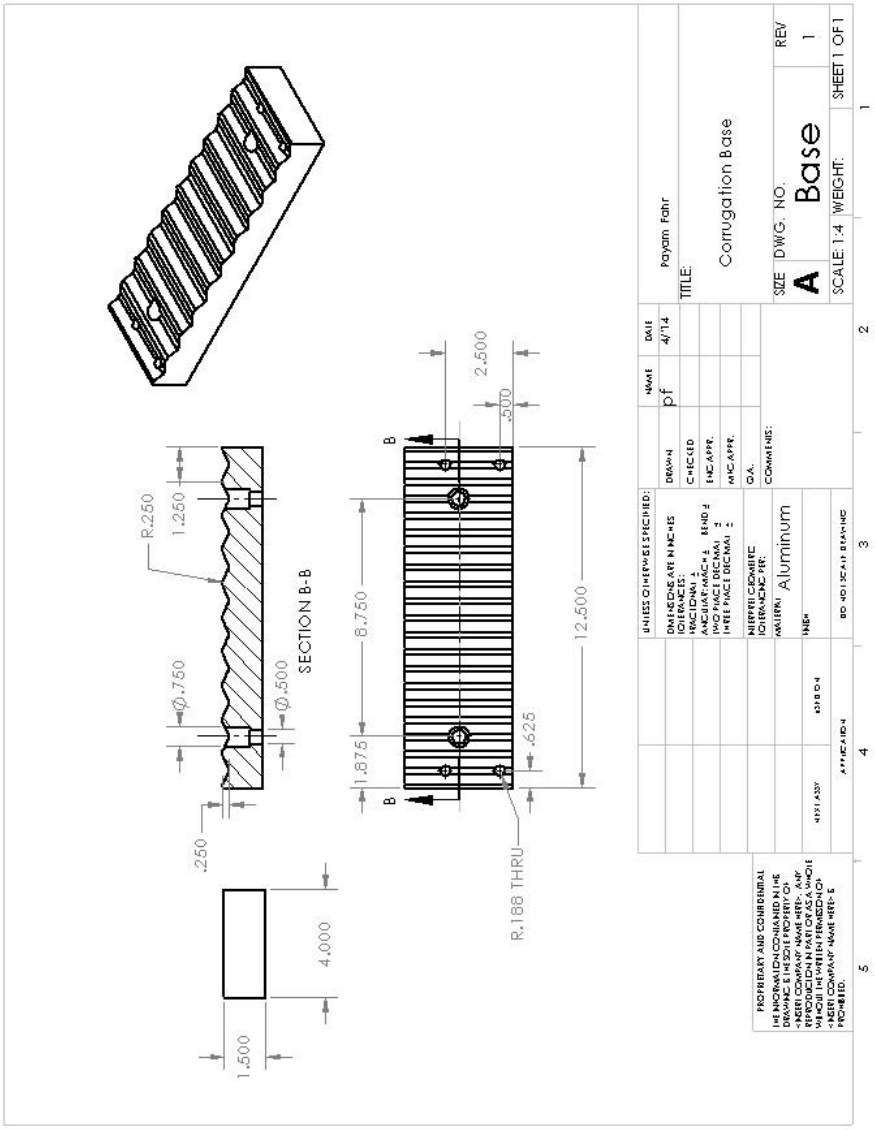
R.250
1.250
Ø.750
Ø.500
SECTION B-B
.250
4.000
1.500
8.750
1.875
2.500
.500
12.500
.625
R.188 THRU
Payam Fahr
Corrugation Base
Aluminum
A
Base
SIZE
DWG. NO.
REV
SCALE: 1:4
WEIGHT:
SHEET 1 OF 1

Schematic B

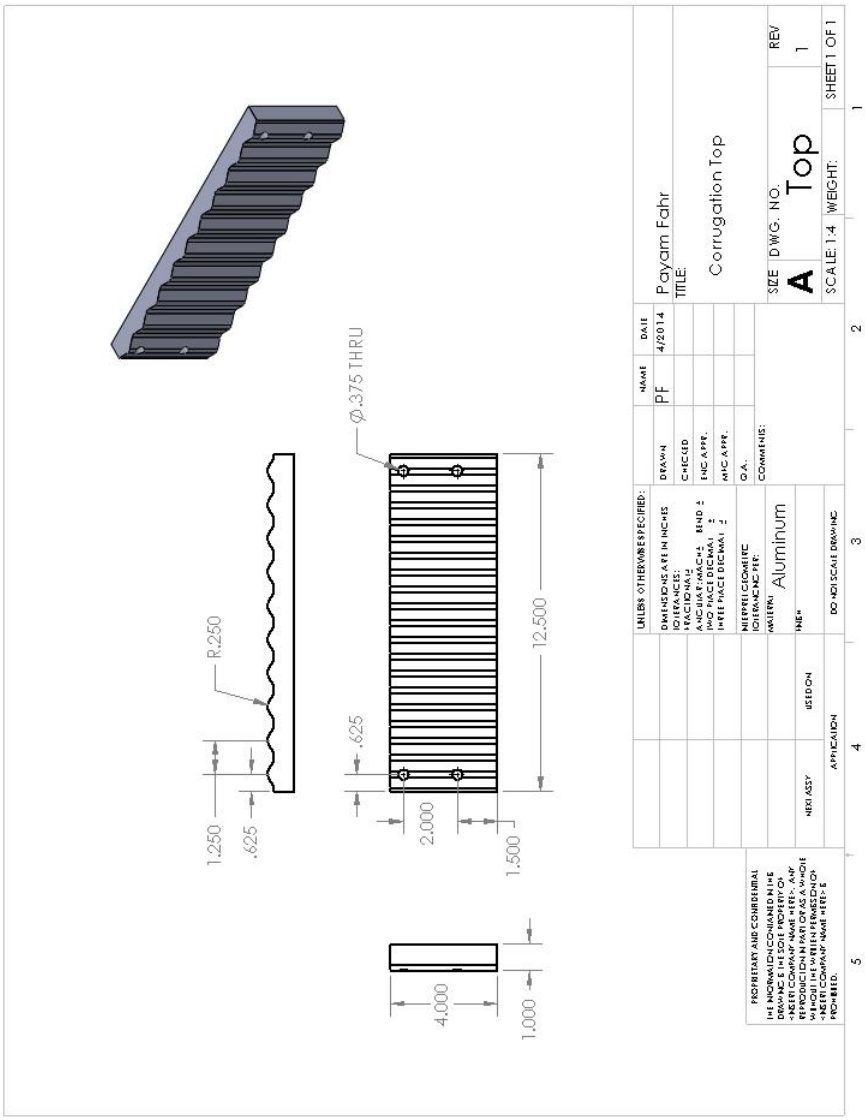
R.250
1.250
.625
Ø.375 THRU
.625
2.000
1.500
12.500
4.000
1.000
Payam Fahr
Corrugation Top
Top
A
SIZE
DWG. NO.
REV
SCALE: 1:4
WEIGHT:
SHEET 1 OF 1

APPENDIX B: METHOD FOR EXTRUDING FILLER MATERIAL

APPENDIX C: DETAILED SCHEMATIC OF EXPERIMENTAL SETUP

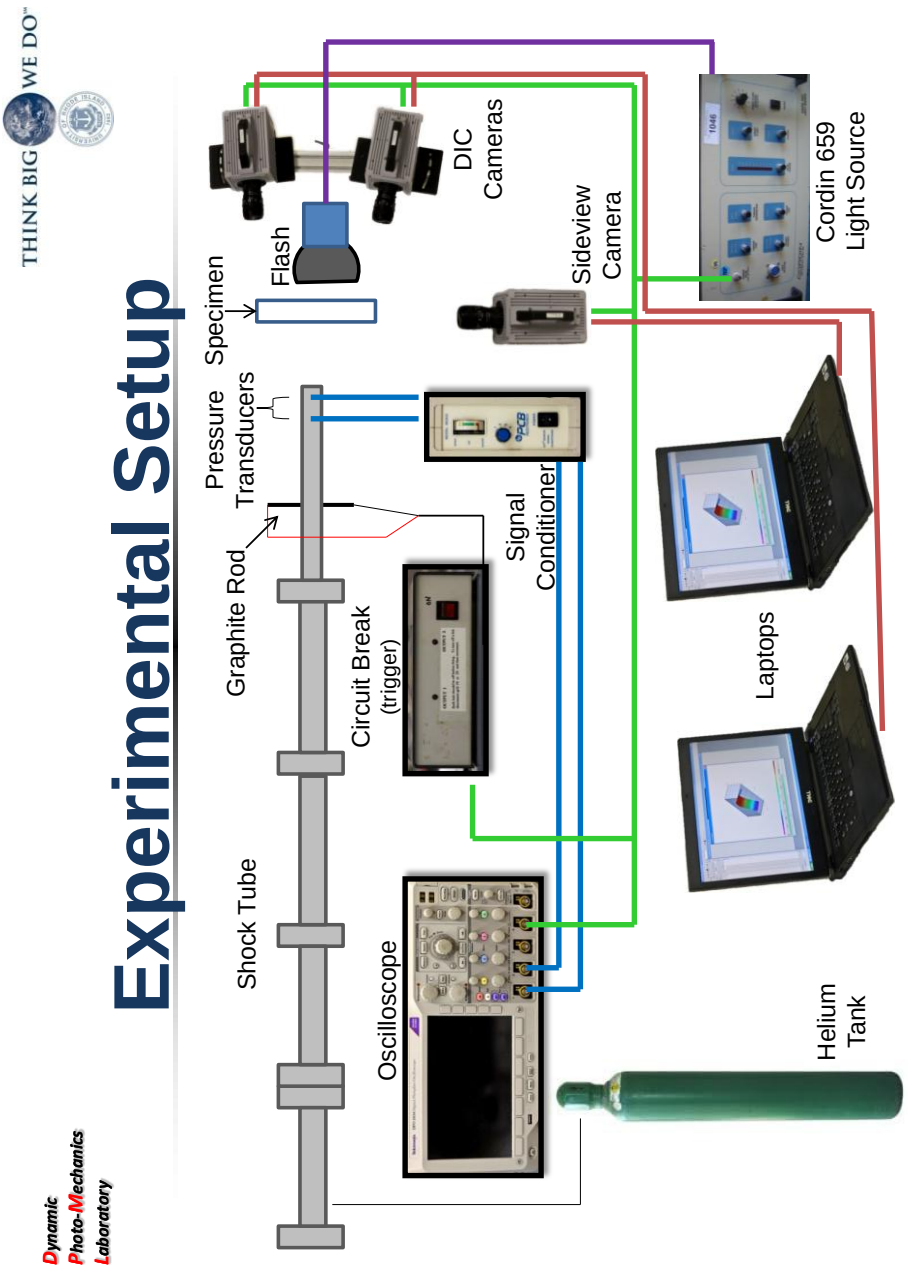

Note: While the use of graphite rod/circuit break is most reliable for triggering, it was later discontinued in favor of using an Oscilloscope capable of generating a negative TTL pulse after a pressure spike was received by the pressure transducers. This was in an effort to reduce any unnecessary transfer of kinetic energy as the graphite particles would strike the specimen.

APPENDIX D: MATLAB CODES

MATLAB Code to analyze side view images

```
%%%%%%%%%%%%%%%%%%%%%%%%%%%%%%%%%%%%
% This program is written by Erheng Wang. The copy right belongs the
% Dynamic Photo-Mechanics Laboratory.
%
% Code has been modified by Payam Fahr to add reference lines for load   % area based on muzzle configuration. July 2013
%
% This program is for calculating the deformation energy of the gas,
% the momentum and the kinetic energy of the specimen in a shock tube
% experiment.
%%%%%%%%%%%%%%%%%%%%%%%%%%%%%%%%%%%%

clear all;
close all;
clc;
format long;

disp('%%%%%%%%%%%%%%%%%%%%%%%%%%%%%%%%%%%%');
disp('This program is for calculating the deformation energy of the gas,');
disp('the momentum and the kinetic energy of the specimen in a shock tube');
disp('experiment.');
disp(' ');
disp('Please follow the instruction.');
disp('%%%%%%%%%%%%%%%%%%%%%%%%%%%%%%%%%%%%');
disp(' ');

disp('%%%%%%%%%%%%%%%%%%%%%%%%%%%%%%%%%%%%');
disp('First Step: load the reflection pressure profile.');
disp(' ');
disp('The reflection pressure profile should have following form:');
disp('0.00001  124');
disp('0.00002  160');
disp('0.00003  215');
disp('0.00004  260');
disp('0.00005  302');
disp('The first column is time. And second column is pressure.');
disp('You need to input the unit of time and pressure. Please check the unit carefully.');
disp('Please follow the instruction.');
disp(' ');

eval(['load ref_sp.dat;'])
disp(' ');
```

```
disp('We have following time unit:');
disp('1. second');
disp('2. millisecond');
disp('3. microsecond');
unit_judge=true;
time_unit=0; % this number can be any integer except 1, 2 and 3.
while unit_judge==true
   time_unit=input('Please choose the unit you use (input the No. before the unit):');
   if time_unit==1
      disp(' ');
      disp('The time unit you use is second;');
      eval(['ref_sp(:,1)=ref_sp(:,1);'])
      unit_judge=false;
   elseif time_unit==2
      disp(' ');
      disp('The time unit you use is millisecond;');
      eval(['ref_sp(:,1)=ref_sp(:,1)./1000;'])
      unit_judge=false;
   elseif time_unit==3
      disp(' ');
      disp('The time unit you use is microsecond;');
      eval(['ref_sp(:,1)=ref_sp(:,1)./1000000;'])
      unit_judge=false;
   else
      disp('Wrong input. Please choose again.');
      unit_judge=true;
   end
end
disp(' ');

disp('We have following pressure unit:');
disp('1. psi');
disp('2. MPa');
disp('3. Pa');
unit_judge=true;
pressure_unit=0; % this number can be any integer except 1, 2 and 3.
while unit_judge==true
   pressure_unit=input('Please choose the unit you use (input the No. before the
unit):');
   if pressure_unit==1
      disp(' ');
      disp('The pressure unit you use is psi;');
      eval(['ref_sp(:,2)=ref_sp(:,2);'])
      unit_judge=false;
   elseif pressure_unit==2
```

```
        disp(' ');
        disp('The pressure unit you use is MPa;');
        eval(['ref_sp(:,2)=ref_sp(:,2).*1000000./6894.7;'])
        unit_judge=false;
    elseif pressure_unit==3
        disp(' ');
        disp('The pressure unit you use is Pa;');
        eval(['ref_sp(:,2)=ref_sp(:,2)./6894.7;'])
        unit_judge=false;
    else
        disp('Wrong input. Please choose again.');
        unit_judge=true;
    end
end
disp(' ');

disp('The pressure data has been resaved into variable ref_sp.');
disp('There are two columns in ref_sp. The first column is time and unit is s (second).');
disp('The second column is pressure and unit is psi.');
disp('First Step end');
disp('%%%%%%%%%%%%%%%%%%%%%%%%%%%%%%%%%%%');
disp(' ');

disp('%%%%%%%%%%%%%%%%%%%%%%%%%%%%%%%%%%%');
disp('Second Step: load the time series of the images.');
disp(' ');

disp('You have three ways to load the time series of the images.');
disp('1. The time between two frames is same.');
disp('   You can input total number of frames and time between two frames.')
disp('   The code will generate the time series automatically.');
disp(' ');

disp('2. The time between two frames is not same.');
disp('    You can input total number of frames and input time between two frames frame by frame.')
disp(' ');

disp('3. The time between two frames is not same.');
disp('   And you have saved the time series into one data file.')
disp('   Then you can just load that time series data file.');
disp(' ');

time_series_judge=true;
time_series=0; % this number can be any integer except 1, 2 and 3.
```

```
while time_series_judge==true
   time_series=input('Please choose which method you want to use (input the No. before the method):');
   if time_series==1
      frames=input('Please input the total number of frames for calculating(integer): '); % the number of images for calculating
      frame_time=input('Please input the time between two frames (unit: microsecond): ')/1000000;
      for i=1:frames
         t_frame(i,1)=(i-1)*frame_time;
      end
      time_series_judge=false;
   elseif time_series==2
      frames=input('Please input the total number of frames for calculating(integer): '); % the number of images for calculating
      sum_time=0;
      for i=1:frames
         disp('recent frame is')
         i
         disp('frame.')
         disp('Please input 0 when i=1;');
         sum_time=input('Please input the time between this frame and one frame before(unit: \mus): ')/1000000+sum_time;
         t_frame(i,1)=sum_time;
      end
      time_series_judge=false;
   elseif time_series==3
      time_series_name=input('Please input the filename of the time serise (without extension):','s')
      time_series_extension=input('Please input the extension of the time serise:','s')
      eval(['load ',time_series_name,'.',time_series_extension,';'])
      eval(['t_frame=',time_series_name,';'])
      time_series_judge=false;
   else
      disp('Wrong input. Please choose again.');
      time_series_judge=true;
   end
end
disp(' ');

disp('Second Step end');
disp('%%%%%%%%%%%%%%%%%%%%%%%%%%%%%%%%%%%%');
disp(' ' );


disp('%%%%%%%%%%%%%%%%%%%%%%%%%%%%%%%%%%%%');
```

```
disp('Third Step: length calibration.');
disp(' ');
disp('you can choose any image for length calibration.');
disp('On the image, you need to choose two points and the vertical distance between these two points will be used to calibrate the length');
disp('Therefore, you need to know one real vertical scale in the image.');
disp('For example:');
disp('the span of the supports is 6 inches');
disp('the outer diameter of the shock tube is 5 inches');
disp('');
disp('The process will repeat three times. Thus, totally you will pick six times');
disp('Please follow the instruction.');
disp(' ');

disp('Please enter image filename for length calibration:');
I=input('(for example: calibration.jpg) ','s');
Judge1='n';
while Judge1=='n'
   % load the jpg file
   imshow(I);
   hold on

   xlabel('Length Calculation')
   title('Please pick first point for calibration');
   [xc(1),yc(1)] = ginput(1);
   title('Please pick second point for calibration');
   [xc(2),yc(2)] = ginput(1);
   title('Please pick third point for calibration');
   [xc(3),yc(3)] = ginput(1);
   title('Please pick fourth point for calibration');
   [xc(4),yc(4)] = ginput(1);
   title('Please pick fifth point for calibration');
   [xc(5),yc(5)] = ginput(1);
   title('Please pick sixth point for calibration');
   [xc(6),yc(6)] = ginput(1);

   title('Please go to the matlab main window and input the real distance');
   % average point between two calibration points
   Y(1) = abs(yc(1)-yc(2));
   Y(2) = abs(yc(3)-yc(4));
   Y(3) = abs(yc(5)-yc(6));
   measured = mean(Y);

   % determine the middle position of the shock tube
   ym(1)=(yc(1)+yc(2))/2;
   ym(2)=(yc(3)+yc(4))/2;
```

```
    ym(3)=(yc(5)+yc(6))/2;
    midy=mean(ym);


    % real distance between two calibration points. unit: m
    true = input('Please input the real distance between two points you choose (in): ')*0.0254;

    % The transform from the pixels to distance
    %~Payam Fahr 7/18/2013
    scale = measured/true
    innerdia = (.75*0.0254*scale); %Select this for SMALL MUZZLE
    %innerdia = (1.5*0.0254*scale) % Select this for LARGE MUZZLE
     %~Payam Fahr 7/18/2013

    xlabel('')
    title('Length Calculation End');

    Judge1=input('Is calibration OK? (y/n)','s');

    close all;
end

disp('Third Step end');
disp('%%%%%%%%%%%%%%%%%%%%%%%%%%%%%%%%%%%%');
disp(' ' );

disp('%%%%%%%%%%%%%%%%%%%%%%%%%%%%%%%%%%%%');
disp('Fourth Step: real measurement.');
disp(' ');
disp('you need to measure the deformation shape of front face for every image.');
disp('For each image, you need to choose seven points on the front face.');
disp('There will be a symmetric line on the image.');
disp('It is better to choose these points symmetric to this line.');
disp('Please follow the instruction.');
disp(' ');

frames = input('Please input the total number of frames for calculating(integer): '); % the number of pictures for calculating
%Tube_d=0.0762;     % the real scale of the large muzzle diameter of shock tube - Payam Fahr
Tube_d=0.0762/2     % the real scale of the large muzzle diameter of shock tube - Payam Fahr

% point_number=input('How many points will you choose for face shape fitting? (integer) ');
```

```
point_number=7;

x=zeros(point_number,frames);
y=zeros(point_number,frames);
for i = 1:frames

   disp(' ');
   if i==1
      disp('Please enter the first image filename for measurement:');
      I=input('(for example: measure_image.jpg) ','s');
   else
      I=input('Please enter next image filename for measurement: ','s');
   end


   % Simulate the Front Surface Shape with Cubic Spline interpolation method
   Judge2='n';
   while Judge2=='n'
      imshow(I);
      hold on;
      xlabel('Simulate the Front Surface');

      %~Payam Fahr 7/18/2013
      plot ([0;1200],[midy;midy],'r'), hold on
      plot ([0;1200],[midy+innerdia;midy+innerdia],'r'), hold on
      plot ([0;1200],[midy-innerdia;midy-innerdia],'r'), hold on
      % Given the scale based on picked points and length input, this
      % will project horizontal markers on the centerline of specimen and
      % the upper and lower boundaries of the inner diameter of the
      % muzzle depending on which has been selected above (large or
      % small) This will aid in keeping all profile measurements about
      % the loading area
      %~Payam Fahr 7/18/2013

      title('Please pick the top point for shape calculation');
      [x(1,i),y(1,i)] = ginput(1);
      plot(x(1,i),y(1,i),'go'),hold on;

      title('Please pick the bottom point for shape calculation');
      [x(7,i),y(7,i)] = ginput(1);
      plot(x(7,i),y(7,i),'go'),hold on;

      for j=1:point_number
         yfl(j,1)=(y(1,i)+y(7,i))/2-abs(y(1,i)-y(7,i))/2+(j-1)*abs(y(1,i)-
y(7,i))/(point_number-1);
```

```
        end
        x1=linspace(0,1200);
        for j=1:point_number
           clear y1;
           y1=linspace(yfl(j),yfl(j));
           plot(x1,y1,'c'), hold on;
        end
%        if i==1
%        else
%           plot(xx(:,(i-1)),yy(:,(i-1)),'y','linewidth',0.25), hold on;
%           legend('symmetric line','previous shape');
%        end

        % choose seven points for the surface shape fit

        title('Please pick the second point for shape calculation');
        [x(2,i),y(2,i)] = ginput(1);
        plot(x(2,i),y(2,i),'go'),hold on;

        title('Please pick the third point for shape calculation');
        [x(3,i),y(3,i)] = ginput(1);
        plot(x(3,i),y(3,i),'go'),hold on;

        title('Please pick the fourth point for shape calculation');
        [x(4,i),y(4,i)] = ginput(1);
        plot(x(4,i),y(4,i),'go'),hold on;

        title('Please pick the fifth point for shape calculation');
        [x(5,i),y(5,i)] = ginput(1);
        plot(x(5,i),y(5,i),'go'),hold on;

        title('Please pick the sixth point for shape calculation');
        [x(6,i),y(6,i)] = ginput(1);
        plot(x(6,i),y(6,i),'go'),hold on;

% d=Tube_d*scale;
% the pixes scale of the diameter of shock tube
        dD=abs(y(1,i)-y(7,i))/100;
        dd=Tube_d*scale/100;
        for m=1:101
           yy(m,i)=(y(1,i)+y(7,i))/2-abs(y(1,i)-y(7,i))/2+(m-1)*dD;
% the range of shock applied
           yys(m,i)=midy-(Tube_d*scale/2)+(m-1)*dd;
% the range of shock applied
        end
        xx(:,i)=spline(y(:,i),x(:,i),yy(:,i));
```

```
% cubic spline data interpolation
      xxs(:,i)=spline(y(:,i),x(:,i),yys(:,i));
% cubic spline data interpolation
      plot(xx(:,i),yy(:,i),'r'), hold on;
      plot(xxs(:,i),yys(:,i),'g'), hold on;

      title('Press any key to continue');
      pause;

      Judge2=input('Is that curve OK? (y/n)','s');

      close all;
   end
end

disp('Fourth Step end');
disp('%%%%%%%%%%%%%%%%%%%%%%%%%%%%%%%%%%%%');
disp(' ' );

disp('%%%%%%%%%%%%%%%%%%%%%%%%%%%%%%%%%%%%');
disp('Fifth Step: real measurement.');
disp(' ');
disp('The measured position of the specimen will be used to calculate the force
displacement, ');
disp('velocity of the specimen.');
disp('Most parts of this step are automatic.');
disp('Please follow the instruction.');
disp(' ');

% calculate the surface position of every frame
xf=xx(:,1);
yf=yy(:,1);
xfs=xxs(:,1);
yfs=yys(:,1);

specimen_M=input('Please input the total mass of the specimen (g):   ')/1000;
sumimpulse(:,1)=t_frame;
sumyimpulse(:,1)=t_frame;
sumKE(:,1)=t_frame;
for i = 1:frames
   sumimpulse(i,2)=0;
   sumyimpulse(i,2)=0;
   sumKE(i,2)=0;
   for j=1:101
      xd(j,i)=(xx(j,i)-xf(i))/scale;
      yd(j,i)=(yy(j,i)-yf(i))/scale;
```

```
      xds(j,i)=(xxs(j,i)-xfs(i))/scale;
      yds(j,i)=(yys(j,i)-yfs(i))/scale;
      if i==1
         xv(j,i)=0;
         yv(j,i)=0;
         average_v(j,i)=0;
      else
         xv(j,i)=((xx(j,i-1)-xx(j,i))/scale)/frame_time;
         yv(j,i)=((yy(j,i-1)-yy(j,i))/scale)/frame_time;
         average_v(j,i)=sqrt(xv(j,i)^2+yv(j,i)^2);
      end
      sumimpulse(i,2)=sumimpulse(i,2)+(specimen_M/101)*xv(j,i);
      sumyimpulse(i,2)=sumyimpulse(i,2)+(specimen_M/101)*yv(j,i);
      sumKE(i,2)=sumKE(i,2)+((specimen_M/101)*average_v(j,i)^2)/2;
   end
end

% calculate the deflection for every points of every frame

for j=1:101;
   for i=1:frames
      xdd(j,i)=abs(xd(j,i)-xd(j,1));
      ydd(j,i)=abs(yd(j,i)-yd(j,1));
      xdds(j,i)=abs(xds(j,i)-xds(j,1));
      ydds(j,i)=abs(yds(j,i)-yds(j,1));
   end
end

% figure(2)
% for i=1:frames;
%     plot(-xdd(:,i),yy(:,i)/scale,'k'),hold on
%     plot(-xdd(:,2),yy(:,1)/scale,'k--'),hold on
%     plot(-xdd(:,3),yy(:,1)/scale,'r'),hold on
%     plot(-xdd(:,4),yy(:,1)/scale,'r--'),hold on
%     plot(-xdd(:,5),yy(:,1)/scale,'g'),hold on
%     plot(-xdd(:,6),yy(:,1)/scale,'g--'),hold on
%     plot(-xdd(:,7),yy(:,1)/scale,'b'),hold on
%     plot(-xdd(:,8),yy(:,1)/scale,'b--'),hold on
%     plot(-xdd(:,9),yy(:,1)/scale,'m'),hold on
% end
% plot(-xdd(:,10),yy(:,1)/scale,'m--'),hold on
% plot(-xdd(:,11),yy(:,1)/scale,'y'),hold on
% plot(-xdd(:,12),yy(:,1)/scale,'c'),hold on
% plot(-xdd(:,13),yy(:,1)/scale,'c--'),hold on
% xlabel('unit: m');
% ylabel('unit: m');
```

```
% title('Deflection Sketch');
% axis tight

% choose the biggest time to normalize data

for i=1:10000
   t(i,1)=(i-1)*2E-6;
   if (t(i,1)>=t_frame(frames,1))
      break;
   end
end

ref=spline(ref_sp(:,1),ref_sp(:,2),t);

% normalize the time for deflection data
for j=1:101
   De(:,j)=spline(t_frame,xdd(j,:),t);
   Des(:,j)=spline(t_frame,xdds(j,:),t);
end

S_x_impulse(:,1)=t;
S_x_impulse(:,2)=spline(sumimpulse(:,1),sumimpulse(:,2),t);


%~Payam Fahr 7/18/2013
%S_y_impulse(:,1)=t;
%S_y_impulse(:,2)=spline(sumyimpulse(:,2),sumyimpulse(:,2),t);
%This is causing error possibly because there is no deviation in y
%direction if points are selected on the projected horizontal points
%~Payam Fahr 7/18/2013

S_KE(:,1)=t;
S_KE(:,2)=spline(sumKE(:,1),sumKE(:,2),t);

% calculate the energy increase between every two closed frame
n0=length(t);
egy(1)=0;
delta_d=(Tube_d*0.99)/99;
for i=2:n0
   A(i)=0;
   for j=1:100
      B(j)=((ref(i)+ref(i-1))*6894.7)*(Des(i,j)-Des(i-1,j))*delta_d*(sqrt((Tube_d/2)^2-
((Tube_d/2)-j*delta_d)^2)+sqrt((Tube_d/2)^2-((Tube_d/2)-(j-1)*delta_d)^2))/2;
      A(i)=B(j)+A(i);
   end
   egy(i)=A(i);
```

```
end

% calculate the energy increase between every frame and initial frame
for i=1:n0
   A1=0;
   for j=1:i
      B1=egy(j);
      A1=A1+B1;
   end
   energy(i,1)=A1;
end

DFLE(:,1)=t;
DFLE(:,2)=energy(:,1);

Center(:,1)=t;
Center(:,2)=De(:,51);

figure(1)
plot(t,De(:,51),'r','linewidth',3),hold on
ylabel('Deflection (m)');
xlabel('Time (s)');
grid on;
title('Maxi Deflection-Time Curve(Middle Point)');

figure(2),plot(t,S_x_impulse(:,2),'r','linewidth',3);
xlabel('Time (s)');
ylabel('Horizontal momentum (kgm/s or Ns)');
% axis tight;
grid on;

%~ Payam Fahr 7/18/2013
%figure(3),plot(t,S_y_impulse(:,2),'r','linewidth',3);
%xlabel('Time (s)');
%ylabel('Vertical momentum (kgm/s or Ns)');
% axis tight;
%grid on;
%~ Payam Fahr 7/18/2013

figure(3),plot(t,S_KE(:,2),'r','linewidth',3);
xlabel('Time (s)');
ylabel('Kinetic Energy (J)');
% axis tight;
grid on;

figure(4),plot(t,energy(:,1),'r','linewidth',3);
```

```
xlabel('Time (s)');
ylabel('Deformation Energy (J)');
% axis tight;
grid on;

disp(' ');
disp('After runing this code, there will be Five dat files with following name: ');
disp('filename_deformation_E.DAT            Deformation energy');
disp('filename_x_momentum.DAT               Horizontal momentum');
%~ Payam Fahr 7/18/2013
%disp('filename_y_momentum.DAT              Vertical momentum');
%~ Payam Fahr 7/18/2013
disp('filename_Kinetic_E.DAT                Kinetic energy');
disp('filename_center_displacement.DAT      Center displacement');
disp(' ');
disp('All of other data have been save into the file entitled filename_specimen.mat.');

filename=input('Now, please input the filename you want to save the final data into:
','s');

eval(['save ',filename,'_specimen.mat'])
eval(['save ',filename,'_deformation_E.DAT',' DFLE',' /ascii'])
eval(['save ',filename,'_x_momentum.DAT',' S_x_impulse',' /ascii'])
%~ Payam Fahr 7/18/2013
%eval(['save ',filename,'_y_momentum.DAT',' S_y_impulse',' /ascii'])
%~ Payam Fahr 7/18/2013
eval(['save ',filename,'_Kinetic_E.DAT',' S_KE',' /ascii'])
eval(['save ',filename,'_center_displacement.DAT',' Center',' /ascii'])

disp('Fifth Step end');
disp('%%%%%%%%%%%%%%%%%%%%%%%%%%%%%%%%%%%%%%%%%%%%%%%%%%%%%%%%%%%%%%%%%%%%%%');
disp(' ' );
```

APPENDIX E: 3M™ Glass Bubbles (Types A and D) MSDS and Data Sheet

Safety Data Sheet

Document Group:	11-4410-4	**Version Number:**	37.07
Issue Date:	12/13/13	**Supercedes Date:**	11/25/13

SECTION 1: Identification

1.1. Product identifier
3M™ Glass Bubbles, Types A and D

Product Identification Numbers
70-0704-8395-6, 70-0704-8396-4, 70-0704-8398-0, 75-0299-0514-0, 75-0299-0517-3, 75-0299-0521-5, 75-5410-0014-9, 75-5800-0032-3, 75-5800-0035-6

1.2. Recommended use and restrictions on use

Recommended use
Lightweight Filler

1.3. Supplier's details

MANUFACTURER:	3M
DIVISION:	Advanced Materials Division
ADDRESS:	3M Center, St. Paul, MN 55144-1000, USA
Telephone:	1-888-3M HELPS (1-888-364-3577)

1.4. Emergency telephone number
1-800-364-3577 or (651) 737-6501 (24 hours)

SECTION 2: Hazard identification

2.1. Hazard classification
Not classified as hazardous according to OSHA Hazard Communication Standard, 29 CFR 1910.1200.

2.2. Label elements
Signal word
Not applicable.

Symbols
Not applicable.

Pictograms
Not applicable.

2.3. Hazards not otherwise classified

None.

SECTION 3: Composition/information on ingredients

Ingredient	C.A.S. No.	% by Wt
Soda Lime Bororsilicate Glass	65997-17-3	> 99
Chromium, Aqua Chloro Hydroxy Methacrylate Complexes	111031-82-4	< 1

SECTION 4: First aid measures

4.1. Description of first aid measures

Inhalation:
No need for first aid is anticipated.

Skin Contact:
Wash with soap and water. If signs/symptoms develop, get medical attention.

Eye Contact:
Flush with large amounts of water. Remove contact lenses if easy to do. Continue rinsing. If signs/symptoms persist, get medical attention.

If Swallowed:
Rinse mouth. If you feel unwell, get medical attention.

4.2. Most important symptoms and effects, both acute and delayed
See Section 11.1. Information on toxicological effects.

4.3. Indication of any immediate medical attention and special treatment required
Not applicable

SECTION 5: Fire-fighting measures

5.1. Suitable extinguishing media
Material will not burn. Non-combustible. Use a fire fighting agent suitable for surrounding fire.

5.2. Special hazards arising from the substance or mixture
None inherent in this product.

5.3. Special protective actions for fire-fighters
No unusual fire or explosion hazards are anticipated.

SECTION 6: Accidental release measures

6.1. Personal precautions, protective equipment and emergency procedures
Ventilate the area with fresh air. Refer to other sections of this SDS for information regarding physical and health hazards, respiratory protection, ventilation, and personal protective equipment.

6.2. Environmental precautions
Avoid release to the environment.

6.3. Methods and material for containment and cleaning up

Collect as much of the spilled material as possible. Use wet sweeping compound or water to avoid dusting. Sweep up. Place in a closed container approved for transportation by appropriate authorities. Clean up residue. Seal the container. Dispose of collected material as soon as possible.

SECTION 7: Handling and storage

7.1. Precautions for safe handling
For industrial or professional use only. Avoid breathing dust/fume/gas/mist/vapors/spray. Do not eat, drink or smoke when using this product. Wash thoroughly after handling.

7.2. Conditions for safe storage including any incompatibilities
No special storage requirements.

SECTION 8: Exposure controls/personal protection

8.1. Control parameters

Occupational exposure limits

Ingredient	C.A.S. No.	Agency	Limit type	Additional Comments
CHROMIUM (III) COMPOUNDS	111031-82-4	US Dept of Labor - OSHA	TWA(as Cr):0.5 mg/m3	
Chromium, insoluble salts	111031-82-4	US Dept of Labor - OSHA	TWA(as Cr):1 mg/m3	
Soda Lime Bororsilicate Glass	65997-17-3	Manufacturer determined	TWA(as dust):10 mg/m3	

Amer Conf of Gov. Indust. Hyg. : American Conference of Governmental Industrial Hygienists
American Indust. Hygiene Assoc : American Industrial Hygiene Association
Chemical Manufacturer Rec Guid : Chemical Manufacturer's Recommended Guidelines
US Dept of Labor - OSHA : United States Department of Labor - Occupational Safety and Health Administration
TWA: Time-Weighted-Average
STEL: Short Term Exposure Limit
CEIL: Ceiling

8.2. Exposure controls

8.2.1. Engineering controls
Provide local exhaust ventilation at transfer points. Use general dilution ventilation and/or local exhaust ventilation to control airborne exposures to below relevant Exposure Limits and/or control dust/fume/gas/mist/vapors/spray. If ventilation is not adequate, use respiratory protection equipment.

8.2.2. Personal protective equipment (PPE)

Eye/face protection

Wear eye/face protection. Select and use eye/face protection to prevent contact based on the results of an exposure assessment. The following eye/face protection(s) are recommended:
Safety Glasses with side shields

Skin/hand protection
Select and use gloves and/or protective clothing approved to relevant local standards to prevent skin contact based on the results of an exposure assessment. Selection should be based on use factors such as exposure levels, concentration of the substance or mixture, frequency and duration, physical challenges such as temperature extremes, and other use conditions. Consult with your glove and/or protective clothing manufacturer for selection of appropriate compatible gloves/protective clothing. Wear appropriate gloves to minimize risk of injury to skin from contact with dust or physical abrasion from grinding or sanding.

Gloves made from the following material(s) are recommended: Neoprene
Nitrile Rubber

Respiratory protection

Wear respiratory protection if ventilation is inadequate to prevent overexposure. An exposure assessment may be needed to decide if a respirator is required. If a respirator is needed, use respirators as part of a full respiratory protection program. Based on the results of the exposure assessment, select from the following respirator type(s) to reduce inhalation exposure: Half facepiece or full facepiece air-purifying respirator suitable for particulates

For questions about suitability for a specific application, consult with your respirator manufacturer.

SECTION 9: Physical and chemical properties

9.1. Information on basic physical and chemical properties

General Physical Form:	Solid
Specific Physical Form:	Low Density Fine Powder (< 200 microns)
Odor, Color, Grade:	White, Odorless
Odor threshold	*Not Applicable*
Melting point	*No Data Available*
Boiling Point	*Not Applicable*
Flash Point	*Not Applicable*
Evaporation rate	*Not Applicable*
Flammability (solid, gas)	Not Classified
Flammable Limits(LEL)	*Not Applicable*
Flammable Limits(UEL)	*Not Applicable*
Vapor Pressure	*Not Applicable*
Vapor Density	*Not Applicable*
Density	0.1 - 0.6 g/cm3
Specific Gravity	0.1 - 0.6 [*Ref Std:* WATER=1]
Solubility in Water	Negligible
Solubility- non-water	*Not Applicable*
Partition coefficient: n-octanol/ water	*No Data Available*
Autoignition temperature	*Not Applicable*
Decomposition temperature	*Not Applicable*
Viscosity	*Not Applicable*
Volatile Organic Compounds	*Not Applicable*
Percent volatile	< 0.5 % weight
Softening point	>=600 ºC
VOC Less H2O & Exempt Solvents	*Not Applicable*

SECTION 10: Stability and reactivity

10.1. Reactivity
This material is considered to be non reactive under normal use conditions.

10.2. Chemical stability
Stable.

10.3. Possibility of hazardous reactions
Hazardous polymerization will not occur.

10.4. Conditions to avoid
None known.

10.5. Incompatible materials
None known.

10.6. Hazardous decomposition products

Substance	Condition
None known.	Not Specified

SECTION 11: Toxicological information

The information below may not be consistent with the material classification in Section 2 if specific ingredient classifications are mandated by a competent authority. In addition, toxicological data on ingredients may not be reflected in the material classification and/or the signs and symptoms of exposure, because an ingredient may be present below the threshold for labeling, an ingredient may not be available for exposure, or the data may not be relevant to the material as a whole.

11.1. Information on Toxicological effects

Signs and Symptoms of Exposure

Based on test data and/or information on the components, this material may produce the following health effects:

Inhalation:
No health effects are expected.

Skin Contact:
Mechanical Skin irritation: Signs/symptoms may include abrasion, redness, pain, and itching.

Eye Contact:
Mechanical eye irritation: Signs/symptoms may include pain, redness, tearing and corneal abrasion.

Ingestion:
May be harmful if swallowed.
Gastrointestinal Irritation: Signs/symptoms may include abdominal pain, stomach upset, nausea, vomiting and diarrhea.

Additional Information:
This product, when used under reasonable conditions and in accordance with the 3M directions for use, should not present a health hazard. However, use or processing of the product in a manner not in accordance with the product's directions for use may affect the performance of the product and may present potential health and safety hazards.

Toxicological Data

Acute Toxicity

Name	Route	Species	Value
Overall product	Ingestion		No data available; calculated ATE 2,500 mg/kg
Soda Lime Borosilicate Glass	Dermal		LD50 estimated to be > 5,000 mg/kg
Soda Lime Borosilicate Glass	Ingestion		LD50 estimated to be 2,000 - 5,000 mg/kg
Chromium, Aqua Chloro Hydroxy Methacrylate Complexes			Data not available or insufficient for classification

ATE = acute toxicity estimate

Skin Corrosion/Irritation

Name	Species	Value
Soda Lime Borosilicate Glass		No significant irritation
Chromium, Aqua Chloro Hydroxy Methacrylate Complexes		Data not available or insufficient for classification

Serious Eye Damage/Irritation

Name	Species	Value
Soda Lime Borosilicate Glass		No significant irritation
Chromium, Aqua Chloro Hydroxy Methacrylate Complexes		Data not available or insufficient for classification

Skin Sensitization

Name	Species	Value
Soda Lime Borosilicate Glass		Data not available or insufficient for classification
Chromium, Aqua Chloro Hydroxy Methacrylate Complexes		Data not available or insufficient for classification

Respiratory Sensitization

Name	Species	Value
Soda Lime Borosilicate Glass		Data not available or insufficient for classification
Chromium, Aqua Chloro Hydroxy Methacrylate Complexes		Data not available or insufficient for classification

Germ Cell Mutagenicity

Name	Route	Value
Soda Lime Borosilicate Glass	In Vitro	Some positive data exist, but the data are not sufficient for classification
Chromium, Aqua Chloro Hydroxy Methacrylate Complexes		Data not available or insufficient for classification

Carcinogenicity

Name	Route	Species	Value
Soda Lime Borosilicate Glass	Inhalation	Multiple animal species	Some positive data exist, but the data are not sufficient for classification
Chromium, Aqua Chloro Hydroxy Methacrylate Complexes			Data not available or insufficient for classification

Reproductive Toxicity

Reproductive and/or Developmental Effects

Name	Route	Value	Species	Test Result	Exposure Duration
Soda Lime Borosilicate Glass		Data not available or insufficient for classification			
Chromium, Aqua Chloro Hydroxy Methacrylate Complexes		Data not available or insufficient for classification			

Target Organ(s)

Specific Target Organ Toxicity - single exposure

Name	Route	Target Organ(s)	Value	Species	Test Result	Exposure Duration
Chromium, Aqua Chloro Hydroxy Methacrylate Complexes			Data not available or insufficient for classification			

Specific Target Organ Toxicity - repeated exposure

Name	Route	Target Organ(s)	Value	Species	Test Result	Exposure Duration
Soda Lime Borosilicate Glass	Inhalation	respiratory system	Some positive data exist, but the data are not sufficient for classification	Human	NOAEL not available	occupational exposure
Chromium, Aqua Chloro Hydroxy Methacrylate			Data not available or insufficient for classification			

Complexes						

Aspiration Hazard

Name	Value
Soda Lime Borosilicate Glass	Not an aspiration hazard
Chromium, Aqua Chloro Hydroxy Methacrylate Complexes	Not an aspiration hazard

Please contact the address or phone number listed on the first page of the SDS for additional toxicological information on this material and/or its components.

SECTION 12: Ecological information

Ecotoxicological information

Please contact the address or phone number listed on the first page of the SDS for additional ecotoxicological information on this material and/or its components.

Chemical fate information

Please contact the address or phone number listed on the first page of the SDS for additional chemical fate information on this material and/or its components.

SECTION 13: Disposal considerations

13.1. Disposal methods

Dispose of contents/ container in accordance with the local/regional/national/international regulations.

Dispose of waste product in a permitted industrial waste facility.

EPA Hazardous Waste Number (RCRA): Not regulated

SECTION 14: Transport Information

Not regulated per U.S. DOT, IATA or IMO.

These transportation classifications are provided as a customer service. ***As the shipper YOU remain responsible for complying with all applicable laws and regulations, including proper transportation classification and packaging.*** *3M transportation classifications are based on product formulation, packaging, 3M policies and 3M understanding of applicable current regulations. 3M does not guarantee the accuracy of this classification information. This information applies only to transportation classification and* ***not*** ***the packaging, labeling, or marking requirements.*** *The original 3M package is certified for U.S. ground shipment only. If you are shipping by air or ocean, the package may not meet applicable regulatory requirements.*

SECTION 15: Regulatory information

15.1. US Federal Regulations

Contact 3M for more information.

311/312 Hazard Categories:

Fire Hazard - No Pressure Hazard - No Reactivity Hazard - No Immediate Hazard - Yes Delayed Hazard - No

15.2. State Regulations

Contact 3M for more information.

California Proposition 65

Ingredient	C.A.S. No.	Classification
GLASS FILAMENTS	None	Carcinogen

WARNING: This product contains a chemical known to the State of California to cause cancer.

15.3. Chemical Inventories

This product is an article as defined by TSCA regulations, and is exempt from TSCA Inventory listing requirements.

This product complies with the New Zealand Hazardous Substances and New Organisms Act (1996).

Contact 3M for more information.

15.4. International Regulations

Contact 3M for more information.

This SDS has been prepared to meet the U.S. OSHA Hazard Communication Standard, 29 CFR 1910.1200.

SECTION 16: Other information

NFPA Hazard Classification
Health: 1 **Flammability:** 0 **Instability:** 0 **Special Hazards:** None

National Fire Protection Association (NFPA) hazard ratings are designed for use by emergency response personnel to address the hazards that are presented by short-term, acute exposure to a material under conditions of fire, spill, or similar emergencies. Hazard ratings are primarily based on the inherent physical and toxic properties of the material but also include the toxic properties of combustion or decomposition products that are known to be generated in significant quantities.

HMIS Hazard Classification
Health: 1 **Flammability:** 0 **Physical Hazard:** 0 **Personal Protection:** X - See PPE section.

Hazardous Material Identification System (HMIS® III) hazard ratings are designed to inform employees of chemical hazards in the workplace. These ratings are based on the inherent properties of the material under expected conditions of normal use and are not intended for use in emergency situations. HMIS® III ratings are to be used with a fully implemented HMIS® III program. HMIS® is a registered mark of the American Coatings Association (ACA).

Document Group:	11-4410-4	**Version Number:**	37.07
Issue Date:	12/13/13	**Supercedes Date:**	11/25/13

DISCLAIMER: The information in this Safety Data Sheet (SDS) is believed to be correct as of the date issued. 3M MAKES NO WARRANTIES, EXPRESSED OR IMPLIED, INCLUDING, BUT NOT LIMITED TO, ANY IMPLIED WARRANTY OF MERCHANTABILITY OR FITNESS FOR A PARTICULAR PURPOSE OR COURSE OF PERFORMANCE OR USAGE OF TRADE. User is responsible for determining whether the 3M product is fit for a particular purpose and suitable for user's method of use or application. Given the variety of factors that can affect the use and application of a 3M product, some of which are uniquely within the user's knowledge and control, it is essential that the user evaluate the 3M product to determine whether it is fit for a particular purpose and suitable for user's method of use or application.

3M provides information in electronic form as a service to its customers. Due to the remote possibility that electronic transfer may have resulted in errors, omissions or alterations in this information, 3M makes no representations as to its completeness or accuracy. In addition, information obtained from a database may not be as current as the information in the SDS available directly from 3M

3M™ Glass Bubbles
Floated Product Series

Introduction

3M™ Glass Bubbles are engineered hollow glass microspheres that are alternatives to conventional fillers and additives such as silicas, calcium carbonate, talc, clay, etc., for many demanding applications. These low-density particles are used in a wide range of industries to reduce part weight, lower costs and enhance product properties.

The spherical shape of 3M glass bubbles offers a number of important benefits, including: higher filler loading, lower viscosity/improved flow, and reduced shrinkage and warpage. It also helps the 3M glass bubbles blend readily into compounds, and makes them adaptable to a variety of production processes, including spraying, casting and molding. In addition, they offer greater survivability under demanding processing conditions, such as injection molding, and also produce stable voids, which results in low thermal conductivity and a low dielectric constant.

The chemically stable soda-lime-borosilicate glass composition of 3M glass bubbles provides excellent water resistance, to create more stable emulsions. They are also non-combustible and non-porous, so they do not absorb resin. And, their low alkalinity gives 3M glass bubbles compatibility with most resins, stable viscosity and long shelf life.

3M Glass Bubbles Floated Series offer the same combination of strength and light weight as standard 3M glass bubbles, with an added surface treatment of special coupling agents, for use in high-tech applications such as aerospace and hydrospace syntactic foam, radomes and printed wire boards.

They are available in a variety of sizes and grades for various product and processing requirements.

Typical Properties (Not for specification purposes)

Nitrogen Isostatic Crush Strength (3M QCM 14.1.5)

Product	Test Pressure (psi)	Target Fractional Survival	Minimum Fractional Survival
A16/500	500	90%	80%
A20/1000	1,000	90%	80%
H20/1000	1,000	90%	80%
D32/4500	4,500	90%	80%
H50/10,000 EPX*	6,000	90%	90%

*Per ASTM D3102-78 in glycerol.

True Density (3M QCM 14.24.6)

Product	Typical	True Density (g/cc)	
		Minimum	Maximum
A16/500	0.16	0.14	0.18
A20/1000	0.20	0.18	0.22
H20/1000	0.20	0.18	0.22
D32/4500	0.32	0.30	0.34
H50/10,000 EPX	0.50	0.48	0.52

Chemical Resistance

In general, the chemical properties of 3M glass bubbles resemble those of a soda-lime-borosilicate glass.

Surface Treatment

A16/500, A20/1000 and D32/4500 glass bubbles have methacrylato chromic chloride surface treatment, H20/1000 and H50/10,000 EPX glass bubbles have epoxy silane surface treatment.

Packing Factor (Ratio of bulk density to true particle density)

Varies from 55% to 68%.

Oil Absorption

31-36 g oil/100 cc of 3M glass bubbles, per ASTM D1483.

Typical Properties (Continued)

Thermal Properties: Conductivity

0.06-0.16 W/m•K at 68°F (20°C), based on theoretical calculations. Conductivity increases with temperature and product density. The thermal conductivity of a composite will depend on the matrix material and volume loading of 3M glass bubbles.

Thermal Properties: Stability

Appreciable changes in bubble properties may occur above 1112°F (600°C) depending on temperature and duration of exposure.

Flotation (3M QCM 37.2)

Product	Floaters (% by bulk volume) Minimum
A16/500	99%
A20/1000	99%
H20/1000	99%
D32/4500	99%
H50/10,000 EPX	99%

Volatile Content (3M QCM 1.5.7)

Maximum of 0.5 percent by weight.

Alkalinity (3M QCM 55.19)

Maximum of 0.3 milliequivalents per gram

pH

Because 3M™ Glass Bubbles are a dry powder, pH is not defined. The pH effect will be determined by the alkalinity as indicated above. When 3M glass bubbles are mixed with deionized water at 5 volume percent loading, the resulting pH of the slurry is typically 9.1 to 9.9, as measured by a pH meter.

Dielectric Constant

1.3 to 1.5 @ 100 MHz, based on theoretical calculations. The dielectric constant of a composite will depend on the matrix material and volume loading of 3M glass bubbles.

Size

Product	Particle Size (microns, by volume) (3M QCM 193.2) Distribution			Effective Top Size
	10th%	50th%	90th%	95th%
A16/500	30	60	95	115
A20/1000	25	60	90	105
H20/1000	25	60	90	105
D32/4500	20	40	65	80
H50/10,000 EPX	15	30	55	70

Hard Particles (3M QCM 93.4.3)

No hard particles (e.g., glass slag, flow agent, etc.) greater than U.S. number 40 (420 microns) standard sieve will exist.

Sieve Analysis (3M QCM 93.4.4)

For *A16/500, A20/1000, H20/1000* glass bubbles: Using a 10 gram sample on a U.S. number 80 standard sieve (177 microns), a maximum of five percent by weight glass bubbles will be retained on the sieve.

For *D32/4500, H50/10,000 EPX* glass bubbles: Using a 10 gram sample on a U.S. number 200 sieve (74 microns), a maximum of three percent by weight glass bubbles will be retained on the sieve.

Appearance (3M QCM 22.85)

White to the unaided eye. *A16/500, A20/1000, and D3L/4500* have a green tint from the surface treatment.

Flowability (3M QCM 22.83)

3M glass bubbles remain free flowing for at least one year from the date of manufacture if stored in the original, unopened container in the minimum storage conditions of an unheated warehouse.

Labeling

3M glass bubbles will be packaged in suitable containers to help prevent damage during normal handling and shipping. Each container will be labeled with:

1. Name of manufacturer
2. Type of 3M glass bubbles
3. Lot number
4. Quantity in pounds

Storage and Handling

To help ensure ease of storage and handling while maintaining free flowing properties, 3M™ Glass Bubbles have been made from a chemically stable glass and are packaged in a heavy duty polyethylene bag within a cardboard container.

Minimum storage conditions should be unopened cartons in an unheated warehouse.

Under high humidity conditions with the ambient temperature cycling over a wide range, moisture can be drawn into the bag as the temperature drops and the air contracts. The result may be moisture condensation within the bag. Extended exposure to these conditions may result in "caking" of the 3M glass bubbles to various degrees. To minimize the potential for "caking" and prolong the storage life, the following suggestions are made:

1. Carefully re-tie open bags after use.
2. If the polyethylene bag is punctured during shipping or handling, use this bag as soon as possible, patch the hole, or insert the contents into an undamaged bag.
3. During hot and humid months, store in the driest, coolest space available.
4. If controlled storage conditions are unavailable, carry a minimum inventory, and process on a first in/first out basis.

Dusting that may occur while handling and processing can be minimized by the following procedures:

1. For eye protection wear chemical safety goggles. For respiratory system protection wear an appropriate NIOSH/MSHA-approved respirator. (For additional information about personal protective equipment, refer to Material Safety Data Sheet.)
2. Use appropriate ventilation in the work area.
3. Pneumatic conveyor systems have been used successfully to transport 3M glass bubbles without dusting from shipping containers to batch mixing equipment. Static eliminators should be used to help prevent static charges.

   Diaphragm pumps have been used to successfully convey 3M glass bubbles. Vendors should be consulted for specific recommendations.

3M glass bubble breakage may occur if the product is improperly processed. To minimize breakage, avoid high shear processes such as high-speed Cowles™ Dissolvers, point contact shear such as gear pumps or 3-roll mills, and processing pressures above the strength test pressure for each product.

Health and Safety Information

For product Health and Safety Information, refer to product label and Material Safety Data Sheet (MSDS) before using product.

Packaging Information

Mini-Box

A single corrugated box with a plastic liner.
Box dimensions are 16 in. × 16 in. × 20 in.

Small Box (10 Cubic ft.)

A single corrugated box with a plastic liner. All boxes are banded together and to the wooden pallet. 4 boxes per pallet.

Box dimensions are 22 in. × 19 in. × 39 in.
Pallet size is 42 in. × 48 in.

Box Weights

Product	Mini-Box	Small Box
A16/500	10 lb.	50 lb.
A20/1000	10 lb.	50 lb.
H20/1000	10 lb.	50 lb.
D32/4500	10 lb.	100 lb.
H50/10,000 EPX	10 lb.	100 lb.

Additional Information

3M™ Glass Bubbles are supported by global sales, technical and customer service resources, with fully-staffed technical service laboratories in the U.S., Europe, Japan, Latin America and Southeast Asia. Users benefit from 3M's broad technology base and continuing attention to product development, performance, safety and environmental issues.

For additional technical information on 3M glass bubbles in the United States, call 3M Energy and Advanced Materials Division, **800-367-8905**.

For other 3M global offices, and information on additional 3M products, visit our web site at: **www.3M.com/oilandgas**.

3M

Energy and Advanced Materials Division
3M Center, Building 223-6S-04
St. Paul, MN 55144-1000
www.3M.com/oilandgas

Please recycle. Printed in USA.
Issued: 9/08 © 3M 2008.
All rights reserved. 6317HB
98-0212-4117-3

APPENDIX F: Quickrete MSDS and Data Sheet

MATERIAL SAFETY DATA SHEET

QUIKRETE®

CEMENT & CONCRETE PRODUCTS™

Masonry Mortars

MATERIAL SAFETY DATA SHEET
(Complies with OSHA 29 CFR 1910.1200)

SECTION I: PRODUCT IDENTIFICATION

The QUIKRETE® Companies
One Securities Centre
3490 Piedmont Road, Suite 1300
Atlanta, GA 30329

Emergency Telephone Number
(770) 216-9580

Information Telephone Number
(770) 216-9580

MSDS E1
Revision: May-12

QUIKRETE® Product Name	Code #
MORTAR MIX	1102
MASON MIX	1136
GLASS BLOCK MORTAR	1610
ROOF TILE MORTAR	1140
CSC-4	1191-84
VENEER STONE MORTAR	1137
POLYMER MODIFIED VENEER STONE MORTAR	1137-85
QUIKRETE® PRO-FINISH BLENDED MORTAR MIX	1136-58
ALL-STAR MORTAR MIX	1122
ALL-STAR MASON MIX	1136
ALL-STAR VENEER STONE MORTAR	1137
HANDICRETE MORTAR MIX	
NATURAL STONE MORTAR	
RED-E-CRETE MORTAR	

BULK MASONRY MORTARS: MIX 101M, 102 S, 104 N, 112 M, 112 N, 112 S, 122 M, 122 N, 122 S, 132 S, 142, 201 M, 202 PLN, 202 S, 203 PLS, 203 S, 203 N, 204 N, 205 P/L type O, 203 M, 212 M, 212 N, 212 S, 222 M, 222 S, 253 S, 294 N

PRODUCT USE: MASONRY MORTARS FOR CONSTRUCTION WITH BLOCK, BRICK, VENEER STONES, ETC.

SECTION II - HAZARD IDENTIFICATION

Route(s) of Entry: Inhalation, Skin, Ingestion
Acute Exposure: Product becomes alkaline when exposed to moisture. Exposure can dry the skin, cause alkali burns and affect the mucous membranes. Dust can irritate the eyes and upper respiratory system. Toxic effects noted in animals include, for acute exposures, alveolar damage with pulmonary edema.
Chronic Exposure: Dust can cause inflammation of the lining tissue of the interior of the nose and inflammation of the cornea. Hypersensitive individuals may develop an allergic dermatitis.
Carcinogenicity: Since Portland cement and blended cements are manufactured from raw materials mined from the earth (limestone, marl, sand, shale, etc.) and process heat is provided by burning fossil fuels, trace, but detectable, amounts of naturally occurring, and possibly harmful, elements may be found during chemical

analysis. Under ASTM standards, Portland cement may contain 0.75 % insoluble residue. A fraction of these residues may be free crystalline silica. Respirable crystalline silica (quartz) can cause silicosis, a fibrosis (scarring) of the lungs and possibly cancer. There is evidence that exposure to respirable silica or the disease silicosis is associated with an increased incidence of Scleroderma, tuberculosis and kidney disorders.

Carcinogenicity Listings:		
	NTP:	Known carcinogen
	OSHA:	Not listed as a carcinogen
	IARC Monographs:	Group 1 Carcinogen
	California Proposition 65:	Known carcinogen

NTP: The National Toxicology Program, in its "Ninth Report on Carcinogens" (released May 15, 2000) concluded that "Respirable crystalline silica (RCS), primarily quartz dusts occurring in industrial and occupational settings, is *known to be a human carcinogen*, based on sufficient evidence of carcinogenicity from studies in humans indicating a causal relationship between exposure to RCS and increased lung cancer rates in workers exposed to crystalline silica dust (reviewed in IAC, 1997; Brown *et al*., 1997; Hind *et al*., 1997)

IARC: The International Agency for Research on Cancer ("IARC") concluded that there was "*sufficient evidence* in humans for the carcinogenicity of crystalline silica in the forms of quartz or cristobalite from occupational sources", and that there is "*sufficient evidence* in experimental animals for the carcinogenicity of quartz or cristobalite." The overall IARC evaluation was that "crystalline silica inhaled in the form of quartz or cristobalite from occupational sources is *carcinogenic to humans (*Group 1)." The IARC evaluation noted that "carcinogenicity was not detected in all industrial circumstances or studies. Carcinogenicity may be dependent on inherent characteristics of the crystalline silica or on external factors affecting its biological activity or distribution of its polymorphs." For further information on the IARC evaluation, see IARC Monographs on the Evaluation of carcinogenic Risks to Humans, Volume 68, "Silica, Some Silicates." (1997)

Signs and Symptoms of Exposure: Symptoms of excessive exposure to the dust include shortness of breath and reduced pulmonary function. Excessive exposure to skin and eyes especially when mixed with water can cause caustic burns as severe as third degree.

Medical Conditions Generally Aggravated by Exposure: Individuals with sensitive skin and with pulmonary and/or respiratory disease, including, but not limited to, asthma and bronchitis, or subject to eye irritation, should be precluded from exposure. Exposure to crystalline silica or the disease silicosis is associated with increased incidence of scleroderma, Tuberculosis and possibly increased incidence of kidney lesions.

Chronic Exposure: Dust can cause inflammation of the lining tissue of the interior of the nose and inflammation of the cornea. Hypersensitive individuals may develop an allergic dermatitis. (May contain trace (<0.05 %) amounts of chromium salts or compounds including hexavalent chromium, or other metals found to be hazardous or toxic in some chemical forms. These metals are mostly present as trace substitutions within the principal minerals)

Medical Conditions Generally Aggravated by Exposure: Individuals with sensitive skin and with pulmonary and/or respiratory disease, including, but not limited to, asthma and bronchitis, or subject to eye irritation, should be precluded from exposure.

SECTION III - HAZARDOUS INGREDIENTS/IDENTITY INFORMATION

Hazardous Components	CAS No.	PEL (OSHA)	TLV (ACGIH)

		mg/M^3	mg/M^3
Portland Cement	65997-15-1	5	5
Silica Sand, crystalline	14808-60-7	$\frac{10}{\%SiO_2+2}$	0.05 (respirable)
May contain one or more of the following ingredients:			
Lime	01305-62-0	5	5
Pulverized Limestone	01317-65-3	5	5
Iron Oxide Pigments	01309-37-1	5	5
Clay	01332-58-7	5	5

Other Limits: National Institute for Occupational Safety and Health (NIOSH). Recommended standard maximum permissible concentration=0.05 mg/M^3 (respirable free silica) as determined by a full-shift sample up to 10-hour working day, 40-hour work week. See NIOSH Criteria for a Recommended Standard Occupational Exposure to Crystalline Silica.

SECTION IV – First Aid Measures

Eyes: Immediately flush eye thoroughly with water. Continue flushing eye for at least 15 minutes, including under lids, to remove all particles. Call physician immediately.
Skin: Wash skin with cool water and pH-neutral soap or a mild detergent. Seek medical treatment if irritation or inflammation develops or persists. Seek immediate medical treatment in the event of burns.
Inhalation: Remove person to fresh air. If breathing is difficult, administer oxygen. If not breathing, give artificial respiration. Seek medical help if coughing and other symptoms do not subside. Inhalations of large amounts of Portland cement require immediate medical attention.
Ingestion: Do not induce vomiting. If conscious, have the victim drink plenty of water and call a physician immediately.

SECTION V - FIRE AND EXPLOSION HAZARD DATA

Flammability: Noncombustible and not explosive.
Auto-ignition Temperature: Not Applicable
Flash Points: Not Applicable

SECTION VI – ACCIDENTAL RELEASE MEASURES

If spilled, use dustless methods (vacuum) and place into covered container for disposal (if not contaminated or wet). Use adequate ventilation to keep exposure to airborne contaminants below the exposure limit.

SECTION VII - PRECAUTIONS FOR SAFE HANDLING AND STORAGE

Do not allow water to contact the product until time of use. DO NOT BREATHE DUST. In dusty environments, the use of an OSHA, MSHA or NIOSH approved respirator and tight fitting goggles is recommended.

SECTION VIII – EXPOSURE CONTROL MEASURES

Engineering Controls: Local exhaust can be used, if necessary, to control airborne dust levels.

Personal Protection: The use of barrier creams or impervious gloves, boots and clothing to protect the skin from contact is recommended. Following work, workers should shower with soap and water. Precautions must be observed because burns occur with little warning -- little heat is sensed.

WARN EMPLOYEES AND/OR CUSTOMERS OF THE HAZARDS AND REQUIRED OSHA PRECAUTIONS ASSOCIATED WITH THE USE OF THIS PRODUCT.

Exposure Limits: Consult local authorities for acceptable exposure limits

SECTION IX - PHYSICAL/CHEMICAL CHARACTERISTICS

Appearance: Gray to gray-brown colored powder;

Specific Gravity:	2.6 to 3.15	**Melting Point:**	>2700°F
Boiling Point:	>2700°F	**Vapor Pressure:**	Not Available
Vapor Density:	Not Available	**Evaporation Rate:**	Not Available
Solubility in Water:	Slight	**Odor:**	Not Available

SECTION X - REACTIVITY DATA

Stability: Stable.
Incompatibility (Materials to Avoid): Contact of silica with powerful oxidizing agents such as fluorine, chlorine trifluoride, manganese trioxide, or oxygen difluoride may cause fires
Hazardous Decomposition or By-products: Silica will dissolve in Hydrofluoric Acid and produce a corrosive gas – silicon tetrafluoride.
Hazardous Polymerization: Will Not Occur.
Condition to Avoid: Keep dry until used to preserve product utility.

SECTION XI – TOXICOLOGICAL INFORMATION

Routes of Entry: Inhalation, Ingestion
Toxicity to Animals:
LD50: Not Available
LC50: Not Available
Chronic Effects on Humans: Conditions aggravated by exposure include eye disease, skin disorders and Chronic Respiratory conditions.
Special Remarks on Toxicity: Not Available

SECTION XII – ECOLOGICAL INFORMATION

Ecotoxicity: Not Available
BOD5 and COD: Not Available
Products of Biodegradation: Not available
Toxicity of the Products of Biodegradation: Not available
Special Remarks on the Products of Biodegradation: Not available

SECTION XIII – DISPOSAL CONSIDERATIONS

Waste Disposal Method: The packaging and material may be land filled; however, material should be covered to minimize generation of airborne dust. This product is not classified as a hazardous waste under the authority of the RCRA (40CFR 261) or CERCLA (40CFR 117&302).

SECTION XIV – TRANSPORT INFORMATION

Not hazardous under U.S. DOT and TDG regulations.

SECTION XV – OTHER REGULATORY INFORMATION

US OSHA 29CFR 1910.1200: Considered hazardous under this regulation and should be included in the employers' hazard communication program
SARA (Title III) Sections 311 & 312: Qualifies as a hazardous substance with delayed health effects
SARA (Title III) Section 313: Not subject to reporting requirements
TSCA (May 1997): Some substances are on the TSCA inventory list
Federal Hazardous Substances Act: Is a hazardous substance subject to statues promulgated under the subject act
California Regulation: WARNING: This product contains chemicals known to the State of California to cause cancer, birth defects or other reproductive harm.
Canadian Environmental Protection Act: Not listed
Canadian WHMIS: Considered to be a hazardous material under the Hazardous Products Act as defined by the Controlled Products Regulations (Class D2A, E- Corrosive Material) and subject to the requirements of Health Canada's Workplace Hazardous Material Information (WHMIS). This product has been classified according to the hazard criteria of the Controlled Products Regulation (CPR). This document complies with the WHMIS requirements of the Hazardous Products Act (HPA) and the CPR.

SECTION XVI – OTHER INFORMATION

HMIS-III:

Health –
0 = No significant health risk
1 = Irritation or minor reversible injury possible
2 = Temporary or minor injury possible
3 = Major injury possible unless prompt action is taken
4 = Life threatening, major or permanent damage possible

Flammability-
0 = Material will not burn
1 = Material must be preheated before ignition will occur
2 = Material must be exposed to high temperatures before ignition
3 = Material capable of ignition under normal temperatures
4 = Flammable gases or very volatile liquids; may ignite spontaneously

Physical Hazard-
0 = Material is normally stable, even under fire conditions
1 = Material normally stable but may become unstable at high temps
2 = Materials that are unstable and may undergo react at room temp
3 = Materials that may form explosive mixtures with water
4 = Materials that are readily capable of explosive water reaction

Abbreviations:

ACGIH American Conference of Government Industrial Hygienists

QUIKRETE®

CEMENT & CONCRETE PRODUCTS™

CAS	Chemical Abstract Service
CERCLA	Comprehensive Environmental Response, Compensation and Liability Act
CFR	Code of Federal Regulations
CPR	Controlled Products Regulations (Canada)
DOT	Department of Transportation
IARC	International Agency for Research
MSHA	Mine Safety and Health Administration
NIOSH	National Institute for Occupational Safety and Health
NTP	National Toxicity Program
OSHA	Occupational Safety and Health Administration
PEL	Permissible Exposure Limit
RCRA	Resource Conservation and Recovery Act
SARA	Superfund Amendments and Reauthorization Act
TLV	Threshold Limit Value
TWA	Time-weighted Average
WHMIS	Workplace Hazardous Material Information System

Last Updated: May 8, 2012

NOTE: The information and recommendations contained herein are based upon data believed to be correct. However, no guarantee or warranty of any kind, express or implied, is made with respect to the information contained herein. We accept no responsibility and disclaim all liability for any harmful effects which may be caused by exposure to silica contained in our products. END OF MSDS.

ONE SECURITIES CENTRE, 3490 PIEDMONT ROAD NE, SUITE 1300, ATLANTA, GA 30305 TEL 404-634-9100 WWW.QUIKRETE.COM

QUIKRETE®
CEMENT & CONCRETE PRODUCTS™

MORTAR MIX

PRODUCT NO. 1102

DIVISION **4**

Masonry Mortaring
04 05 13

PRODUCT DESCRIPTION

QUIKRETE® Mortar Mix is a construction grade mortar mix designed for laying brick, concrete masonry units and stone.

PRODUCT USE

QUIKRETE® Mortar Mix is a construction grade mortar mix designed for laying brick, concrete masonry units and stone. QUIKRETE® Mortar Mix is a pre-blended, sanded product. The standard formulation meets ASTM C 270 and C 1714 for Type N mortar.

COLORS

QUIKRETE® Mortar Mix is available in gray and additional colors by special order. Color can also be added to the product as it is mixed by adding QUIKRETE® Stucco and Mortar Color (#1319) to the mixing water. Twenty standard colors are available.

SIZES

- QUIKRETE® Mortar Mix -
  - 60 lb (27.2 kg) bags
  - 80 lb (36.3 kg) bags

YIELD

- Each 80 lb (36.3 kg) bag of QUIKRETE® Mortar Mix will lay up to 37 standard bricks or 13 standard (8" x 8" x 16" [200 x 200 x 400 mm]) blocks.

TECHNICAL DATA

APPLICABLE STANDARDS

ASTM International

- ASTM C 270 Specification for Mortar for Unit Masonry
- ASTM C 387 Specification for Packaged, Dry, Combined Materials for Mortar and Concrete
- ASTM C 1714 Specification for Preblended Dry Mortar Mix for Unit Masonry

PHYSICAL/CHEMICAL PROPERTIES

QUIKRETE® Mortar Mix meets or exceeds the property requirements of ASTM C 270, ASTM C 387 and ASTM C 1714 for the type selected. Refer to Appendix XI of ASTM C270 for guidance in selecting the proper mortar type. See Table 1.

INSTALLATION

SURFACE PREPARATION

Surfaces to receive Mortar Mix should be clean and free of dirt, loose debris, grease, oil, etc., for the best possible bond.

MIXING

- For each 80 lb (36.3 kg) bag, add 9 pt (4.3 L) of fresh water to mixer
- Turn the mixer on and begin adding bags of Mortar Mix
- If the material becomes too difficult to mix, add additional water until a workable mix of trowelable consistency is obtained

Note - Final water content should be 9 - 14 pt (4.3 - 6.6 L) for each 80 lb (36.3 kg) bag and 7 - 10 pt (3.3 - 4.7 L) for each 60 lb (27.2 kg) bag.

INSTALLATION

- Apply a full bed of mortar onto the base, approximately 1/2" - 3/4" (12.7 - 19.1 mm) thick
- Push downward into the mortar bed and sideways against the previously laid block with a slight twisting motion
- Tool the mortar joints when they become thumbprint hard. This will make the mortar joint watertight and provide a neat appearance

Table 1

Hydraulic Cement- Lime Mortars or Cement Mortars			
Type	Minimum Compressive Strength, psi (MPa)	Water Retention Minimum %	Air content Maximum %
M	2500 (17.2)	75	12
S	1800 (12.4)	75	12
N	750 (5.2)	75	14[1]
O	350 (2.4)	75	14[1]
Masonry Cement Mortars			
Type	Minimum Compressive Strength, psi (MPa)	Water Retention Minimum %	Air content Maximum %
M	2500 (17.2)	75	18
S	1800 (12.4)	75	18
N	750 (5.2)	75	20[2]
O	350 (2.4)	75	20[2]

[1] When structural reinforcement is included, the maximum air content shall be 12%
[2] When structural reinforcement is included, the maximum air content shall be 18%

CURING

Curing of masonry mortars is required only if conditions are very hot, dry or windy. In such cases, a gentle mist of water applied to the surface will prevent premature drying and improve the strength of the mortar.

PRECAUTIONS

Variations in mix water amount, mix time, curing conditions and finishing will cause color variations.

WARRANTY

The QUIKRETE® Companies warrant this product to be of merchantable quality when used or applied in accordance with the instructions herein. The product is not warranted as suitable for any purpose or use other than the general purpose for which it is intended. Liability under this warranty is limited to the replacement of its product (as purchased) found to be defective, or at the shipping companies' option, to refund the purchase price. In the event of a claim under this warranty, notice must be given to The QUIKRETE® Companies in writing. This limited warranty is issued and accepted in lieu of all other express warranties and expressly excludes liability for consequential damages.

The QUIKRETE® Companies
One Securities Centre
3490 Piedmont Rd., NE, Suite 1300, Atlanta, GA 30305
(404) 634-9100 • Fax: (404) 842-1425

** Refer to www.quikrete.com for the most current technical data, MSDS, and guide specifications*

BIBLIOGRAPHY

Abotula S, Heeder N, Chona R, Shukla A. Dynamic Thermo-mechanical Response of Hastelloy X to Shock Wave Loading. *Experimental Mechanics.* 2014 Feb 1;54(2):279–291.

Ai S, Mao Y, Pei Y, Fang D, Tang L. Study on aluminum honeycomb sandwich panels with random skin/core weld defects. *Journal of Sandwich Structures and Materials.* 2013 Nov 1;15(6):704–717.

Alberto Corigliano ER. Experimental characterization and numerical simulations of a syntactic-foam/glass-fibre composite sandwich.*Composites Science and Technology.* 2000;(11):2169–2180.

Arioz O. Effects of elevated temperatures on properties of concrete. *Fire Safety Journal.* 2007 Nov;42(8):516–522.

Bardella L, Genna F. Elastic design of syntactic foamed sandwiches obtained by filling of three-dimensional sandwich-fabric panels.*International Journal of Solids and Structures.* 2001 Jan 11;38(2):307–333.

Chen Q, Pugno N, Zhao K, Li Z. Mechanical properties of a hollow-cylindrical-joint honeycomb. *Composite Structures.* 2014 Mar;109:68–74.

Dharmasena KP, Wadley HNG, Xue Z, Hutchinson JW. Mechanical response of metallic honeycomb sandwich panel structures to high-intensity dynamic loading. *International Journal of Impact Engineering.* 2008 Sep;35(9):1063–1074.

Ebrahimi H, Vaziri A. Metallic sandwich panels subjected to multiple intense shocks. *International Journal of Solids and Structures.*2013 Apr;50(7–8):1164–1176.

Ergün A, Kürklü G, M. Serhat B, Mansour MY. The effect of cement dosage on mechanical properties of concrete exposed to high temperatures. *Fire Safety Journal.* 2013 Jan;55:160–167.

Erik S Weiser TFJ. Polyimide Foams for Aerospace Vehicles. *High Performance Polymers.*2000;12(1):1–12.

François Grosjean NB. Comprehensive analyses of syntactic foam behaviour in deepwater environment. *Journal of Materials Science.*2009;44(6):1462–1468.

G. M. Gladysz BP. Three-phase syntactic foams: structure-property relationships. *Journal of Materials Science.* 2006;41(13):4085–4092.

Guan ZW, Aktas A, Potluri P, Cantwell WJ, Langdon G, Nurick GN. The blast resistance of stitched sandwich panels. *International Journal of Impact Engineering.* 2014 Mar;65:137–145.

Hassan MZ, Guan ZW, Cantwell WJ, Langdon GS, Nurick GN. The influence of core density on the blast resistance of foam-based sandwich structures. *International Journal of Impact Engineering.* 2012 Dec;50:9–16.

Husem M. The effects of high temperature on compressive and flexural strengths of ordinary and high-performance concrete. *Fire Safety Journal.* 2006 Mar;41(2):155–163.

Johnson G.R. and Cook W.H.. *Proc. 7th Int. Symp. on Ballistics*, The Hague, The Netherlands, 1983, 541–47.

Kessler M, Schnettler A. Investigation of the DC breakdown mechanism in elastic syntactic foams. *IEEE Transactions on Dielectrics and Electrical Insulation.* 2010 Jun;17(3):898–905.

Langdon GS, Karagiozova D, von Klemperer CJ, Nurick GN, Ozinsky A, Pickering EG. The air-blast response of sandwich panels with composite face sheets and polymer foam cores: Experiments and predictions. *International Journal of Impact Engineering.*2013 Apr;54:64–82.

Langdon GS, von Klemperer CJ, Rowland BK, Nurick GN. The response of sandwich structures with composite face sheets and polymer foam cores to air-blast loading: Preliminary experiments. *Engineering Structures.* 2012 Mar;36:104–112.

Li G, Jones N. Development of rubberized syntactic foam. *Composites Part A: Applied Science and Manufacturing.* 2007 Jun;38(6):1483–1492.

Li M, Qian C, Sun W. Mechanical properties of high-strength concrete after fire. *Cement and Concrete Research.* 2004 Jun;34(6):1001–1005.

Liang C-C, Yang M-F, Wu P-W. Optimum design of metallic corrugated core sandwich panels subjected to blast loads. *Ocean Engineering.* 2001 Jul;28(7):825–861.

Lin TC, Gupta N, Talalayev A. Thermoanalytical characterization of epoxy matrix-glass microballoon syntactic foams. *J Mater Sci.*2009 Mar 1;44(6):1520–1527.

Liu H, Cao ZK, Yao GC, Luo HJ, Zu GY. Performance of aluminum foam–steel panel sandwich composites subjected to blast loading.*Materials & Design.* 2013 May;47:483–488.

M. Porfiri NQN. Thermal conductivity of multiphase particulate composite materials. 44(6):1540–1550.

Momchil Dimchev RC. Effect of carbon nanofibers on tensile and compressive characteristics of hollow particle filled composites.*Materials & Design.* 2010;31(3):1332–1337.

Mutua FN. Surface Modification of Hollow Glass Microspheres. *Materials Sciences and Applications.* 2012;03(12):856–860.

Nadège Bouchonneau VS-M. Experimental testing and modelling of an industrial insulated pipeline for deep sea application. *Journal of Petroleum Science and Engineering.* 2010;:1–12.

Nikhil Gupta EW. Compression properties of syntactic foams: effect of cenosphere radius ratio and specimen aspect ratio. *Composites Part A: Applied Science and Manufacturing.* 2003;(1):103–111.

Nikhil Gupta VCS. High strain rate compressive response of syntactic foams: Trends in mechanical properties and failure mechanisms.*Materials Science and Engineering A- Structural Materials Properties Microstructure and Processing.* 2011;528(25):7596–7605.

Phan VT, Choqueuse D, Cognard JY, Sohier L. Experimental analysis and modelling of the long term thermo-mechanical behaviour of glass/polypropylene syntactic used on thermally insulated offshore pipeline. *Progress in Organic Coatings.* 2013 Feb;76(2-3):341–350.

Poon C-S, Azhar S, Anson M, Wong Y-L. Comparison of the strength and durability performance of normal- and high-strength pozzolanic concretes at elevated temperatures. *Cement and Concrete Research.* 2001 Sep;31(9):1291–1300.

Poveda RL, Achar S, Gupta N. Thermal Expansion of Carbon Nanofiber-Reinforced Multiscale Polymer Composites. *Journal Of Materials.*2012;64(10):1148 – 1157.

Rahul Jhaver HT. Characterization and modeling of compression behavior of syntactic foam-filled honeycombs. *Journal of Reinforced Plastics and Composites.* 2010;29(12).

Rubino V, Deshpande VS, Fleck NA. The dynamic response of clamped rectangular Y-frame and corrugated core sandwich plates.*European Journal of Mechanics - A/Solids.* 2009 Jan;28(1):14–24.

Shabde VS, Hoo KA, Gladysz GM. Experimental determination of the thermal conductivity of three-phase syntactic foams. *Journal of Material Science.* 2006 Jul 1;41(13):4061–4073.

Sohel KMA, Richard Liew JY, Yan JB, Zhang MH, Chia KS. Behavior of Steel–Concrete–Steel sandwich structures with lightweight cement composite and novel shear connectors. *Composite Structures.* 2012 Dec;94(12):3500–3509.

Song B, Chen W, Yanagita T, Frew DJ. Temperature effects on dynamic compressive behavior of an epoxy syntactic foam. *Composite Structures.* 2005 Mar;67(3):289–298.

Stuckey CI, Reinarts TR, Davis D. Thermal characterization of an epoxy-based composite sandwich nose cap design for the space shuttle solid rocket booster. AIP Conference Proceedings, 552, 2001 : p. 298–303.

Tekalur SA, Shukla A, Shivakumar K. Blast resistance of polyurea based layered composite materials. *Composite Structures.* 2008 Jul;84(3):271–281.

Thangavelu Muthukumar AA. Fouling and stability of polymers and composites in marine environment. *International Biodeterioration & Biodegradation.* 2011;65(2):276–284.

Vasanth Chakravarthy Shunmugasamy DP. Thermal expansion behavior of hollow glass particle/vinyl ester composites. *Journal of Materials Science.* 2012;47(14):5596–5604.

Vural M, Ravichandran G, Rittel D. Large strain mechanical behavior of 1018 cold-rolled steel over a wide range of strain rates. *Metallurgical and Material Transactions A.* 2003 Dec 1;34(12):2873–2885.

Wadley HNG, Dharmasena KP, O'Masta MR, Wetzel JJ. Impact response of aluminum corrugated core sandwich panels.*International Journal of Impact Engineering.* 2013 Dec;62:114–128.

Wang E, Gardner N, Shukla A. The blast resistance of sandwich composites with stepwise graded cores. *International Journal of Solids and Structures.* 2009 Sep;46(18–19):3492–3502.

Wang E, Shukla A. Analytical and experimental evaluation of energies during shock wave loading. *International Journal of Impact Engineering.* 2010 Dec;37(12):1188–1196.

Wang E, Wright J, Shukla A. Analytical and experimental study on the fluid structure interaction during air blast loading. *Journal of Applied Physics.* 2011 Dec 1;110(11):114901.

Xiao J, König G. Study on concrete at high temperature in China—an overview. *Fire Safety Journal.* 2004 Feb;39(1):89–103.

Xiong J, Vaziri A, Ma L, Papadopoulos J, Wu L. Compression and impact testing of two-layer composite pyramidal-core sandwich panels. *Composite Structures.* 2012 Jan;94(2):793–801.

Xue Z, Hutchinson JW. A comparative study of impulse-resistant metal sandwich plates. *International Journal of Impact Engineering.* 2004 Nov;30(10):1283–1305.

Yang Y, Fallah AS, Saunders M, Louca LA. On the dynamic response of sandwich panels with different core set-ups subject to global and local blast loads. *Engineering Structures.* 2011 Oct;33(10):2781–2793.

Yazici, M, Fahr, P, Shukla, A, Güneş Ş, Akay S. Development of a Polymer Based Syntactic Foam for High Temperature Applications.*Acta Physica Polonica A.* 2014 Feb 24**;** 125(2): 526-528

Yazıcı Ş, Sezer Gİ, Şengül H. The effect of high temperature on the compressive strength of mortars. *Construction and Building Materials.* 2012 Oct;35:97–100.

Youssef MA, Moftah M. General stress–strain relationship for concrete at elevated temperatures. *Engineering Structures.* 2007 Oct;29(10):2618–2634.

Yüzer N, Aköz F, Öztürk LD. Compressive strength–color change relation in mortars at high temperature. *Cement and Concrete Research.* 2004 Oct;34(10):1803–1807.